DISSERTATION

LONG-TERM-ROBUST ADAPTATION STRATEGIES FOR RESERVOIR OPERATION CONSIDERING MAGNITUDE AND TIMING OF CLIMATE CHANGE: APPLICATION TO DIYALA RIVER BASIN IN IRAQ

Submitted by

Saddam Qahtan Waheed

Department of Civil and Environmental Engineering

In partial fulfillment of the requirements

For the Degree of Doctor of Philosophy

Colorado State University

Fort Collins, Colorado

Spring 2020

Doctoral Committee:

Advisor: Neil S. Grigg

Jorge A. Ramirez
Ryan T. Bailey
Steven R. Fassnacht

ABSTRACT

LONG-TERM-ROBUST ADAPTATION STRATEGIES FOR RESERVOIR OPERATION CONSIDERING MAGNITUDE AND TIMING OF CLIMATE CHANGE: APPLICATION TO DIYALA RIVER BASIN IN IRAQ

Vulnerability assessment due to climate change impacts is of paramount importance for reservoir operation to achieve the goals of water resources management. This requires accurate forcing and basin data to build a valid hydrology model and assessment of the sensitivity of model results to the forcing data and uncertainty of model parameters. The **first objective** of this study is to construct the model and identify its sensitivity to the model parameters and uncertainty of the forcing data. The **second objective** is to develop a Parametric Regional Weather Generator (RP-WG) for use in areas with limited data availability that mimics observed characteristics. The **third objective** is to propose and assess a decision-making framework to evaluate pre-specified reservoir operation plans, determine the theoretical optimal plan, and identify the anticipated best timeframe for implementation by considering all possible climate scenarios.

To construct the model, the Variable Infiltration Capacity (VIC) platform was selected to simulate the characteristics of the Diyala River Basin (DRB) in Iraq. Several methods were used to obtain the forcing data and they were validated using the Kling–Gupta efficiency (KGE) metric. Variables considered include precipitation, temperature, and wind speed. Model sensitivity and uncertainty were examined by the Generalized Likelihood Uncertainty Estimation (GLUE) and the Differential Evolution Adaptive Metropolis (DREAM) techniques. The proposed RP-WG was based on (1) a First-order, Two-state Markov Chain to simulate precipitation occurrences; (2) use of Wilks' technique to produce correlated weather variables at multiple sites with conservation of

spatial, temporal, and cross correlations; and (3) the capability to produce a wide range of synthetic climate scenarios.

A probabilistic decision-making framework under nonstationary hydroclimatic conditions was proposed with four stages: (1) climate exposure generation (2) supply scenario calculations, (3) demand scenario calculations, and (4) multi-objective performance assessment. The framework incorporated a new metric called Maximum Allowable Time to examine the timeframe for robust adaptations. Three synthetic pre-suggested plans were examined to avoid undesirable long-term climate change impacts, while the theoretical-optimal plan was identified by the Non-dominated Sorting Genetic Algorithm II.

The multiplicative random cascade and Schaake Shuffle techniques were used to determine daily precipitation data, while a set of correction equations was developed to adjust the daily temperature and wind speed. The depth of the second soil layer caused most sensitivity in the VIC model, and the uncertainty intervals demonstrated the validity of the VIC model to generate reasonable forecasts. The daily VIC outputs were calibrated with a KGE average of 0.743, and they were free from non-normality, heteroscedasticity, and auto-correlation. Results of the PR-WG evaluation show that it exhibited high values of the KGE, preserved the statistical properties of the observed variables, and conserved the spatial, temporal, and cross correlations among the weather variables at all sites. Finally, risk assessment results show that current operational rules are robust for flood protection but vulnerable in drought periods. This implies that the project managers should pay special attention to the drought and spur new technologies to counteract. Precipitation changes were dominant in flood and drought management, and temperature and wind speed changes effects were significant during drought. The results

demonstrated the framework's effectiveness to quantify detrimental climate change effects in magnitude and timing with the ability to provide a long-term guide (and timeframe) to avert the negative impacts.

ACKNOWLEGMENTS

First of all, thanks to God Almighty for giving me the strength, ability, and knowledge to complete this research. Foremost, I would like to express my sincere gratitude to my advisor Dr. Neil Grigg for the continuous support, patience, motivation, enthusiasm, immense knowledge, and guidance in my Ph. D research and writing. I will forever be thankful to my previous advisor soul Dr. Jorge Ramirez. This thesis would not have been possible without his assistance through reading the papers, comments, and suggestions during past five years. Besides, I would like to thank the rest of my exceptional committee: Dr. Ryan T. Bailey and Dr. Steven R. Fassnacht for their invaluable discussion, insightful comments, and feedback. Earnest thanks are due to the Higher Committee for Education Development (HCED) and Ministry of Water Resources (MoWR) in Iraq for financial support and sharing the data. Deep gratitude to all my family members for the continuous encourage and support. I am always indebted to my parents, wife, and kids for their unparalleled love and countless sacrifices throughout this journey as well as the inspiration to follow my dreams. Special thanks to Mr. Muhammad Ukasha for his invaluable helping in running the VIC model. Last but not least, I express my deepest gratitude to my friends and colleagues at Colorado State University for their friendship.

DEDICATION

To my darling parents ... for your love, support, and unwavering belief in me… without you, I would not be the person I am today,

To my wife … for the unconditional love and endless encouragement… for all the late nights and early mornings… for keeping me sane over the study years .... I owe you everything.

To my lovely kids … I love you to the moon and back,

To my beloved brothers, sister, nieces, and nephews ... my source of inspiration… near or far, you are always in my heart…

TABLE OF CONTENTS

LIST OF TABLES

LIST OF FIGURES

CHAPTER 1

INTRODUCTION AND MOTIVATION

1.1. Objective and Expected Significance

Water resources planning and management are being affected by climate change impacts, and assessment of its risk is an important task for hydrologists and scientists. To approach this task, the overall goal of this dissertation is to develop and test a probabilistic decision-making framework for application under a non-stationary hydroclimatic assumption to evaluate the magnitude and timing of climate change for management of water resources systems. Basic data analysis and testing of results are on the Diyala River Basin (DRB) reservoir system in Iraq.

The framework can aid decision makers to adapt system operational rules to long-term climate change and help them gain insights about risk characteristics. It is also capable of identifying the long-term-robust management plans that avoid undesirable climate change impacts among pre-specified plans, and of implementing an optimization technique to provide the best plan for multi-objective operational purposes. Although the framework is applied for a paradigm in Iraq, it is effective to use in other basins for quantifying detrimental climate change effects and providing a long-term guide for water resources management and planning in similar basins with limited data.

The study involved the following specific objectives:

1) Build a valid hydrologic model to project future water availability in the DRB by addressing data scarcity issues. The observed forcing data, obtained from the Iraqi Ministry of Water Resources (MoWR), were augmented by data from the Tropical Rainfall Measuring

Mission (TRMM) and the Global Implemented Data (GIDAL) [Adam and Lettenmaier, 2003 and Adam et al., 2006]. The validity and applicability of these datasets were examined through comparing with ground observation data. Then, the sensitivity and uncertainty of the selected model platform, the Variable Infiltration Capacity (VIC) model, were investigated to identify model applicability in the region. The approaches used to address the sensitivity and uncertainty are the Generalized Likelihood Uncertainty Estimation (GLUE) proposed by Beven and Binley, (1992) and the Differential Evolution Adaptive Metropolis (DREAM) [e.g., Vrugt et al., 2009a; Vrugt et al., 2009b; and Vrugt, 2016].

2) Develop a Parametric Regional-Multivariate Statistical Weather Generator (PR-WG) to produce a wide range of possible climate scenarios in the basin. The suggested PR-WG is straightforward to develop and can employ any distribution function for variables such as precipitation or temperature. The model developed is capable of conserving the spatial, temporal, and cross-correlations among the variables, producing scenarios beyond the range of the observations and applying to periods longer than the observation period. It also enables relatively simple alteration of statistical parameters.
3) Model a probabilistic decision-making framework, with new performance indicators and approaches to assess climate change impacts in both magnitude and timing. The framework utilizes the VIC model and PR-WG developed in objectives 1 and 2. The framework is capable of evaluating different pre-suggested alternative plans to select the most robust adaptation plan, implementing an optimization technique to suggest the theoretical-optimal adaptation plan, and identifying the optimal timeframe to start applying the robust plan(s) to minimize the negative climate change impacts. The

framework is also capable of evaluating the impact of different weather variables including wind speed change on the decision-making process.

1.2. Background

Assessment of climate change impacts on water resources infrastructure performance, including reservoirs and regulatory controls, is a growing concern in water resources management and creates a need for new strategies or adaptations to avert undesirable impacts and cope with shifting climate regimes [Kundzewicz et al., 2008; Azhoni et al., 2018].

In this content, there have been extensive efforts to develop approaches to assess climate change impacts. These can be divided into two main groups: top-down and bottom-up. Top-down is considered as the traditional approach, where the performance of a water resources system is examined under specific scenarios that are usually obtained from GCM outputs. Although the top-down approach is widely used, it limits the decision-making abilities since the GCM scenarios represent only specific discrete scenarios for climatic variability and lead to uncertain conclusions. Therefore, it is not suitable to evaluate the risks and examine the degree of undesirable system performances in these scenarios [Wilby and Dessai, 2010; Hallegatte et al., 2012; Brown and Wilby, 2012; Stephenson et al., 2012; Whateley et al., 2014; Culley et al., 2016; Taner et al., 2019]. Moreover, GCMs are spatially coarse to capture the high-intensity at which precipitation occurs at fine spatial scales, thus leading to difficult selection for an adaptation strategy [Spence and Brown, 2016; Van Tra et al., 2018].

The second group of “bottom-up” approaches is considered as an alternative to overcome the “top-down” approach drawbacks. Using this approach, a wide range of plausible synthetic future scenarios is generated using SWG and including values beyond the GCMs bounds. Those

scenarios are fed into hydrologic models to produce the corresponding water supply scenarios. Afterwards, the system response against each supply scenario can be evaluated. The bottom-up approach provides more insights regarding system performance under climate change and enables better testing and selecting for robust alternative management [Weaver et al., 2013; Turner et al., 2014; Steinschneider et al., 2015a; Zhang et al., 2018]. Furthermore, Moody and Brown, (2013); Steinschneider et al., (2015b); and Taner et al., (2017) linked SWG scenarios with GCM scenarios so that a probability of occurrence of each scenario generated by SWG can be estimated. This weighting procedure enables better identification for robust alternative management.

An example of a simple comparison between the outputs of GCM and SWG is shown in Figure 1.1. It is seen that some internal weather conditions cannot be obtained by the GCMs, while SWG can generate any condition of interest including for those beyond the GCM bounds, which demonstrates the importance of the SWG usage.

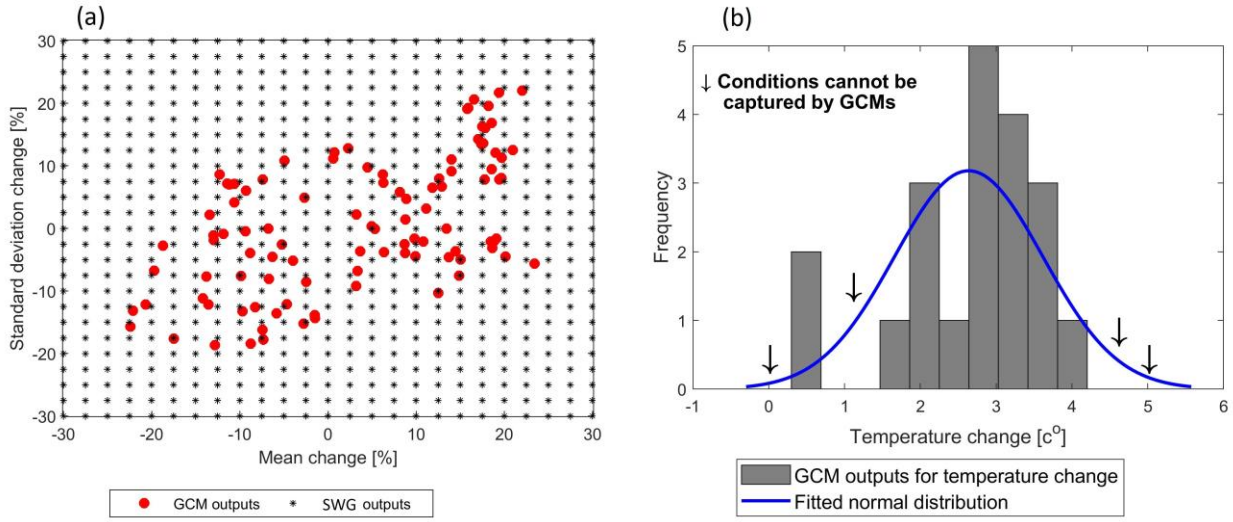

Figure 1.1: Comparison of the GCM outputs versus SWG outputs.

However, system performance can be evaluated using different indicators. For example, Whateley, et al., (2014) developed a binary performance function called the Robustness Index (RI). In it, the binary performance function returns a value of 1 (acceptable performance) or 0 (unacceptable performance) for each climate scenario by comparing the system performance with the threshold value, Z, as follows:

$$\Lambda\,(t,j) = 1 \qquad if \quad Z_t^j \leq 0 \tag{1.1}$$

$$\Lambda\,(t,j) = 0 \qquad if \quad Z_t^j > 0 \tag{1.2}$$

$$R(j) = \frac{\sum_{t=1}^{T} \Lambda(t,j)}{T} \tag{1.3}$$

In these equations, Λ is the system performance function, j is the climate scenario index, t is the time index in month, Z(t,j) is the system performance threshold corresponding to the given scenario j at time step t ($Z(t,j) = 0.8\,D(t,j)\ - S(t,j)$), R is the system Reliability, and T is the scenario time length in months. Dam performance is assigned "acceptance" if the water supply (S) meets 80% or more of the demand (D) at the time step t. Then, the RI is computed by integrating the performance function over the range of climate scenarios and dividing by the entire climate change space:

$$RI = \frac{\int_1^J R\,(j)\,dj}{\int_1^J dj} \tag{1.4}$$

The RI can be used to evaluate the system performance of the system status quo relative to climate change effects and then used to compare different adaptation strategies. An example of the RI is shown in Figure 1.2.

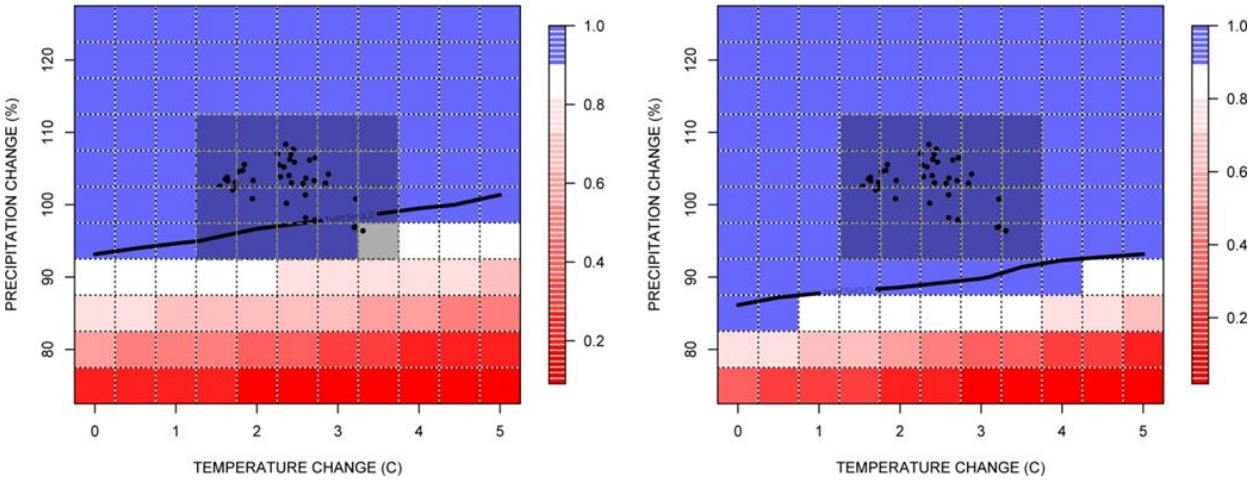

Figure 1.2: Climate response surfaces over climate change space for water supply reliability under (a) standard operation (RI=0.55) and (b) alternative operation (RI= 0.7) for Connecticut River Basin [*Whateley, et al., 2014].*

Steinschneider et al., (2015b) modified the Whateley, et al., (2014) approach to account for the probability of each scenario and developed an indicator called "Robustness Score", as follows:

$$R - Score_z = \sum_{j=1}^{J} w(j) \frac{1}{B} \sum_{b=1}^{B} R_z(t,j,b) \tag{1.5}$$

Here w(j) is the weight of each scenario for a given climate condition, B is the number of internal realizations for a given scenario j, and z is the index of adaptation strategies. Let $\Phi^{-1}(.)$ and $\psi(.)$ be the density and distribution function of a standard normal random. The weights based on the probabilities of occurrence, Pr, for each realization of future variability can be calculated as:

$$w_j = \frac{\Phi\left[\psi^{-1}\left(p_j\right)\right]}{\sum_{j=1}^{J} \Phi\left[\psi^{-1}\left(p_j\right)\right]} \tag{1.6}$$

In this way, the adaptation strategy (or the status quo) performance is considered acceptable if the R-Score is greater than a threshold value, which is assumed to be 0.7. An example is shown in Figure 1.3.

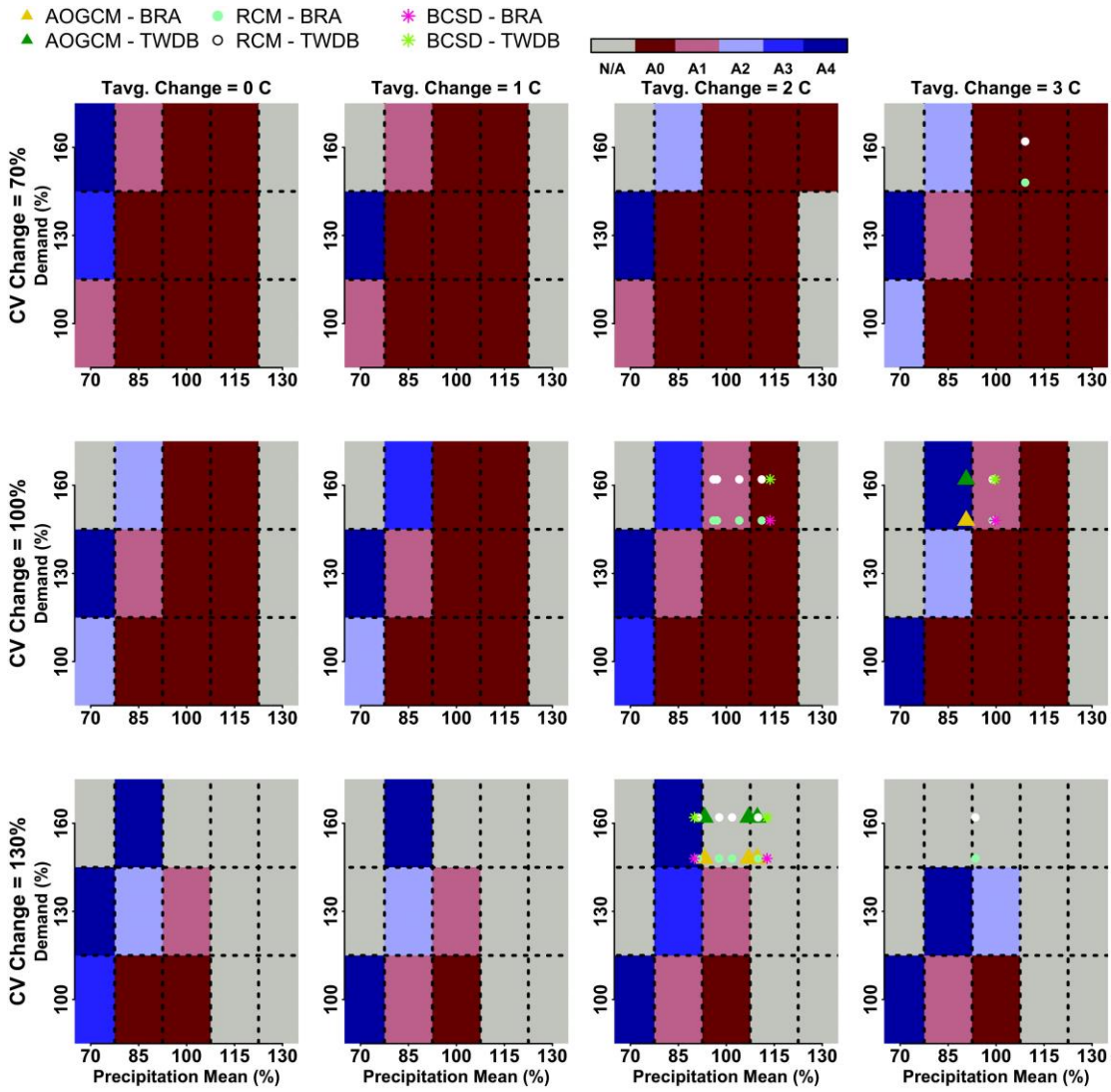

Figure 1.3: (Color) Robust Management plans; A0: the status quo plan, (Gray) no plan is; 19 projections of climate models projections, and future water demand from BRA and TWDB scenarios, for Belton Lake watershed [Steinschneider et al., 2015b].

Similarly, Culley et al., (2016) modified an approach to assess the optimal operation of the system. Instead of calculating a value using a performance function, an objective function is used to evaluate the system performance to be either “Success” or “Failure”, as follows:

$$OF = \text{Success } if \left(R_f \leq T_f \; and \; R_s \leq T_R\right) \tag{1.7}$$

$$OF = \text{Failure } if \left(R_f > T_f \; or \; R_s > T_R\right) \tag{1.8}$$

$$C_Z = \frac{\int_1^J SN_z}{\int_1^J SN_0} \tag{1.9}$$

R_f and R_S are the magnitude of flood and irrigation deficit, respectively, T_F and T_R are the thresholds for flood (100 m^2/day of flooded area) and irrigation (400 kL^2 of squared water deficit), respectively. SN is the number of success scenarios for the system under the adaptation strategy z, SN_0 is the number of success scenarios under the status qua of the system, and C is the maximum operational adaptive capacity. So, the system performance is considered "fail" if its operations result in the daily average flooded area exceed T_F and/or a daily average deficit exceeds T_R. Then, the adaptation strategy that maximizes the system performance (e.g., maximum C_Z) can be identified. This indicator can allow the decision maker to examine all optimal adaptation strategies as well as to identify the limits of them according to the indicator C. An example is shown in Figure 1.4.

Other indicators were also suggested for the climate change assessment such as the "vulnerability" approach. Foti, et al., (2014) defined it as the probability of demand D exceeding the supply S, as follows:

$$V = Pr[S < D] = Pr[S - D < 0] \tag{1.10}$$

Let Z be the difference between supply and demand (S-D), then equation), then equation (1.10) becomes,

$$V = Pr[Z > 0] = Pr[\frac{Z - \mu_Z}{\sigma_Z} < -\frac{\mu_Z}{\sigma_Z} = -\frac{\mu_Z}{\sigma_Z}] \quad (1.11)$$

In this equation, $\mu_Z = \mu_S - \mu_D$, $\sigma_Z^2 = \sigma_Z^2 - \sigma_Z^2 - COV(S, D)$, and μ_S, μ_D, σ_S, σ_D, and $COV(S, D)$, are the mean, standard deviation and covariance of water supply and water demand. If the supply and demand are assumed normally distributed, equation (1.11) yields:

$$V = Pr = [2\,\pi\,\sigma_Z^2]^{-0.5} \int_{-\infty}^{0} e^{-\frac{(Z-\mu_Z)^2}{2\sigma_Z^2}}\, dZ \quad (1.12)$$

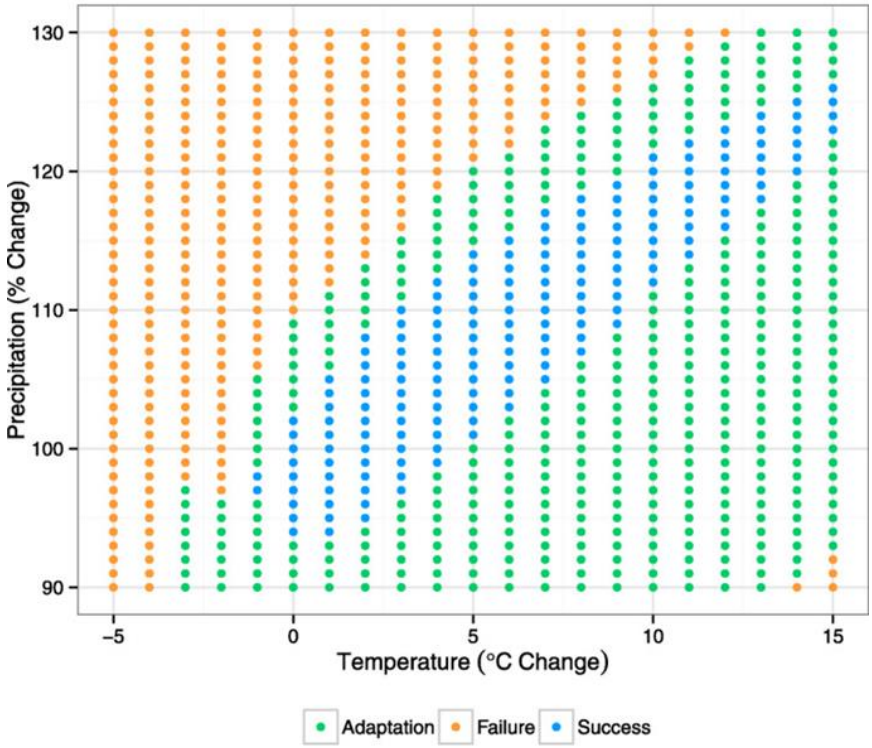

Figure 1.4: The operational adaptive capacity for Lake Como watershed for an adaptation strategy with C = 3.23 [Culley et al., 2016].

However, Zhang et al., (2018) defined the vulnerability as a three-parameter function: exposure, sensitivity, and adaptive capacity based on the conceptual model developed by Dong et al., (2015), as follows;

$$Vulnerability = \frac{Sensitivity \times ExposureDegree}{AdaptiveCapacity} \quad (1.13)$$

Here, Sensitivity is the degree to which the system influenced by climate change, Adaptive Capacity is the capability of a system absorb or recover from the effects, and Exposure Degree is the presence of people and infrastructure in the place of being affected. These are computed as follows;

$$Sensitivity = 1 + \frac{WA_{c,max} - WA_{c,min}}{WA_{T,impacted}} \quad (1.14)$$

$$Adaptive\ Capacity = \frac{WA_{T,impacted} \mp WT}{WA_{T,impacted}} \quad (1.15)$$

$$Exposure\ Degree = \frac{1}{2} \times \left(\sqrt{\frac{PD}{PD_0}} + \sqrt{\frac{GDP_P}{GDP_{P,0}}} \right) \quad (1.16)$$

Where, WA is the water availability, WA_T is the long-term average component of WA, WA_c is a fluctuating component affected by climatic factors, WA_t is the volume of water availability at year t, $WA_{c,t}$ is climate affected water availability at period t, WA is the volume of water transferred into or out of the region, and GPD is population density (PD) per capita. The runoff series is divided into two periods: natural period ($WA_{T,\mathrm{natural}}$) and impacted period ($WA_{T,\mathrm{impacted}}$). The donor region was set (an average of region 1 and 2) by using population density (PD_0) and per capita GDP ($GPD_{P,0}$) as benchmarks to facilitate a comprehensive comparison among all regions.

Tuner et al., (2019) proposed Bayesian Networks Decision Scaling to examine the water resources system or investment plans across the pre-specified set of environmental, demographic, and financial uncertainties.

It can be concluded from those studies, in essence, that there is still a need for other indicators regarding the optimal time to start applying the adaptation(s). i.e., besides specifying the robustness of the system or the vulnerability for a specific period. It is of utmost essential to compute the time when the system cannot exceed the minimum acceptance performance, then compare the adaptation strategies to cope the climate change effects on the system.

1.3. River Systems in Iraq

Iraq has two main rivers, the Tigris and Euphrates, and depends mainly on surface water for irrigation. There are about 120 irrigation projects in Iraq and about 15% of the land is irrigable. Any changes on water availability will have bad consequences on agricultural activities and the life quality of farmers. Therefore, the future of the water supply is a major concern for project developments upstream across the national border and climate change impacts [Waheed, 2013]. Table 1.1 illustrates the reduction in water amounts in the Euphrates and Tigris rivers. As seen, future water availability is subject to large reductions, which require new management strategies as a result of project developments in the upstream countries and climate change influences.

Table 1.1: Total annual amount of water in Tigers and Euphrates Rivers (MoWR, 2011; unpublished data)

	Duration	Total annual water	Remarks
Tigris River	1932 - 1998	49.2 billion m3	Natural streamflow
	1999 - 2010	33.1 billion m3	After dam construction in the upstream
Euphrates River	1932 - 1972	30.4 billion m3	Natural streamflow
	1973 - 1989	26.2 billion m3	After construction of Kipan dam in the upstream
	1990 - 2000	19.7 billion m3	After filling Ataturk dam
	2001 - 2010	12.8 billion m3	After building more dams in the upstream

The Diyala River is the third largest tributary of Tigris River in Iraq. It is a transboundary river between Iran and Iraq starts from the Zagros Mountains in Iran and crosses the Iran-Iraq border with a confluence with the Tigris River in south of Baghdad, as shown in Figure 1.5. The total river length is about 445 km with total watershed area of 32,600 km^2, of which 43% lies in Iraq. The basin is situated between 33.216° N and 35.833° N, and 44.500° E and 46.833° E. The main sub-tributaries of the river are the Sirwan, Tanjeru and Wand Rivers. Two large dams were built within the Iraqi part of the watershed: Derbendikhan and Hemrin [Hamza, 2012; Al-Faraj and Scholz, 2014; Al-Faraj et al., 2015; Abbas et al., 2016].

Only a few studies to investigate climate change impacts on the water availability in DRB were identified. Waheed, (2013) studied the effects of climate change on water availability for the period (1990-2010) using the Hydrologic Engineering Center's Hydrologic Modeling System (USACE-HEC, 1998). The analysis removed the trend in the weather variables, then compared the resultant runoff with the observed. The results showed an increment in the monthly evapotranspiration of 4% to 13%, and a decrement in the surface runoff of 4.7 %. Al-Faraj et al., (2014) examined the sensitivity of the runoff reduction due to climate change. The results showed a change in the median flow between +5.3% to -62.7% for the period (1983–2013), and -28.2% to -77.5% for (1999–2013) and -23.6% to -76.8% for (2004–2013), as a comparison with the period (1955–1982). Abbas et al., (2016) studied the climate impact and the Reconnaissance Drought Index using the Soil and Water Assessment Tool (SWAT) with different six GCM outputs (e.g., top-down approach). With comparison to the period between 1979 and 2004, the results showed a decrease of 56%, 50% and 39% under A2, A1B and B1, respectively; and an increase of 14% under A2 and A1B scenarios. Al-Khafaji and Al-Chalabi, (2019) studied the impact of climate

change on the streamflow and sediment yield with aid of SWAT for the period until 2050 of five GCM scenarios. Results showed a decrease in average monthly streamflow up to 49% as compared with the historic period 1948 to 2013. Neither Abbas et al., 2016 nor Al-Khafaji and Al-Chalabi, 2019 studied or removed the bias in the GCM scenarios, which can explain the huge decrease in the future water availability.

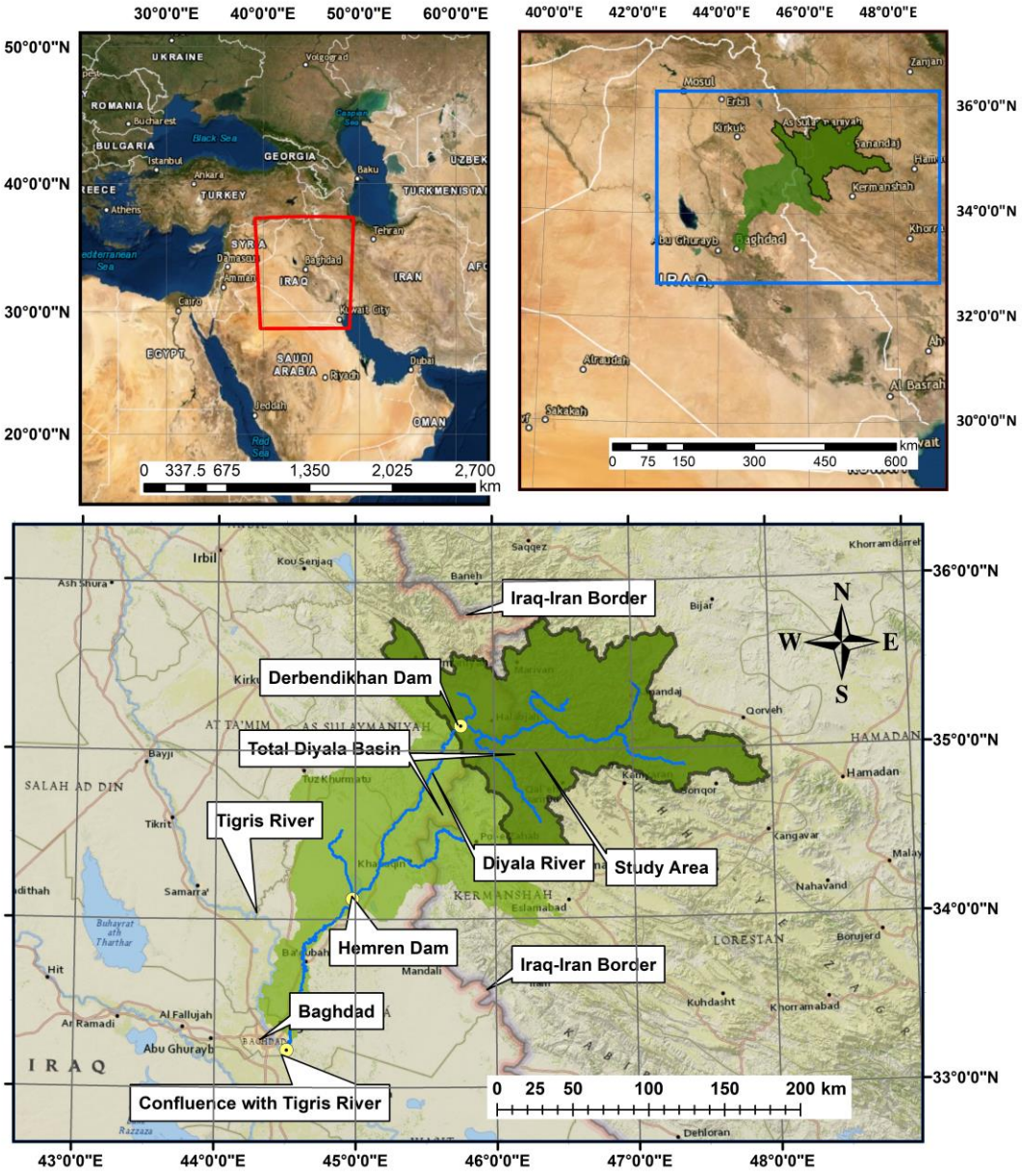

Figure 1.5: Location of the study area in Iraq.

Al-Jawad et al., (2019a) developed and applied a comprehensive optimal operation technique for a multiple-objective function. The methodology was applied for the historic period from 1981 and 2013 and projected two future scenarios by including the trends in the last seven years and the entire 33 years period. Although their results show improvement in the dam operation using the proposed model to decrease water deficit and recommended guidance to cope with it, the authors did not provide a framework to compare different plans to overcome the climate change impact.

It can be inferred from the above studies that a more comprehensive study using a bottom-up approach is required to evaluate the climate change impacts as well as a comparison of different adaptation scenarios to examine the most promising plan. In addition, more analysis is needed to examine the most probable future scenarios that may occur to help the decision makers to determine the desirable adaptation strategy. However, one of the most significant issues the researchers encountered in Iraq is data limitation to apply the bottom-up approaches. Therefore, the major part of this study is to overcome the data scarcity issues in Iraq and suggest valid hydrology models and SWG to make the bottom-up approach applicable. Then, the bottom-up framework will have more features to examine climate change impact in both timing and magnitude, identify optimal timeframe of the robust plan(s), and evaluate the impact of wind speed change and variation on the system performance.

1.4. Identified Issues and the Research Contributions

1) There is a limitation in the Historic daily forcing data availability, they are often missing in the basin. Therefore, two data sources were used to augment the ground observations of MoWR and obtain complete daily forcing data. These were the Tropical

Rainfall Measuring Mission (TRMM) data and Global Implemented Data (GIDAL) [Adam and Lettenmaier, 2003 and Adam et al., 2006]. A framework was suggested to provide complete and accurate daily forcing data in Iraq to make facilitate decision-making studies. This produced the first complete daily forcing dataset for DRB using different sources and is the first study in Iraq to identify the applicability of the hydrology model by uncertainty analysis of the model parameters and to build a valid-calibrated model to generate synthetic future scenario supply.

2) There is a need for a more functional and adaptable SWG to conserve spatial, cross, and temporal correlation as well as independence of the observational record length, since the developed weather estimates are not applicable in areas with limited data availability. The projected forcing data length is limited to the historic length and inability to preserve correlations among the forcing data. A SWG for the bottom-up approach was developed that is capable of conserving all correlations and is independent of the historic record length. It is easy to alter statistical parameters and the frequency distribution function of the forcing data can be changed so that it can be used according to the scope of the study as well as the data availability.

3) It is required to develop new approaches to examine the climate change impact in both timing and magnitude and suggest the most promising (robust) plan to cope with the negative impacts, as well as the optimal time of applying the best plan. These were achieved by developing a framework with new techniques and performance indicators under the probabilistic and non-stationary assumptions. The impact of wind speed change and variation were also examined on the decision-making studies since they

were not considered previously. The study represented the first attempt to provide a time frame to apply the robust adaptation plan, beside comparing the plan effectiveness for long-term, so as to avert the negative climate change influence. Also, this is considered as the first study to develop and apply a framework that utilizes the bottom-up approach in DRB and in Iraq. Moreover, the novelty of the developed framework is the consideration of the non-stationary assumption in simulating the future water supply, demand, and system losses' scenarios.

1.5. Organization of the Dissertation

The main part of the dissertation is organized in four chapters. CHAPTER 1 discusses the background and objectives of the study. CHAPTER 2 reports construction of a hydrology model through preparation of datasets and studying the model sensitivity and parameter uncertainty of the hydrology model. CHAPTER 3 develops a SWG, that is capable to preserve the observed statistical properties and to assess climate change impacts on water resources systems for cases of limited data availability. CHAPTER 4 suggests a bottom-up decision-making framework under nonstationary hydroclimatic conditions to evaluate the long-term water resources system rules for multi-objective purposes. CHAPTER 5 presents the overall conclusions of the study and recommendations for future work.

References

Abbas, Nahla, Saleh A. Wasimi, and Nadhir Al-Ansari. "Impacts of Climate Change on Water Resources in Diyala River Basin, Iraq." Journal of Civil Engineering and Architecture 10.9 (2016): 1059-1074.

Adam, Jennifer C., Elizabeth A. Clark, Dennis P. Lettenmaier, and Eric F. Wood. "Correction of global precipitation products for orographic effects." Journal of Climate 19.1 (2006): 15-38.

Adam, Jennifer C., and Dennis P. Lettenmaier. "Adjustment of global gridded precipitation for systematic bias." Journal of Geophysical Research: Atmospheres 108.D9 (2003).

Al-Faraj, Furat AM, and Miklas Scholz. "Assessment of temporal hydrologic anomalies coupled with drought impact for a transboundary river flow regime: the Diyala watershed case study." Journal of hydrology 517 (2014): 64-73.

Al-Faraj, Furat AM, Miklas Scholz, and Dimitris Tigkas. "Sensitivity of surface runoff to drought and climate change: Application for shared river basins." Water 6.10 (2014): 3033-3048.

Al-Jawad, Jafar Y., Hassan M. Alsaffar, Douglas Bertram, and Robert M. Kalin. "A comprehensive optimum integrated water resources management approach for multidisciplinary water resources management problems." Journal of environmental management 239 (2019): 211-224.

Al-Khafaji, Mahmoud S., and Rana D. Al-Chalabi. "Assessment and Mitigation of Streamflow and Sediment Yield under Climate Change Conditions in Diyala River Basin, Iraq." Hydrology 6.3 (2019): 63.

Azhoni, Adani, Simon Jude, and Ian Holman. "Adapting to climate change by water management organisations: Enablers and barriers." Journal of Hydrology (2018).

Beven, Keith, and Andrew Binley. "The future of distributed models: model calibration and uncertainty prediction." Hydrological processes 6.3 (1992): 279-298.

Brown, Casey, and Robert L. Wilby. "An alternate approach to assessing climate risks." Eos, Transactions American Geophysical Union 93.41 (2012): 401-402.

Culley, Sam, S. Noble, A. Yates, M. Timbs, S. Westra, H. R. Maier, Matteo Giuliani, and Andrea Castelletti. "A bottom-up approach to identifying the maximum operational adaptive capacity of water resource systems to a changing climate." Water Resources Research 52.9 (2016): 6751-6768.

Foti, Romano, Jorge A. Ramirez, and Thomas C. Brown. "A probabilistic framework for assessing vulnerability to climate variability and change: the case of the US water supply system." Climatic change 125.3-4 (2014): 413-427.

Hallegatte, Stéphane, Ankur Shah, Robert Lempert, Casey Brown, and Stuart Gill. "Investment decision making under deep uncertainty." Policy research working paper 6193 (2012): 1-41.

Hamza, Nahida H. "Evaluation of water quality of Diyala River for irrigation purposes." Diyala Journal of Engineering Sciences 5.2 (2012): 82-98.

Kundzewicz, Zbigniew W., L. J. Mata, Nigel William Arnell, P. Döll, B. Jimenez, K. Miller, T. Oki, Z. Şen, and I. Shiklomanov. "The implications of projected climate change for freshwater resources and their management." (2008): 3-10.

Moody, Paul, and Casey Brown. "Robustness indicators for evaluation under climate change: Application to the upper Great Lakes." Water Resources Research 49.6 (2013): 3576-3588.

Spence, Caitlin M., and Casey M. Brown. "Nonstationary decision model for flood risk decision scaling." Water Resources Research 52.11 (2016): 8650-8667.

Steinschneider, Scott, Sungwook Wi, and Casey Brown. "The integrated effects of climate and hydrologic uncertainty on future flood risk assessments." Hydrological Processes 29.12 (2015a): 2823-2839.

Steinschneider, Scott, Rachel McCrary, Sungwook Wi, Kevin Mulligan, Linda O. Mearns, and Casey Brown. "Expanded decision-scaling framework to select robust long-term water-system plans under hydroclimatic uncertainties." Journal of Water Resources Planning and Management 141.11 (2015b): 04015023.

Stephenson, David B., Matthew Collins, Jonathan C. Rougier, and Richard E. Chandler. "Statistical problems in the probabilistic prediction of climate change." Environmetrics23.5 (2012): 364-372.

Taner, Mehmet Ümit, Patrick Ray, and Casey Brown. "Robustness-based evaluation of hydropower infrastructure design under climate change." Climate Risk Management 18 (2017): 34-50.

Taner, Mehmet Ümit, Patrick Ray, and Casey Brown. "Incorporating Multidimensional Probabilistic Information Into Robustness-Based Water Systems Planning." Water Resources Research (2019).

Turner, Sean WD, David Marlow, Marie Ekström, Bruce G. Rhodes, Udaya Kularathna, and Paul J. Jeffrey. "Linking climate projections to performance: A yield-based decision scaling assessment of a large urban water resources system." Water Resources Research 50.4 (2014): 3553-3567.

Van Tra, Tran, Nguyen Xuan Thinh, and Stefan Greiving. "Combined top-down and bottom-up climate change impact assessment for the hydrological system in the Vu Gia-Thu Bon River Basin." Science of The Total Environment 630 (2018): 718-727.

Vrugt, Jasper A., Cajo JF Ter Braak, Hoshin V. Gupta, and Bruce A. Robinson. "Equifinality of formal (DREAM) and informal (GLUE) Bayesian approaches in hydrologic modeling?." Stochastic environmental research and risk assessment 23.7 (2009a): 1011-1026.

Vrugt, Jasper A., C. J. F. Ter Braak, C. G. H. Diks, Bruce A. Robinson, James M. Hyman, and Dave Higdon. "Accelerating Markov chain Monte Carlo simulation by differential evolution with self-adaptive randomized subspace sampling." International Journal of Nonlinear Sciences and Numerical Simulation 10.3 (2009b): 273-290.

Vrugt, Jasper A. "Markov chain Monte Carlo simulation using the DREAM software package: Theory, concepts, and MATLAB implementation." Environmental Modelling & Software 75 (2016): 273-316.

Waheed, Saddam Q. 2013. ”Effects of climate change on water availability in Diyala basin in Iraq”, 2nd International Conference on Hydrology & Groundwater Expo. NC, USA

Weaver, Christopher P., Robert J. Lempert, Casey Brown, John A. Hall, David Revell, and Daniel Sarewitz. "Improving the contribution of climate model information to decision making: the value and demands of robust decision frameworks." Wiley Interdisciplinary Reviews: Climate Change 4.1 (2013): 39-60.

Whateley, Sarah, Scott Steinschneider, and Casey Brown. "A climate change range-based method for estimating robustness for water resources supply." Water Resources Research 50.11 (2014): 8944-8961.

Wilby, Robert L., and Suraje Dessai. "Robust adaptation to climate change." Weather 65.7 (2010): 180-185.

Zhang, Enze, et al. "Bottom-up quantification of inter-basin water transfer vulnerability to climate change." Ecological Indicators 92 (2018): 195-206.

CHAPTER 2

Variable Infiltration Capacity Model Sensitivity, Parameter Uncertainty, and Data Augmentation for the Diyala River Basin in Iraq[1]

Chapter Synopsis

construct a valid model, hydrologists face challenges in determining sensitivity to the forcing data and the uncertainty of model parameters. These require basin data and forcing data from different sources, which may be incommensurate. The study reported here calibrated the Variable Infiltration Capacity (VIC) platform to quantify sensitivity of model results to model parameters and the uncertainty of the parameters. The modeled basin was the Diyala River in Iraq, above the Derbendikhan Dam. The study produced the first complete set of daily forcing data for the study basin using different sources. Besides ground observations from the Iraqi Ministry of Water Resources, two additional data sources were tested: Tropical Rainfall Measurement Mission (TRMM) and the Global Implemented Data (GIDAL). Several methods were implemented to adjust the data, and the model sensitivity and parameter uncertainty were examined by the Generalized Likelihood Uncertainty Estimation (GLUE) and the Differential Evolution Adaptive Metropolis (DREAM) techniques. Neither of these techniques has been applied before in Iraq. Then, the VIC model was calibrated manually using Kling–Gupta efficiency (KGE). The analyses indicate that neither TRMM nor GIDAL data are adequate for gridded precipitation analysis in the study basin. TRMM tends to underestimate and GIDAL tends to

[1] Published in American Society of Civil Engineers, Journal of Hydrologic Engineering Saddam Q. Waheed, Neil S. Grigg, Jorge A. Ramirez, (2020). DOI 10.1061/(ASCE)HE.1943-5584.0001975

overestimate actual data. The multiplicative random cascade and Schaake Shuffle methods were used to determine daily precipitation data. A set of correction equations was developed to adjust GIDAL temperature and wind speed. Results of the GLUE and DREAM analyses imply that the depth of the second soil layer is the parameter that causes most sensitivity in the model. The VIC model outputs were calibrated on a daily time scale with KGE average of 0.743.

2.1. Introduction

To obtain reliable information for planning and management of water resources systems under climate change, hydrologic models are needed to simulate the rainfall-runoff relationship [Pradhan and Indu, 2019]. These require valid basin and forcing data and knowledge about model sensitivity to and uncertainty of its parameters. This study built and calibrated a hydrologic model to generate streamflow time series to examine climate change impact on future reservoir operation and management, in a follow up paper. Forcing data considered were precipitation, temperature, and wind speed, and soils and vegetation data comprised the basin data, in addition to topographic parameters.

In some countries, data are scarce and must be augmented. This study addresses data and modeling issues in Iraq where data are scarce. The study site is the Diyala River Basin (DRB), a tributary of the Tigris River in eastern Iraq with upstream length and basin area about 216 km and 16,764 km^2, respectively. The in situ forcing data were obtained from the Iraqi Ministry of Water Resources (MoWR). These were augmented by data from: 1) the Tropical Rainfall Measuring Mission (TRMM) and 2) the Global Implemented Data (GIDAL) [Adam and Lettenmaier, 2003 and Adam et al., 2006]. The validity and applicability of these two datasets

were tested by comparing them with the in situ in the DRB. The study produced the first complete daily forcing dataset for DRB using different sources.

Besides the forcing data, the parameter sensitivity and model output uncertainty are essential to assess the model applicability in the region. Ignoring them in the calibration process will lead to non-unique parameter estimates, a problem known as Equifinality, which makes identifying the optimal model parameter sets impossible [e.g., Beven, 2006]. In addition, the parameter sensitivity and model uncertainty should be determined in any basin before starting the calibration process, especially in studying climate change impacts [Surfleet et al., 2012] as this will provide useful information regarding system responses and relationships among model parameters [Vrugt and Bouten, 2002; Benke et al., 2008; Liu, 2019].

With this in mind, this study also examines the model sensitivity and parameter uncertainty of the Variable Infiltration Capacity (VIC) model version 4.2 in the DRB. VIC is a physically based model that has been used in a number of river basins. The approaches used in this study to address the sensitivity and uncertainty are the Generalized Likelihood Uncertainty Estimation (GLUE) proposed by Beven and Binley, (1992) and the Differential Evolution Adaptive Metropolis (DREAM) [e.g., Vrugt et al., 2009a; Vrugt et al., 2009b; and Vrugt, 2016]. Neither GLUE nor DREAM has been applied before in any region inside Iraq.

2.2. Literature Review

Hydrologic modeling to simulate real world systems has been a major concern for water resource system planning and management in recent years. Even though the actual processes are more complex than model representations, predictive capabilities can be improved through calibration to find optimal model parameters for the best fit between simulated and observed

characteristics. [Guo et al., 2014; Yen et al., 2019]. Typically, model parameters obtained from observations may not require calibration [Choi et al., 2014], but with the limited soil and vegetation information in the DRB, it is necessary. Usually, model outputs are calibrated with observed discharges at basin outlets [Xue et al., 2015]. In all cases, study of model sensitivity and parameter uncertainty is of importance paramount to avoid biased results in the predictions especially for climate change impact analysis [e.g., Surfleet et al., 2012; Yen et al., 2014].

Most hydrologic models incorporate many parameters to characterize hydrological processes. These are measured or estimated from watershed characteristics [e.g., Montanari and Young, 2013; Sood and Smakhtin, 2015; Guse et al., 2017; Patnaik et al., 2019]. Measuring all parameters is practically infeasible, so they are usually estimated through the calibration process [Abbaspour and Rouholahnejad, 2015; Shafii et al., 2015; Pagliero et al., 2019].

Model studies in the DRB using the Soil and Water Assessment Tool (SWAT) with data by the Climate Forecast System Reanalysis (CFSR) have been reported by Abbas et al., (2016), Alwan et al., (2018), Al-Khafaji and Al-Chalabi, (2019). Among them, only Al-Khafaji and Al-Chalabi, (2019) examined the reliability of CFSR precipitation data in one station in DRB, but this cannot indicate data applicability in the region for other data such as temperature and wind speed. No studies of constructing the VIC model have been identified. Many studies have used TRMM and GIDAL data for other regions and purposes [e.g., Chen et al., 2012; Duan et al., 2012; Nastos et al., 2013; Moazami et al., 2014; Maggioni et al., 2016; Tarek et al., 2017; Medhioub et al., 2019; Song et al., 2019] but none have studied their applicability in Iraq.

TRMM provides observation data of the tropical and subtropical regions of earth. It is managed by the U.S. National Aeronautics and Space Administration (NASA) and the Japan

Aerospace Exploration Agency. TRMM data are available on a daily time scale for the period between 2000 and 2015 with spatial resolution of 0.25^{o}. GIDAL, however, was implemented globally by Adam and Lettenmaier, (2003) and Adam et al., (2006) on a daily time scale for the period 1940 to 2007 on a gridded basis with spatial resolution of 0.5^{o}. The GIDAL dataset was developed by inverting generated runoff at 524 global stations into precipitation amounts using the water balance equation and considering climate data [maximum temperature, minimum temperature, and wind speed] obtained from the National Centers for Environmental Prediction and Climate Prediction Center [Adam and Lettenmaier, 2003]. For consistency purposes, these data are referred to as GIDAL.

The VIC model is a semi-distributed, physically based hydrology model that solves the water and surface energy balances in each grid cell [Gao et al., 2009]. The VIC model framework is described in studies such as Liang et al., (1994) and Liang et al., (1996). The reader should refer to Gao et al., (2009); NASA (2013); and Mehta and Markert (2018) for more details of VIC and an example of model set-up and running. Of interest for this study, VIC generates surface runoff and baseflow while accounting for vegetation heterogeneity in each grid cell, different soil layers with variable infiltration, land topography to capture the precipitation and temperature variation in relation to land elevation, coupled water and energy fluxes between the land surface and atmosphere, snow accumulation, melting and ablation, and non-linear base flow. In addition, a streamflow routing model, RVIC, [Lohmann et al., 1996; Lohmann et al., 1998] is used to route the runoff and base flow generated by VIC to the basin outlet based on the unit hydrograph convolution equation coupled with the linearized Saint Venant equations.

Only a few papers exist on the VIC parameter sensitivity and model uncertainty using the GLUE technique [e.g., Demaria et al., 2007; Sun and Yuan, 2013; He and Pang, 2014; Pang, et al., 2014], which is a widely technique [e.g., Quan et al., 2012]. Demaria et al., (2007) showed that VIC outputs are sensitive to the infiltration parameter (B_inf) in dry areas only, to the exponent of the Brooks-Corey drainage equation, and to the second soil layer depth. Sun and Yuan (2013) results indicated that the second soil layer depth are the most sensitive parameter followed by B_inf in Huaihe catchment in China using GLUE. He and Pang (2014) analyzed VIC parameter sensitivity using the GLUE method in the Heihe River Basin (HRB) in the Gansu Province of China. Results showed that the maximum velocity of baseflow or the fraction of the maximum soil moisture where non-linear baseflow occurs and first soil layer depth are the most sensitive parameters. Others including B_inf are not sensitive. Pang et al., (2014) studied the sensitivity using GLUE in Xitiaoxi catchment in China. Results showed that only B_inf and first soil layer depth are sensitive. From these studies, it is apparent that parameter sensitivity differs by region and climate.

In summary, the main objective of this study is to implement a validated and calibrated VIC model in DRB to be used for climate change assessment in a follow-up study. This main objective was achieved by (1) augmenting the forcing data using other data sources such as TRMM and GIDAL, and (2) examining the VIC model sensitivity and parameter uncertainty by GLUE and DREAM techniques.

2.3. Methodology

The Diyala River is a principal tributary of the Tigris River in Iraq. Two large dams are constructed within Iraq, Derbendikhan Dam and Hemrin Dam [Hamza, 2012; Abbas et al., 2016;

Al-Khafaji and Al-Chalabi, 2019]. The transboundary study-reach between Iran and Iraq is upstream of Derbendikhan Dam with a length of 217 km and area about 16,760 km^2, as shown in Figure 2.1. Derbendikhan Dam was constructed between 1956 and 1961 and is located about 285 km northeast of Baghdad (Coordinates 35.107^o N and 45.704^o E). The dam provides irrigation water, flood control, recreation, and hydroelectric power production [Tofiq and Guven, 2014]. Daily discharge data upstream of Derbendikhan Dam are available from 1960 until 2014.

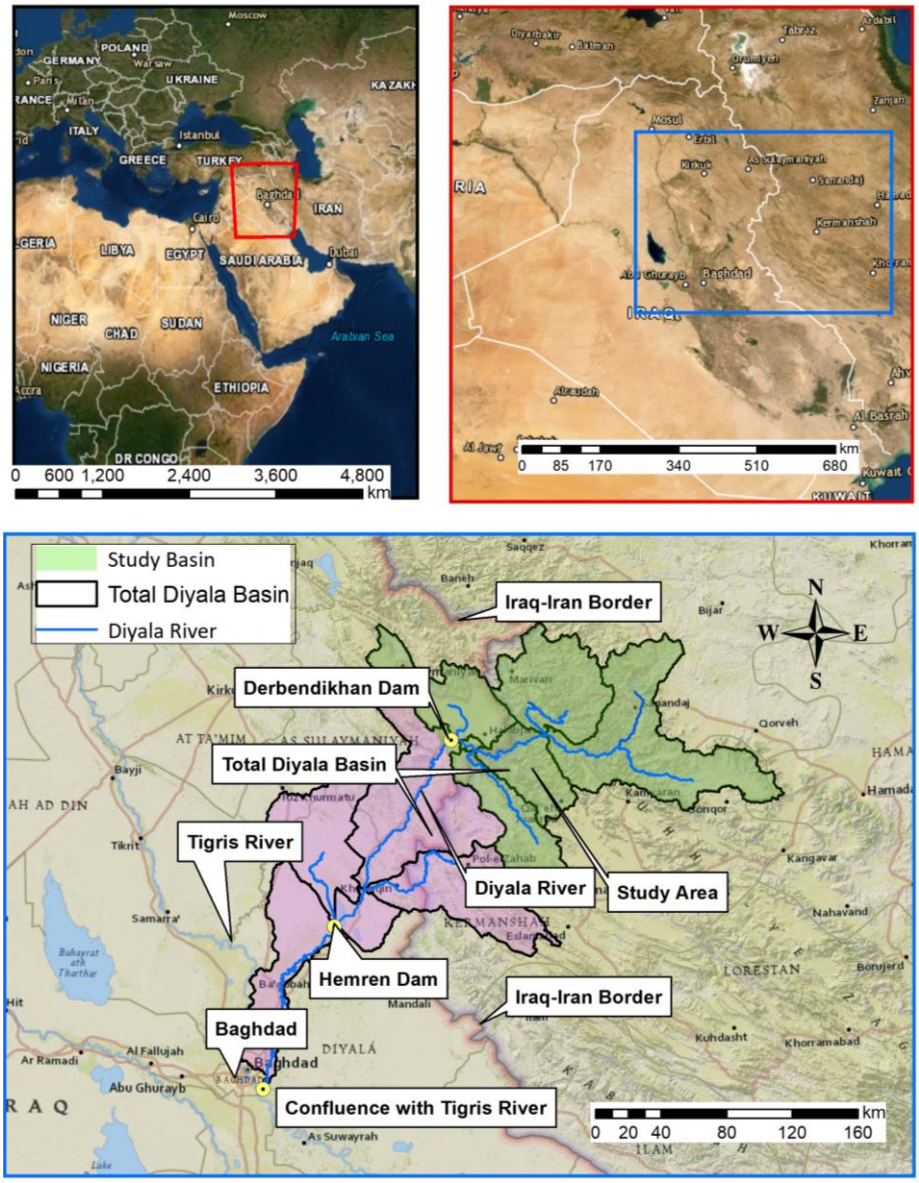

Figure 2.1: Location of Diyala River and its basin.

2.3.1. Data Preparation

The main basin data inputs for the VIC and RVIC models are topography, soils, and vegetation. Due to the limited measured basin data in the study area, and after validation as explained below, the soil and vegetation data used were obtained from studies by Nijssen et al., (2001a) and Nijssen et al., (2001b) with spatial resolution of 0.5°, referred to as NND. Forcing data are precipitation, temperature and wind speed. Station data from MoWR (D_{MWR}) are usually on a monthly time-scale (and some daily) ranging from 1940 to 2014 inside Iraq and some adjacent areas.

Study of the validation of TRMM and GIDAL was through comparing their monthly values with $D_{MWR.}$ Since TRMM and GIDAL are in gridded format, D_{MWR} was transformed into gridded format, hereafter referred to as G_{MWR}, using ordinary co-kriging with elevation as a secondary variable. Ordinary co-kriging is superior to other approaches such as Inverse Distance Weighting, Multi-Quadratic, ordinary kriging, and kriging with an external drift techniques [e.g., Ishida and Kawashima, 1992; Luo et al., 2007; Chahouki et al., 2014; Adhikary et al., 2017]. The metrics for validation were the Coefficient of Determination (R^2) and Kling–Gupta efficiency, KGE, [Gupta et al., 2009] as follows:

$$KGE = 1 - \sqrt{\left(\frac{\mu_{cal}}{\mu_{obs}} - 1\right)^2 + \left(\frac{\sigma_{cal}}{\sigma_{obs}} - 1\right)^2 + (\rho - 1)^2} \quad (2.1)$$

The parameters μ_{obs}, σ_{obs}, μ_{cal}, σ_{cal} are the mean and standard deviation of G_{MWR} and calculations (e.g., with other data sources GIDAL or TRMM), respectively. The variable ρ is the correlation coefficient between G_{MWR} and the calculations. KGE is considered superior to the Nash–Sutcliffe (1970) coefficient efficiency (NSCE) because it examines the bias of mean,

standard deviation, and correlation [Steinschneider et al., 2015]. If both of TRMM and GIDAL metric values are low (i.e., KGE < 0.5), the monthly D_{MWR} will be downscaled to daily using the micro-canonical version of the discrete multiplicative random cascade (MRC) [e.g., Gupta and Waymire, 1993; Over and Gupta, 1994; Over and Gupta, 1996]. The MRC preserves the rainfall mass exactly at all cascade levels and has few parameters [Molnar and Burlando, 2005]. The main idea of this method is to partition the variable (e.g., precipitation depth) at level-m into b=2 branches (j and j+1) depending on the probability of intermittency p_o, such that:

$$\bar{P}(\Delta_m^i) = r_o \prod_{j-1}^{m} W_j\,(i) \quad for\ i = 1,2,\ldots.\, b^m\,; m > 0 \tag{2.2}$$

Where $\Delta_{\mathrm{m}}^{\mathrm{i}}$ denote the i^{th} interval after m levels of sub-division, r_o is the initial monthly precipitation depth (in mm), and W_j is the cascade generator, which is a random variable distributed as a Beta distribution $W_j \sim (\alpha, \beta)$. To implement this method, the daily rainfall must be up-scaled with the same b and m parameters in order to verify the self-similarity of the data by calculating the moments of order 0.5 to 4 in each level [e.g., Molnar and Burlando, 2005; Kang and Ramirez, 2010]. In case no daily data is available at a D_{MWR} station, the MRC parameters are obtained from the nearest station(s).

The resultant daily values of MRC are randomly distributed in time. i.e., the highest precipitation may occur in the 5^{th} day while the actual timing is the 25^{th}. This randomness will affect the peak time and will misrepresent extreme events since high runoff discharge in one sub-basin can be offset by other low runoff discharge in the adjacent sub-basins [e.g., Li, 2014]. Therefore, we used a re-ordering technique called Schaake Shuffle, SS, [e.g., Clark et al., 2004; Vrac and Friederichs, 2015; Li and Babovic, 2018] to rank the downscaled precipitation values. SS

was chosen because it preserves the correlation structure between station pairs and between climate variables [e.g., Clark et al., 2004].

The ranking values for SS reference rank matrix, **R**, can be obtained from GIDAL. An illustration of applying SS is given here. Suppose that the GIDAL of four days and three grid cells of resolution 0.5° of the study area are as shown below. **R** is obtained by assigning ascending rank to the values of each column independently. Now suppose the gridded downscaled daily precipitation, GDP_{MWR}, of the same grid cells are given below. The ranked GDP_{MWR}, $RGDP_{MWR}$, was obtained by re-ordering the values corresponding ranks given in **R**, as shown below. Note that ranking values for days of no precipitation were assigned randomly to re-order the cases when the number of precipitation days are not equal in both GIDAL and GDP_{MWR}. In summary, the final forcing data for the analysis were obtained by (1) applying MRC and SS for D_{MWR} precipitation; and (2) developing sets of adjustments equations to implement temperature and wind speed data from GIDAL.

$$GIDAL = \begin{bmatrix} 0 & 0 & 5.5 \\ 14.8 & 12.8 & 7.3 \\ 0 & 0 & 0 \\ 10.2 & 0 & 9.8 \end{bmatrix}; \qquad \boldsymbol{R} = \begin{bmatrix} 2 & 3 & 2 \\ 4 & 4 & 3 \\ 1 & 2 & 1 \\ 3 & 1 & 4 \end{bmatrix}$$

$$GDP_{MWR} = \begin{bmatrix} 8.1 & 9.2 & 0 \\ 0 & 0 & 8.6 \\ 1.9 & 3.6 & 4.6 \\ 0 & 1.3 & 0 \end{bmatrix}; \quad RGDP_{MWR} = \begin{bmatrix} 0 & 3.6 & 0 \\ 8.1 & 9.2 & 4.6 \\ 0 & 1.3 & 0 \\ 1.9 & 0 & 8.6 \end{bmatrix}$$

2.3.2. Model Sensitivity and Parameter Uncertainty

these data preparation techniques, the sensitivity of VIC parameters and the output uncertainty can be tested. GLUE and DREAM techniques were implemented for seven of VIC model parameters as shown in Table 2.1, by following the suggestions of Demaria et al., (2007), He and Pang, (2014), and Pradhan and Indu, (2019). The GLUE steps are [see Figure 2.2]:

1- Draw a sample of points Θ of size N (2000 sets in this study) using the specified prior distribution, *p(θ)*, depending on the feasible range of each parameter (ζ), as shown in Table 2.1**.** Given that *p(θ)* are unknown, they are assumed as uniform distributions.

2- Calculate the likelihood $L_i = L(\theta_i | Q_t, \bar{Q}_t, \zeta)$ to test the VIC model performance of each parameter set θ^i, i=1,2, …. 2000. Where Q_t and $\bar{Q}_t$ are the observed and calculated streamflow for the time index t in day. In this study, the likelihood was computed using KGE as defined in equation (2.1).

3- Define a threshold value c (e.g., KGE =0), discard all $L_i < c$ and retain the rest of size k as k ≤ n. L_k were then normalized to construct the posterior CDFs, in which $\sum_1^k L(\theta^k \mid Q_t,\ \bar{Q}_t, \zeta) = 1$, and the posterior distribution was calculated as $h(\theta^k) = L(\theta^k \mid Q_t,\ \bar{Q}_t, \zeta) / \sum_1^k L(\theta^k \mid Q_t,\ \bar{Q}_t, \zeta)$.

4- Interpret the results from the shape of $h(\theta^k)$. That is, if $h(\theta^k)$ differs little from the $p(\theta^k)$, the parameter is considered to have a small sensitivity. If it is quite different, then the parameter is considered as highly sensitive. Otherwise, the parameter is non-sensitive [e.g., Beven and Freer, 2001; Sun et al., 2012].

Because no clear approach to differentiate between categories of parameter sensitivity is available, for this study a metric of parameter sensitivity was chosen that compares the quantiles of $h(\theta^k)$ and $p(\theta^k)$. The criteria are for a difference is more than 10% but less than 25%, the parameter is considered as low sensitive; if more than 25%, it is high sensitive; otherwise the parameter is insensitive. Afterwards, the model prediction uncertainty intervals of VIC are given by the median of $h(\theta^k)$ and the 5 and 95% prediction quantiles [Vrugt et al., 2009].

Vrugt et al., (2009a), Vrugt et al., (2009b), and Vrugt, (2016) argued that the residual of the GLUE technique does not account for the error structure using the posterior distribution conditional on the model behavior (i.e., the analysis of GLUE may not distinguish the parameter distribution other than uniform distribution). Therefore, they developed a new technique, DREAM, using Bayesian inference to evaluate the differences between the calculated and corresponding observed streamflow, following the steps of GLUE. With the assumption that the residuals are uncorrelated and normally distributed, the likelihood function (alternative to KGE) for the model performance is:

$$L = \prod_{t=1}^{n} \frac{1}{\sqrt{2\,\pi\,\sigma_t^2}} exp\ [-\frac{1}{2}\left(\frac{\bar{Q}_t - Q_t}{\sigma_t^2}\right)^2] \quad (2.3)$$

Table 2.1: Description and range of VIC model parameters used in the calibration and uncertainty processes.

Parameter	Unit	Description	Limits
B_inf	-	Controlling factor of the variable infiltration curve	0.4 - 0.001
D_{smax}	mm/hr	Maximum velocity of baseflow for each grid cell	30 - 0.001
D_s	-	Fraction of D_{smax} at which non-linear baseflow takes place	2 - 0.001
W_s	-	Maximum soil moisture fraction where non-linear baseflow occurs	2 - 0.001
Depths	M	Depth of the three soil layers (e.g., first, second, and third)	2 - 0.001

Where σ_t is the standard deviation vector of observed streamflow error. A further development for equation (2.3) was done by including the correlation of the residual and applying auto-regressive model of order 1, AR (1); the log-likelihood function of DREAM technique becomes,

$$L = -\frac{n}{2}log(2\pi) + \frac{1}{2}log(1-\Phi^2) - \frac{1}{2}(1-\Phi^2)\,\sigma_1^2\,\varepsilon_1^2 - \sum_{t=2}^{n} log\,\sigma_t - \frac{1}{2}\sum_{t=2}^{n}\left[\frac{\varepsilon_t - \Phi\,\varepsilon_{t-1}}{\sigma_\varepsilon}\right]^2 \quad (2.4)$$

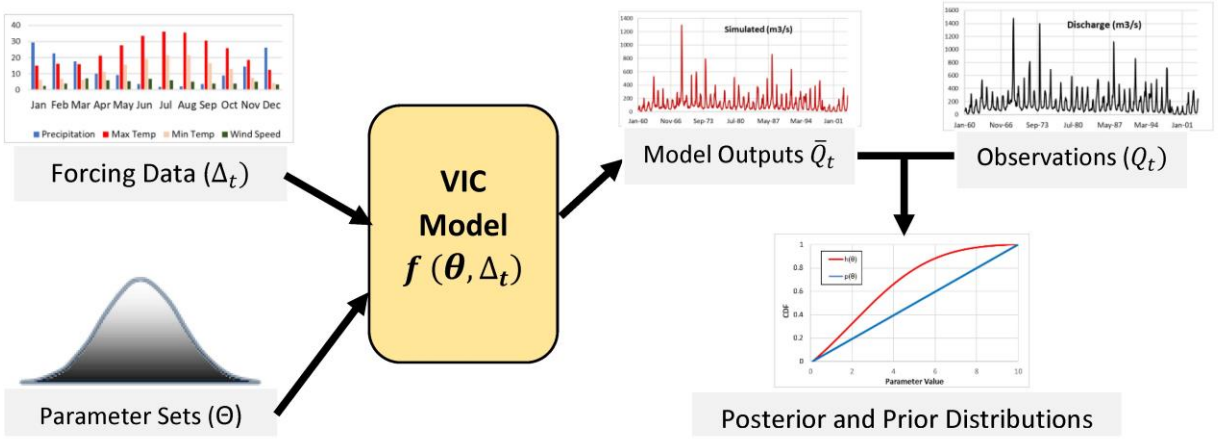

Figure 2.2: Steps in GLUE and DREAM procedures.

2.3.3. Model Calibration Process

Given the condition that direct measurement of all VIC model parameters is not always possible especially in DRB, those parameters shown in Table 2.1 were estimated by the calibration process for the best fit of model outcomes to the observed behavior. The calibrated model is then deemed applicable for simulating periods outside of the used historical record [e.g., Vrugt et al., 2009a]. The calibration process was performed manually using a two-stage process: 1) performance assessment and 2) residual term evaluation. In the first stage, the allowable simulation period was divided into two equal parts, while the first two years were set as a warm-up period to minimize the effect of uncertain initial conditions [e.g., Pang et al., 2014; Xue et al., 2015]. The objective function of the first stage was set to maximize the model performance in these two periods using KGE. The second stage was to examine the model residuals using the procedure proposed by Schoups and Vrugt, (2010), Evin et al., (2013), and Evin et al., (2014), as

explained below. The streamflow observations $Q_{(t)}$ can be expressed as a function of the calculated streamflow $\bar{Q}_{(t)}$ and the residuals, $\epsilon_{(t)}$, as follows:

$$Q_t = \bar{Q}_t\,(\theta, \Delta_t) + \epsilon_{(t)} \tag{2.5}$$

where Δ_t represents forcing data. The standardized residuals, referred to as innovations $\delta_{(t)}$, should be zero-mean, uncorrelated, homoscedastic, and normally distributed, and can be determined using the following system:

$$\eta_{\epsilon(t)} = \epsilon_{(t)} \,/\, \sigma_{\varepsilon(t)} \tag{2.6}$$

$$\sigma_{(t)} = \gamma_o\, \bar{Q}_{(t)} + \gamma_1 \tag{2.7}$$

$$\eta_{\epsilon(t)} = \Phi\, \eta_{e(t-1)} + \delta_{(t)} \tag{2.8}$$

where Δ_t represents forcing data. The standardized residuals, referred to as innovations $\delta_{(t)}$, should be zero-mean, uncorrelated, homoscedastic, and normally distributed, and can be determined using the following system.

2.4. Results and Discussion

2.4.1. Precipitation Data Implementation

A comparison of G_{MWR} against the other data sources (GIDAL and TRMM) is made, as shown in Figure 2.3 (b), (c), (d), and (f) for grids number 9 and 10 since they are located in the heart of the basin. A 1-1 line was also plotted to ease the comparison. The grid-cells were numbered consecutively for grid-cells located inside the basin, and continued for those located outside, as shown in Figure 2.3 (a). GIDAL overestimates both the precipitation amount and its variation while TRMM underestimates them. In addition, R^2 and KGE for GIDAL and TRMM are 0.618, 0.264, 0.219, and -0.227, respectively which are low. Adam et al., (2006) explained that in

some areas, such as the Middle East, where insufficient information was available to the authors to develop GIDAL, precipitation was estimated using the information from the adjacent regions which caused inadequate estimation. As for TRMM, our results are in line with Duan et al., (2012) and Medhioub et al., (2019) that TRMM data tends to underestimate the monthly ground precipitation in some areas due to the high influence of orographic and climatic properties of the region and suggest an adjustment for TRMM data.

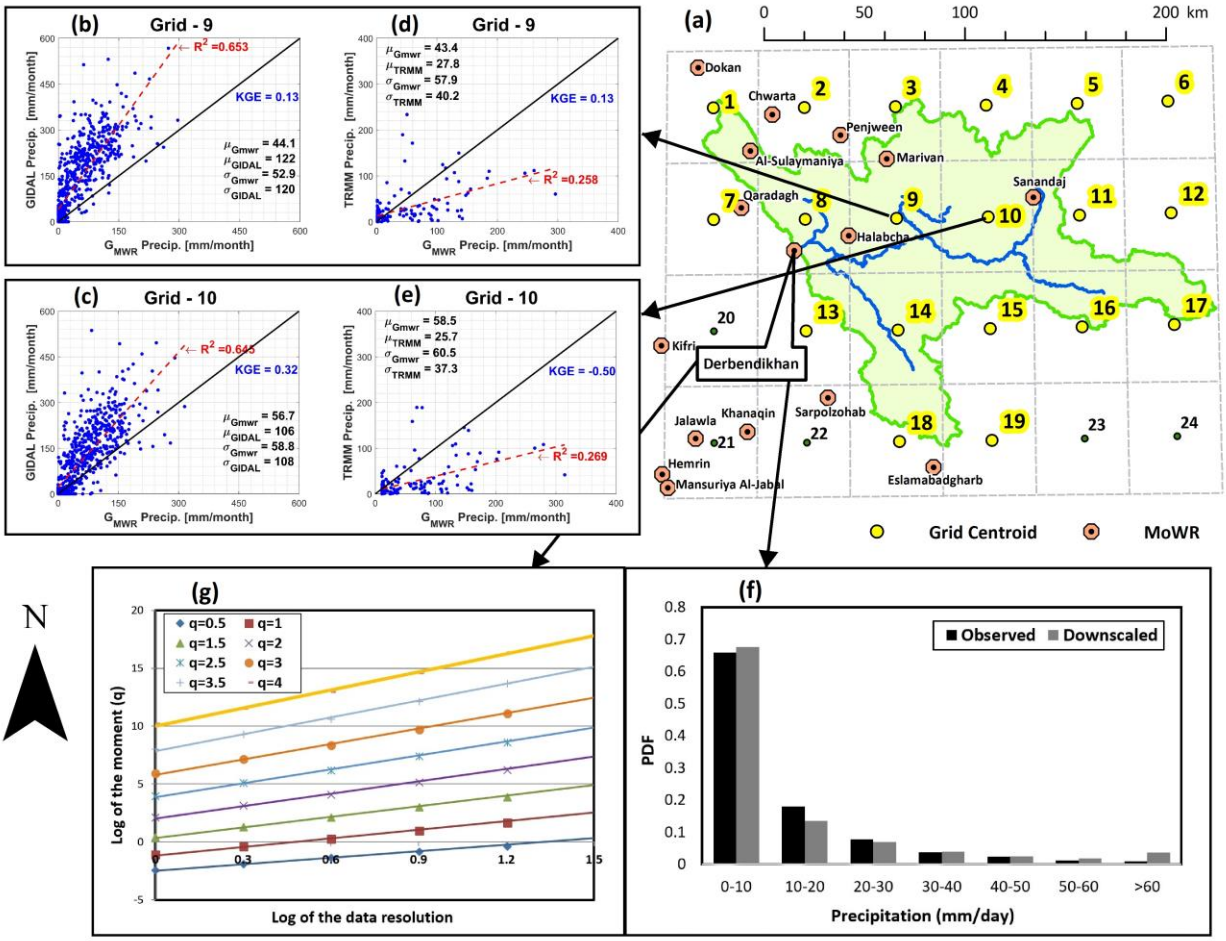

Figure 2.3: (a) MoWR stations and GIDAL grid centroids in DRB. (b), (c), (d), and (e) G_{MWR} precipitation versus GIDAL and TRMM for grids 9 and 10. (f) Histogram comparison of the observed and downscaled, and (g) the moment scaling of observed precipitation data at Derbendikhan station.

Therefore, in order to develop daily precipitation data for DRB in this study, MRC was used to downscale D_{MWR} into daily data, DD_{MWR}. The D_{MWR} in Derbendikhan station was tested

for self-similarity, where the data completeness is 96.6%, and compared the histograms of original daily D_{MWR} with DD_{MWR} by calculating R^2 [0.936], as shown in Figure 2.3 (f) and (g), respectively. The result obtained here is superior to that of Al-Khafaji and Al-Chalabi, (2019) for Khanaqeen gauge station for the period 1984 to 2002 [e.g., R^2 = 0.705]. Afterwards, co-kriging and SS were used to obtain $RGDP_{MWR}$, where **R** matrix is obtained from GIDAL due to its better performance than TRMM (e.g., higher KGE value) and longer coverage years.

2.4.2. Temperature and Wind Speed Data Implementation

Since GIDAL was used partially in implementing precipitation data, it was evaluated to implement temperature and wind speed data. The MoWR ground-stations are shown in Figure 2.4 (a). G_{MWR} temperatures were compared to the GIDAL dataset, as shown in Figure 2.4. (b) and (c) for grids number 9 and 10, and a regression line between G_{MWR} and GIDAL was plotted. It is seen that G_{MWR} and GIDAL are well correlated; but they do not lie on a 1-1 line. Therefore, GIDAL was adjusted to be on a 1:1 line where the adjusted GIDAL and G_{MWR} are nearly the same. However, the coefficients of linear regression (κ_0 and κ_1 as shown in equation (2.9)] between G_{MWR} and GIDAL were plotted against the average grid elevation (Elev), as shown in Figure 2.4 (d) and (e)), which suggest a relationship between κ_1 and Elev, while the relationship between κ_0 and Elev is not as strong and its range is very small (e.g., between 1.02 and 0.98). Therefore, including it in the correction procedure is not very important. A general regression equation to adjust the GIDAL temperature was developed, as follows. Let Y be the raw GIDAL data and X be G_{MWR}, the regression equation is:

$$Y = \kappa_o X + \kappa_1 \quad (2.9)$$

In order to make the relationship Y=X (a perfect relationship), Y was subtracted by κ_1 and divided by κ_0. Letting Y be the T_{GIDAL} and X be the T_{adj}, the relationship becomes;

$$T_{adj} = (T_{GIDAL} - \kappa_1) / \kappa_0 \quad (2.10)$$

$$\kappa_o = 2 \times 10^{-6} Elev + 1.002 \quad (2.11)$$

$$\kappa_1 = -0.002 Elev - 0.921 \quad (2.12)$$

Where, T_{adj} and T_{GIDAL} are the adjusted and raw GIDAL temperatures (C^o), respectively. Again, the range of κ_0 values is very small [1.02-0.98], thus κ_0=1 was assumed. The KGE values for T_{GIDAL} and T_{adj} are 0.73 and 0.97, respectively, as shown in Figure 2.4 (b) and (c).

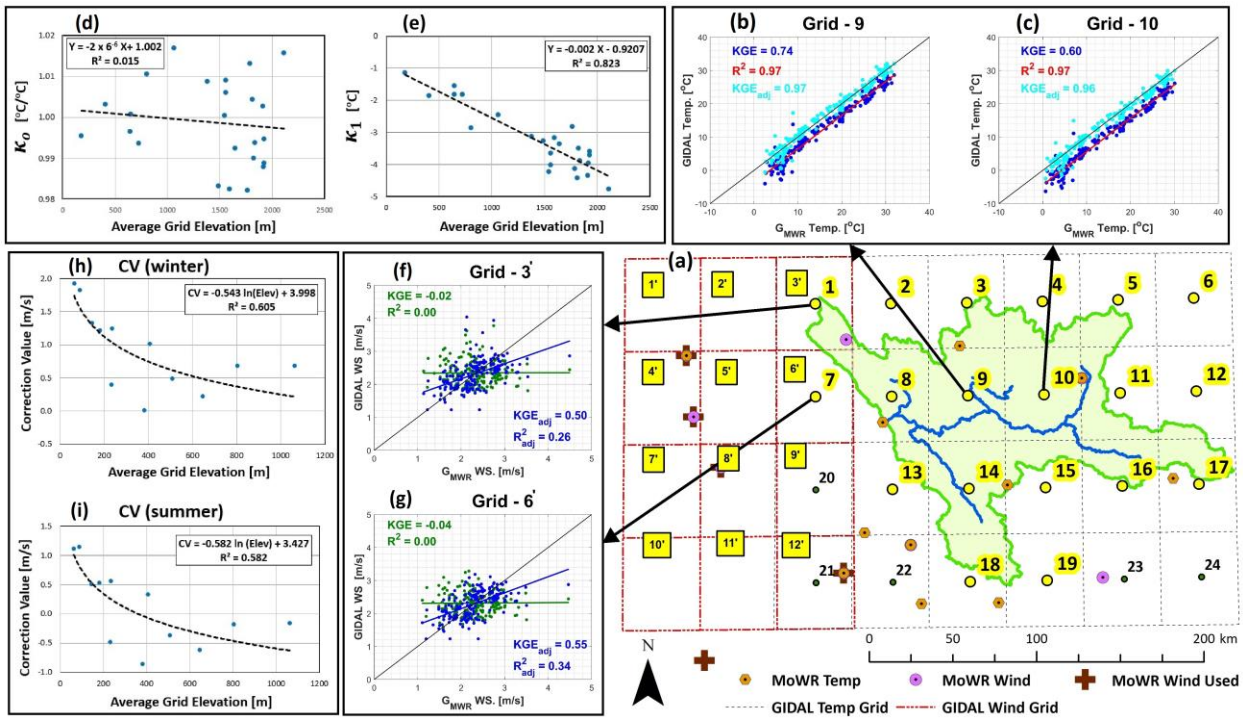

Figure 2.4: (a) and (b) G_{MWR} temperature versus GIDAL before and after adjustment for grids 1 and 2. (c) and (d) β_1 and β_0 versus Elev. (e) and (f) G_{MWR} wind speed versus GIDAL before and after adjustment for grid 3' and 6'. (g), and (h) CV of GIDAL wind speed for winter and spring seasons.

The number of MoWR stations for wind speed in the study area is 10, as shown in Figure 2.4 (a), and only five stations have consistent and complete monthly data for about 14 years and located slightly outside the basin. Therefore, the gridded GIDAL wind speed were used in those

grids for the selected five stations applying similar procedure as done for temperature, but the data was split seasonally. Then, the differences between the means were determined and plotted against elevation. The Correction Values (CV) for each season were developed (as shown Figure 2.4 (h) and (i) for winter and spring), as follows:

$$WS_{adj} = WS_{GIDAL} - CV \quad (2.13)$$

$$CV_{winter} = -0.543\, ln(Elev) + 3.998 \quad ; for\ winter\ season\ months \quad (2.14)$$

$$CV_{spring} = -0.576\, ln(Elev) + 3.117 \quad ; for\ spring\ season\ months \quad (2.15)$$

$$CV_{summer} = -0.543\, ln(Elev) + 3.428 \quad ; for\ summer\ season\ months \quad (2.16)$$

$$CV_{autumn} = -0.54\, ln(Elev) + 3.431 \quad ; for\ autumn\ season\ months \quad (2.17)$$

Where, WS_{adj} and WS_{GIDAL} are the adjusted and raw GIDAL wind speed magnitude, respectively. The overall KGE for adjusted and raw GIDAL are 0.48 and -0.11, respectively. If the CVs were determined without splitting into seasons, KGE for the adjusted data would be 0.01 which demonstrates the importance of splitting the wind speed data seasonally. Even though this procedure does not produce a perfect relationship between adjusted GIDAL and G_{MWR}, it improves the GIDAL wind speed through increasing the KGE value. In summary, the general framework presented above to develop a complete gridded-daily dataset to be used in a hydrology model in the study area and in Iraq is shown in Figure 2.5.

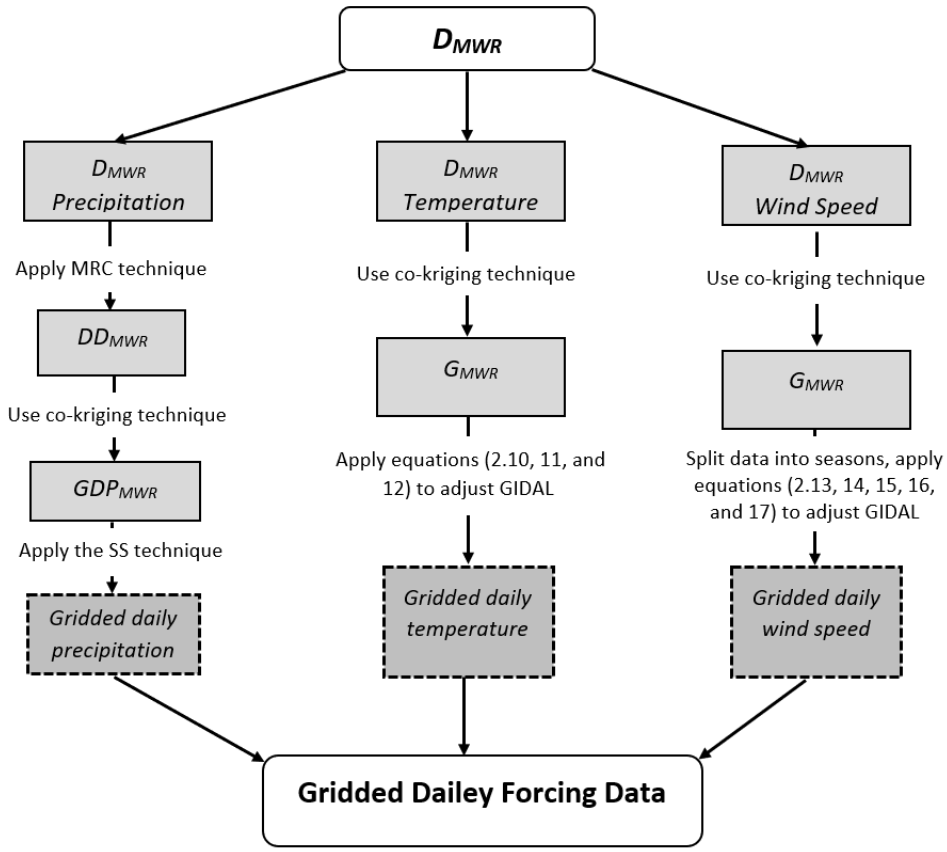

Figure 2.5: Flowchart of forcing data implementation.

2.4.3. GLUE and DREAM Analyses

GLUE and DREAM techniques were applied to VIC daily streamflow at DRB outlet driven by daily forcing data of 0.5^{o} grid spatial resolution from January 1st 1960 to October 31st 2007, with a prior two years for model warm-up. Figure 2.6 and DREAM techniques were applied to VIC daily streamflow at DRB outlet driven by daily forcing data of 0.5^{o} grid spatial resolution from January 1st 1960 to October 31st 2007, with a prior two years for model warm-up.:

1- High: The posterior distribution of the second soil layer depth is very different from its prior distribution. The quantile differences are 52.0% and 53.1% for GLUE and DREAM, respectively. Therefore, the depth of the second soil layer has a great influence on the generated streamflow.

2- Low: The posterior distributions of B_inf, D_{smax}, and first soil layer depth are not very different from the prior. The quantile differences are 10.1%, 12.2%, and 10.3% for GLUE, and 9.1%, 9.5%, and 8.4% for DREAM, respectively.

3- Insensitive: D_s, W_s, and third soil depth posterior distributions are the same as the prior distribution. The quantile differences are 7.8%, 5.9%, and 5.9% for GLUE, and 7.0%, 6.4%, and 6.3% for DREAM, respectively.

Given that DRB is considered as a dry semiarid zone according to the Koppen classification (Pidwirny, 2006), the result here is in line with Demaria et al., (2007) who found that the VIC model is more sensitive to the second soil layer depth in dry areas. In addition, they found that the B_inf sensitivity is significant in dry areas, whereas it is not in wet. They also indicated that the first soil layer depth and saturated hydraulic conductivity K_s are low sensitive in all climate regions, which is consistent with our results for first soil layer depth and D_{smax}, which is equal to K_s multiplied by the grid slope. Moreover, our result is similar to theirs for the third soil layer depth; it is insensitive in all climatic regions. Results obtained here are in line with Sun and Yuan, (2013), as they found that the second soil layer depth is the most sensitive parameter followed by B_inf using GLUE for Huaihe basin in China for the period 1970 to 1999. Our results are also consistent with those of He and Pang, (2014) who found that the third soil layer depth and D_s are insensitive; while B_inf, D_{smax}, and W_s are low sensitive in HRB in China. Nevertheless, He and Pang, (2014) found that the second soil layer depth is insensitive while it is very sensitive in our case. In addition, they found that the first soil layer depth is the most sensitive. These differences might be due to inequality of the simulation length period, their simulation period is 3 years while ours is 47 years. Moreover, the climate zone of HRB is different than DRB, as it is considered as

polar tundra in the south and arid desert in the north of HRB [e.g., Peel et al., 2007] according to Koppen classification, which can also explain the discrepancies in the results according to Demaria et al., (2007). Furthermore, our results differ than Pang et al., (2014). They found that the B_inf and first soil layer depth are the most sensitive parameters in Xitiaoxi basin in China. They also indicated that all other parameters are insensitive. These discrepancies might due to their different used range for the soil layers (e.g., from 0.1 to 1.5 m while it is from 0.001 to 2 m in this study), the simulation period is only 6 years spanning from 1995 to 2000, or the basin climate type is subtropical monsoon which is different than DRB. Finally, Vrugt et al., (2009a) and Jin et al., (2010) revealed that the DREAM and GLUE results can be similar to each other. Therefore, it is not surprising that our results demonstrate the similarity between the two techniques.

Finally, the 90% predictive bounds were generated for the VIC model, as shown in Figure 2.7 (a), which represent the 90% uncertainty in the VIC model outputs using the 5% and 95% quantile estimates of the parameters. The analysis shows that these predictive intervals contain about 93.1% of the observed streamflow which indicates a significant capture of the GLUE and DREAM methods for the model error and uncertainty. Therefore, the VIC model is valid in performing acceptable streamflow forecasting since it can well represent the hydrological behavior of DRB [e.g., Vrugt et al., 2009a; Jin et al., 2010; Beven and Binley, 2014; Pang et al., 2014].

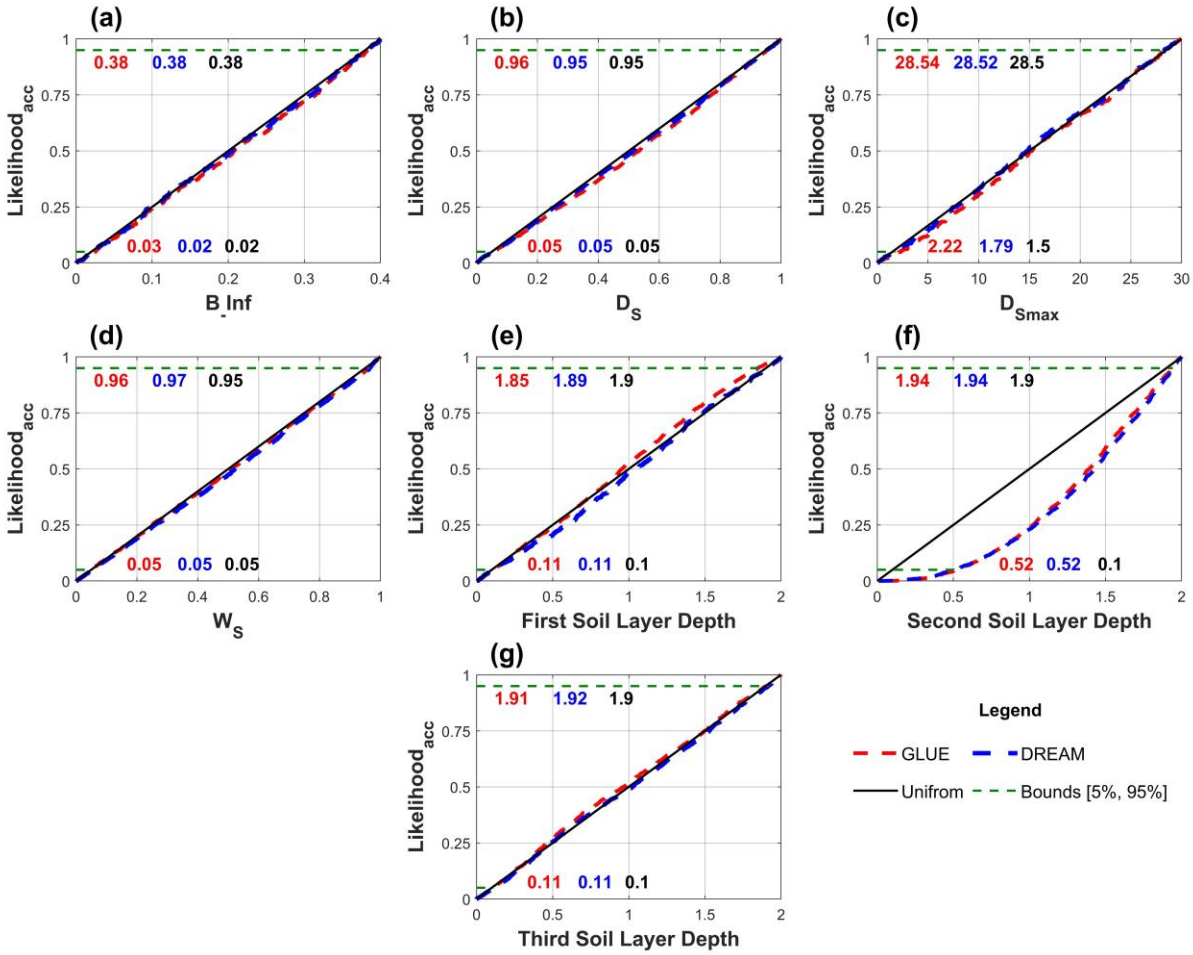

Figure 2.6: The prior and posterior CDFs of the model parameters with the 5 and 95% quantile estimates for GLUE and DREAM.

2.4.4. Model Calibration and Verification

The main objective of the calibration and verification process here is to find the best estimates of the seven calibration parameters shown in Table 2.2 with the original values from NND. The maximum KGE for the calibration and verification period was found to be 0.743 (0.761 and 0.725), as shown in Figure 2.7 (a). Furthermore, the evaluation of the standardized residual term (see equations 5, 6, 7, and 8) are shown in Figure 2.7 (b), (c) and (d). The results glimpsed that the innovations are uncorrelated, normally distributed with zero mean, and homoscedastic (no specific pattern can be detected), as shown in plots (b), (c), and (d) of Figure 2.7, respectively.

The calibrated parameter values are shown in Table 2.2 as well as the quantile estimates from both GLUE and DREAM techniques for the active grid-cells only [see Figure 2.3 (a)].

Table 2.2: The calibrated parameter values of VIC model and the quantile estimates of 5 and 95% percentile using GLUE and DREAM techniques.

Grid	B_inf	D_s	D_{smax}	W_s	First soil layer depth	Second soil layer depth	Third soil layer depth
1	0.203	0.857	20.753	0.881	0.461	0.918	1.437
2	**0.39**	0.263	13.71	0.125	0.2	1.31	0.214
3	0.131	0.098	**29.467**	0.801	0.977	1.855	1.795
4	0.275	0.242	14.81	**0.999**	0.598	1.838	**1.999**
5	0.317	0.326	20.383	0.726	1.072	1.072	0.424
6	0.293	0.78	3.419	0.394	0.835	1.237	1.887
7	0.347	0.456	22.503	0.391	1.205	1.205	1.17
8	**0.394**	0.7	16.822	0.494	**0.096**	1.392	1.828
9	0.309	0.15	5.482	0.091	**0.097**	1.454	1.352
10	0.187	**0.996**	21.725	0.854	0.391	1.341	0.608
11	0.168	0.709	20.683	**0.999**	0.251	0.996	1.053
12	0.187	0.283	20.093	0.531	0.735	0.862	0.696
13	0.314	0.466	22.013	0.176	0.174	1.542	1.752
14	**0.392**	**0.999**	22.795	0.707	0.296	1.311	1.446
15	**0.394**	0.055	16.946	0.598	0.971	1.406	1.824
16	**0.389**	0.197	2.92	0.495	0.465	0.645	**1.999**
17	0.302	**0.035**	29.999	0.199	1.027	1.786	0.231
18	0.196	0.81	9.719	0.328	0.789	0.789	0.453
19	0.183	0.728	20.184	0.337	0.613	0.811	0.538
NND	0.4	0.1	30	1	1	1	0.25
Quantile estimates (GLUE\DREAM)							
5%	0.025\0.022	0.054\0.054	2.21\1.78	0.05\0.053	0.106\0.106	0.521\0.515	0.110\0.114
95%	0.379\0.378	0.950\0.952	28.54\28.52	0.964\0.965	1.846\1.886	1.935\1.942	1.906\1.917

It can be seen that only 15 of the calibrated values, out of 140 (e.g., 11%), are beyond the quantile 5 and 95% quantile estimates, as shown in Table 2.2 in bold style. Due to the limited availability of soil and vegetation information for the basin, it is hard to investigate the physiographic and hydrometeorological characteristics of these values. However, the calibrated values are different form the initial values obtained from NND which demonstrates the importance of the calibration and verification process. Comparing with Al-Khafaji and Al-Chalabi,

(2019) our results are superior in calibrating the model. Their NSCE values are 0.61 and 0.53 for the calibration (Jan- 1984 to Dec-2004) and validation (Jan-2005 to Dec-2013) periods, respectively, whereas our values are higher and we used KGE, a superior performance efficiency to NSCE [e.g., Steinschneider et al., 2015]. Furthermore, the simulation period implemented in this study of 47 years is longer than their simulation length of 30 years.

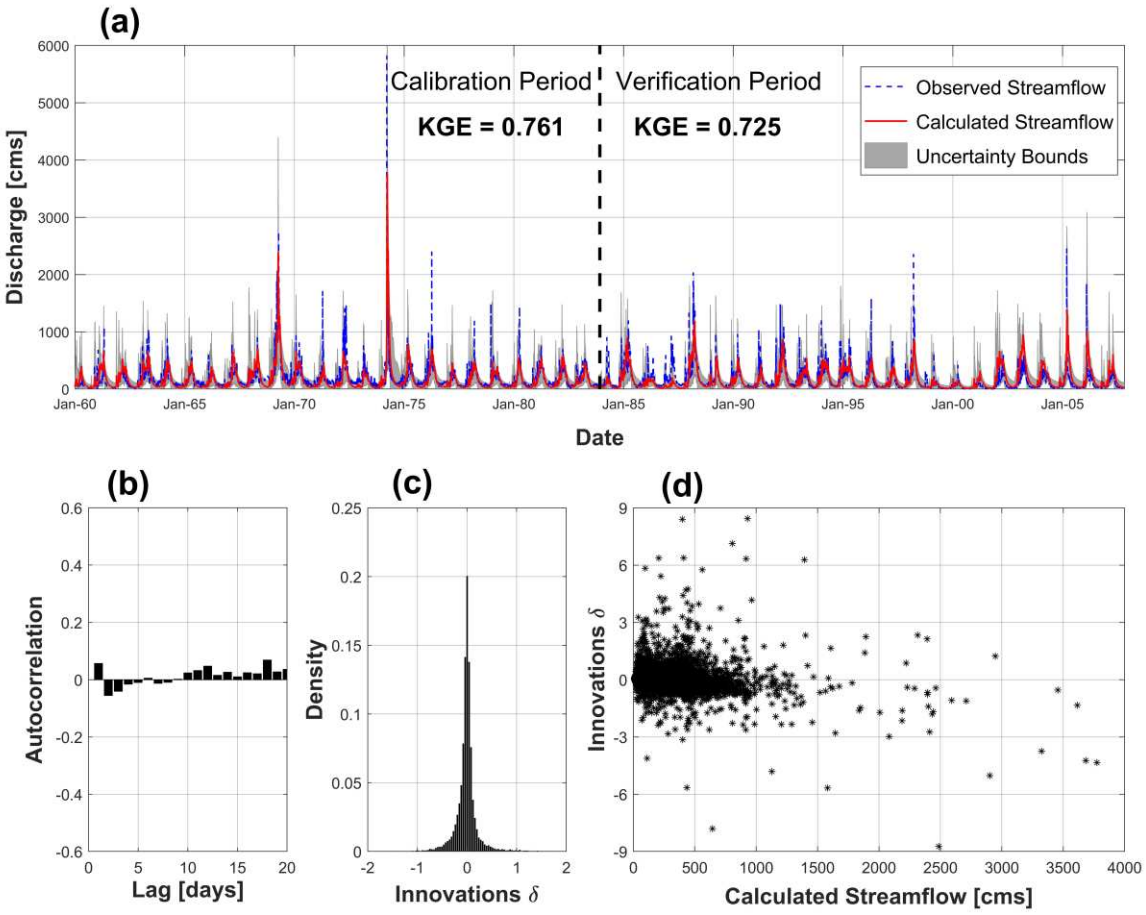

Figure 2.7: (a) streamflow hydrographs for the calibration and verification periods with the uncertainty bands. (b) and (c) correlogram and distribution of the innovations. (d) innovations versus $\overline{Q}_t$.

2.5. Conclusions

The objectives of the study were to develop accurate forcing data for DRB and to evaluate the VIC platform model parameter sensitivity and uncertainty of outcomes using GLUE and

DREAM methods. These will enable construction of a suitable hydrologic model for future management purposes. The study is the first attempt to implement GLUE and DREAM techniques in Iraq.

To augment the available data, the TRMM and GIDAL sources were evaluated. They proved inaccurate for precipitation. TRMM data exhibits smaller means and standard deviations than the ground observed data and GIDAL showed higher values. R^2 were 0.618 and 0.219 while KGE were 0.264 and -0.227 for GIDAL and TRMM, respectively, which indicated they should not be applied without further investigation for adjustment. This is in line with the findings of Duan et al., (2012) and Medhioub et al., (2019). To correct this, the daily precipitation data were developed for D_{MWR} using the MRC and SS techniques. The MRC technique for the Derbendikhan station showed R^2 at 0.936, a higher value than the 0.705 result from Al-Khafaji and Al-Chalabi, (2019). A set of equations was proposed to adjust the temperature and wind speed of GIDAL to be statistically indistinguishable from the ground observed data and to implement daily gridded forcing data. The KGE values for temperature and wind speed before and after adjustment were 0.73, -0.11, 0.97, and 0.48 respectively, which demonstrate the applicability of the proposed procedure. These results comprise a framework to implement daily gridded forcing data in the DRB so that hydrologic analysis can be performed. This framework can also be used in other basins in the region.

GLUE and DREAM techniques revealed that the second soil layer depth parameter causes most sensitivity in model outputs, with the first soil layer depth, B_inf, and D_{smax} causing much less sensitivity. Also, the D_s, W_s, and third soil layer depth are insensitive parameters. The results are consistent with Demaria et al., (2007) and He and Pang, (2014). The uncertainty results show

that 93.1% of the observed streamflow values are within 5 and 95% predictive intervals demonstrating the validity of the VIC model to generate reasonable forecasts.

The VIC model outputs were calibrated on a daily time scale with KGE values of 0.761 and 0.725 (average of 0.743) for the calibration and verification period, respectively. The calibrated model residual was free from non-normality, heteroscedasticity, and auto-correlation, which adds trust to the calibrated model. Results are superior to the calibrated model by Al-Khafaji and Al-Chalabi, (2019), and based on longer period as well as using a more efficient performance test.

Data Availability Statement

Some or all data, models, or code used during the study were provided by a third party. Direct request for these materials may be made to the provider as indicated in the Acknowledgments. The data implemented in this study can be shared conjugated with an approval from MoWR.

Acknowledgements

This study was funded by the Higher Committee for Education Development in Iraq (HCED). The authors are grateful to the Iraqi Ministry of Water Resources (MoWR) for assistance in this study. Data and models are downloaded online (e.g., TRMM is downloaded from https://pmm.nasa.gov/data-access/downloads/trmm, VIC, RVIC, GIDAL, and NND from https://uw-hydro.github.io/code/). The authors are also thankful to the editors and reviewers who offered insightful comments leading to the improvement of this paper**.** The authors are also grateful to Colorado State University for providing its laboratories and supercomputer to perform the model(s) running and analyses.

References

Abbas, Nahla, Saleh Wasimi, and Nadhir Al-Ansari. "Impacts of Climate Change on Water Resources in Diyala River Basin, Iraq: Impacts of Climate Change on Water Resources in Diyala River Basin, Iraq." Journal of Civil Engineering and Architecture 10.10 (2016): 1059-1074.

Abbaspour, K. C. & Rouholahnejad, E. "A continental-scale hydrology and water quality model for Europe: Calibration and uncertainty of a high-resolution large-scale SWAT model." Journal of Hydrology 524 (2015): 733-752.

Adam, J.C., E.A. Clark, D.P. Lettenmaier, and E.F. "Correction of global precipitation products for orographic effects." Journal of Climate 19.1 (2006): 15-38.

Adam, Jennifer C., and Dennis P. Lettenmaier. "Adjustment of global gridded precipitation for systematic bias." Journal of Geophysical Research: Atmospheres 108.D9 (2003).

Adhikary, Sajal Kumar, Nitin Muttil, and Abdullah Gokhan Yilmaz. "Cokriging for enhanced spatial interpolation of rainfall in two Australian catchments." Hydrological processes 31.12 (2017): 2143-2161.

Al-Khafaji, Mahmoud S., and Rana D. Al-Chalabi. "Assessment and Mitigation of Streamflow and Sediment Yield under Climate Change Conditions in Diyala River Basin, Iraq." Hydrology 6.3 (2019): 63.

Alwan, Imzahim Abdulkareem, Ibtisam Karim, and Mahmood Mohamed. "Sediment predictions in Wadi Al-Naft using soil water assessment tool." MATEC Web of Conferences. Vol. 162. EDP Sciences, 2018.

Benke, Kurt K., Kim E. Lowell, and Andrew J. Hamilton. "Parameter uncertainty, sensitivity analysis and prediction error in a water-balance hydrological model." Mathematical and Computer Modelling 47.11 (2008): 1134-1149.

Beven, Keith, and Andrew Binley. "GLUE: 20 years on." Hydrological processes 28.24 (2014): 5897-5918.

Beven, Keith, and Andrew Binley. "The future of distributed models: model calibration and uncertainty prediction." Hydrological processes 6.3 (1992): 279-298.

Beven, Keith, and Jim Freer. "Equifinality, data assimilation, and uncertainty estimation in mechanistic modelling of complex environmental systems using the GLUE methodology." Journal of hydrology 249.1-4 (2001): 11-29.

Beven, Keith. "A manifesto for the equifinality thesis." Journal of hydrology 320.1 (2006): 18-36.

Chahouki, Zare, Mohammadali, Asghar Zare Chahouki, Arash Malekian, Reza Bagheri Fahraji, and S. A. Vesali.. "Evaluation of co-kriging different methods for rainfall estimation in arid region (Central Kavir basin in Iran)." Desert 19.1 (2014): 1-9.

Chen, Cheng, Zhongbo Yu, Li Li, and Chuanguo Yang. "Adaptability evaluation of TRMM satellite rainfall and its application in the Dongjiang River Basin." Procedia Environmental Sciences 10 (2011): 396-402.

Choi, Yun Seok, Cheon Kyu Choi, Hung Soo Kim, Kyung Tak Kim, and Soojun Kim. "Multi-site calibration using a grid-based event rainfall–runoff model: a case study of the upstream areas of the Nakdong River basin in Korea." Hydrological processes 29.9 (2015): 2089-2099.

Clark, Martyn, Subhrendu Gangopadhyay, Lauren Hay, Balaji Rajagopalan, and Robert Wilby. "The Schaake shuffle: A method for reconstructing space–time variability in forecasted precipitation and temperature fields." Journal of Hydrometeorology 5.1 (2004): 243-262.

Demaria, Eleonora M., Bart Nijssen, and Thorsten Wagener. "Monte Carlo sensitivity analysis of land surface parameters using the Variable Infiltration Capacity model." Journal of Geophysical Research: Atmospheres 112.D11 (2007).

Duan, Zheng, W. G. M. Bastiaanssen, and Junzhi Liu. "Monthly and annual validation of TRMM Mulitisatellite Precipitation Analysis (TMPA) products in the Caspian Sea Region for the period 1999–2003." 2012 IEEE International Geoscience and Remote Sensing Symposium. IEEE, 2012.

Evin, Guillaume, et al. "Comparison of joint versus postprocessor approaches for hydrological uncertainty estimation accounting for error autocorrelation and heteroscedasticity." Water Resources Research 50.3 (2014): 2350-2375.

Evin, Guillaume, et al. "Pitfalls and improvements in the joint inference of heteroscedasticity and autocorrelation in hydrological model calibration." Water Resources Research 49.7 (2013): 4518-4524.

Gao, Huilin, et al. "Water budget record from Variable Infiltration Capacity (VIC) model." Algorithm Theoretical Basis Document for Terrestrial Water Cycle Data Records (2010).

Guo, Jun, Jianzhong Zhou, Jiazheng Lu, Qiang Zou, Huajie Zhang, and Sheng Bi. "Multi-objective optimization of empirical hydrological model for streamflow prediction." Journal of Hydrology 511 (2014): 242-253.

Gupta, Hoshin V., Harald Kling, Koray K. Yilmaz, and Guillermo F. Martinez. "Decomposition of the mean squared error and NSE performance criteria: Implications for improving hydrological modelling." Journal of hydrology 377.1-2 (2009): 80-91.

Gupta, Vijay K., and Edward C. Waymire. "A statistical analysis of mesoscale rainfall as a random cascade." Journal of Applied Meteorology 32.2 (1993): 251-267.

Guse, Bjorn, Matthias Pfannerstill, Abror Gafurov, Jens Kiesel, Christian Lehr, and Nicola Fohrer. "Identifying the connective strength between model parameters and performance criteria." (2019).

Hamza, Nahida H. "Evaluation of water quality of Diyala River for irrigation purposes." Diyala Journal of Engineering Sciences 5.2 (2012): 82-98.

He, R., and B. Pang. "Sensitivity and uncertainty analysis of the Variable Infiltration Capacity model in the upstream of Heihe River basin." Proceedings of the International Association of Hydrological Sciences 368 (2014): 312-316.

Ishida, T., and S. Kawashima. "Use of cokriging to estimate surface air temperature from elevation." Theoretical and Applied Climatology 47.3 (1993): 147-157.

Jin, Xiaoli, Chong-Yu Xu, Qi Zhang, and V. P. Singh. "Parameter and modeling uncertainty simulated by GLUE and a formal Bayesian method for a conceptual hydrological model." Journal of Hydrology 383.3-4 (2010): 147-155.

Kang, Boosik, and Jorge A. Ramírez. "A coupled stochastic space-time intermittent random cascade model for rainfall downscaling." Water Resources Research 46.10 (2010).

Li, Xin, and Vladan Babovic. "A new scheme for multivariate, multisite weather generator with inter-variable, inter-site dependence and inter-annual variability based on empirical copula approach." Climate Dynamics 52.3-4 (2019): 2247-2267.

Li, Zhi. "A new framework for multi-site weather generator: a two-stage model combining a parametric method with a distribution-free shuffle procedure." Climate dynamics 43.3-4 (2014): 657-669.

Liang, Xu, Dennis P. Lettenmaier, Eric F. Wood, and Stephen J. Burges. "A simple hydrologically based model of land surface water and energy fluxes for general circulation models." Journal of Geophysical Research: Atmospheres 99.D7 (1994): 14415-14428..

Liang, Xu, Eric F. Wood, and Dennis P. Lettenmaier. "Surface soil moisture parameterization of the VIC-2L model: Evaluation and modification." Global and Planetary Change13.1-4 (1996): 195-206.

Liu, Hongli. "Improved Data Uncertainty Handling in Hydrologic Modeling and Forecasting Applications." (2019).

Lohmann, D. A. G., R. A. L. P. H. NOLTE-HOLUBE, and Ehrhard Raschke. "A large-scale horizontal routing model to be coupled to land surface parametrization schemes." Tellus A48.5 (1996): 708-721.

Lohmann, Dag, Ehrhard Raschke, Bart Nijssen, and D. P. Lettenmaier. "Regional scale hydrology: I. Formulation of the VIC-2L model coupled to a routing model." Hydrological Sciences Journal 43.1 (1998): 131-141.

Luo, W., M. C. Taylor, and S. R. Parker. "A comparison of spatial interpolation methods to estimate continuous wind speed surfaces using irregularly distributed data from England and Wales." International journal of climatology 28.7 (2008): 947-959.

Maggioni, Viviana, Patrick C. Meyers, and Monique D. Robinson. "A review of merged high-resolution satellite precipitation product accuracy during the Tropical Rainfall Measuring Mission (TRMM) era." Journal of Hydrometeorology 17.4 (2016): 1101-1117.

Medhioub, Emna, Moncef Bouaziz, Hammadi Achour, and Samir Bouaziz. "Monthly assessment of TRMM 3B43 rainfall data with high-density gauge stations over Tunisia." Arabian Journal of Geosciences 12.2 (2019): 15.

Mehta, Amita and Kel Markert. "Introduction to Using the VIC Model with NASA Earth Observations." (2018). Available at https://arset.gsfc.nasa.gov/sites/default/files/water/18-VIC/s1.pdf.

Moazami, Saber, Saeed Golian, Yang Hong, Chen Sheng, and M. Reza Kavianpour. "Comprehensive evaluation of four high-resolution satellite precipitation products under diverse climate conditions in Iran." Hydrological Sciences Journal 61.2 (2016): 420-440.

Molnar, Peter, and Paolo Burlando. "Preservation of rainfall properties in stochastic disaggregation by a simple random cascade model." Atmospheric Research 77.1 (2005): 137-151.

Montanari, A., Young, G., Savenije, H.H.G., Hughes, D., Wagener, T., Ren, L.L., Koutsoyiannis, D., Cudennec, C., Toth, E., Grimaldi, S. and Blöschl, G. ""Panta Rhei—everything flows": change in hydrology and society—the IAHS scientific decade 2013–2022." Hydrological Sciences Journal 58.6 (2013): 1256-1275.

NASA, (2013), "Variable Infiltration Capacity (VIC) Model Manual: Step by step manual for setting up, running, calibrating, and validating of VIC model over GBM Basin". Available at http://128.95.45.89/Manual_VIC_V_1.1.pdf.Nash, J. Eamonn, and Jonh V. Sutcliffe. "River flow

forecasting through conceptual models part I—A discussion of principles." Journal of hydrology 10.3 (1970): 282-290.

Nastos, P. T., J. Kapsomenakis, and K. C. Douvis. "Analysis of precipitation extremes based on satellite and high-resolution gridded data set over Mediterranean basin." Atmospheric Research 131 (2013): 46-59.

Nijssen, Bart, Greg M. O'Donnell, Dennis P. Lettenmaier, Dag Lohmann, and Eric F. Wood. "Predicting the discharge of global rivers." Journal of Climate 14.15 (2001a): 3307-3323.

Nijssen, Bart, Reiner Schnur, and Dennis P. Lettenmaier. "Global retrospective estimation of soil moisture using the variable infiltration capacity land surface model, 1980–93." Journal of Climate 14.8 (2001b): 1790-1808.

Over, Thomas M., and Vijay K. Gupta. "A space-time theory of mesoscale rainfall using random cascades." Journal of Geophysical Research: Atmospheres 101.D21 (1996): 26319-26331.

Over, Thomas M., and Vijay K. Gupta. "Statistical analysis of mesoscale rainfall: Dependence of a random cascade generator on large-scale forcing." Journal of Applied Meteorology 33.12 (1994): 1526-1542.

Pagliero, Liliana, Fayçal Bouraoui, Jan Diels, Patrick Willems, and Neil McIntyre. "Investigating regionalization techniques for large-scale hydrological modelling." Journal of Hydrology 570 (2019): 220-235.

Pang, Bo, Rui He, and Lanying Zhang. "Parameter estimation and uncertainty analysis of the variable infiltration capacity model in the Xitiaoxi catchment." 6th International Conference of Flood Management, Sao Paulo, Brazil (2014).

Patnaik, Swagat, Vimal Chandra Sharma, and Basudev Biswal. "Evaluation of an instantaneous dryness index-based calibration-free continuous hydrological model in India." Hydrology Research (2019).

Peel, Murray C., Brian L. Finlayson, and Thomas A. McMahon. "Updated world map of the Köppen-Geiger climate classification." Hydrology and earth system sciences discussions 4.2 (2007): 439-473.

Pidwirny, M. "Climate classification and climatic regions of the world. Fundamentals of Physical Geography." Second edition (2006).

Pradhan, Ankita, and J. Indu. "Uncertainty in Calibration of Variable Infiltration Capacity Model." Hydrology in a Changing World. Springer, Cham, 2019. 89-108.

Quan, Z., J. Teng, W. Sun, T. Cheng, and J. Zhang. "Evaluation of the HYMOD model for rainfall–runoff simulation using the GLUE method." Proceedings of the International Association of Hydrological Sciences 368 (2015): 180-185.

Schoups, Gerrit, and Jasper A. Vrugt. "A formal likelihood function for parameter and predictive inference of hydrologic models with correlated, heteroscedastic, and non-Gaussian errors." Water Resources Research 46.10 (2010).

Shafii, Mahyar, Bryan Tolson, and L. Shawn Matott. "Addressing subjective decision-making inherent in GLUE-based multi-criteria rainfall–runoff model calibration." Journal of Hydrology 523 (2015): 693-705.

Song, Wei, Wei Ye, and Yajuan Li. "The study of the variation law of TRMM rainfall measurement precision on time scale." IOP Conference Series: Earth and Environmental Science. Vol. 252. No. 4. IOP Publishing, 2019.

Sood, Aditya, and Vladimir Smakhtin. "Global hydrological models: a review." Hydrological Sciences Journal 60.4 (2015): 549-565.

Steinschneider, Scott, Sungwook Wi, and Casey Brown. "The integrated effects of climate and hydrologic uncertainty on future flood risk assessments." Hydrological Processes 29.12 (2015): 2823-2839.

Sun, R., and H. Yuan. "Hydrological Ensemble Simulation in Huaihe Catchment Based on VIC Model." AGU Fall Meeting Abstracts. 2013.

Sun, Wenchao, Hiroshi Ishidaira, and Satish Bastola. "Calibration of hydrological models in ungauged basins based on satellite radar altimetry observations of river water level." Hydrological Processes 26.23 (2012): 3524-3537.

Surfleet, Christopher G., Desirèe Tullos, Heejun Chang, and Il-Won Jung. "Selection of hydrologic modeling approaches for climate change assessment: A comparison of model scale and structures." Journal of Hydrology 464 (2012): 233-248.

Tarek, Mehedi Hasan, Adil Hassan, Joy Bhattacharjee, Sayedul Hasan Choudhury, and Abu Borhan Md Badruzzaman. "Assessment of TRMM data for precipitation measurement in B angladesh." Meteorological Applications 24.3 (2017): 349-359.

Tofiq, F. A., and A. Guven. "Prediction of design flood discharge by statistical downscaling and General Circulation Models." Journal of hydrology 517 (2014): 1145-1153.

Vrac, Mathieu, and Petra Friederichs. "Multivariate—intervariable, spatial, and temporal—bias correction." Journal of Climate 28.1 (2015): 218-237.

Vrugt, Jasper A., and Willem Bouten. "Validity of first-order approximations to describe parameter uncertainty in soil hydrologic models." Soil Science Society of America Journal66.6 (2002): 1740-1751.

Vrugt, Jasper A., Cajo JF Ter Braak, Hoshin V. Gupta, and Bruce A. Robinson. "Equifinality of formal (DREAM) and informal (GLUE) Bayesian approaches in hydrologic modeling?." Stochastic environmental research and risk assessment 23.7 (2009a): 1011-1026.

Vrugt, J. A., Ter Braak, C. J. F., Diks, C. G. H., Robinson, B. A., Hyman, J. M., & Higdon, D. "Accelerating Markov chain Monte Carlo simulation by differential evolution with self-adaptive randomized subspace sampling." International Journal of Nonlinear Sciences and Numerical Simulation 10.3 (2009b): 273-290.

Vrugt, Jasper A. "Markov chain Monte Carlo simulation using the DREAM software package: Theory, concepts, and MATLAB implementation." Environmental Modelling & Software 75 (2016): 273-316.

Xue, Xianwu, Ke Zhang, Yang Hong, Jonathan J. Gourley, Wayne Kellogg, Renee A. McPherson, Zhanming Wan, and Barney N. Austin. "New multisite cascading calibration approach for hydrological models: Case study in the red river basin using the VIC model." Journal of Hydrologic Engineering21.2 (2015): 05015019.

Yen, Haw, Xiuying Wang, Darrell G. Fontane, R. Daren Harmel, and Mazdak Arabi. "A framework for propagation of uncertainty contributed by parameterization, input data, model structure, and calibration/validation data in watershed modeling." Environmental Modelling & Software 54 (2014): 211-221.

CHAPTER 3

Development of a Parametric Regional Multivariate Statistical Weather Generator for Risk Assessment Studies in Areas with Limited Data Availability[2]

Chapter Synopsis

Risk analysis of water resources systems can use statistical weather generators coupled with hydrologic models to examine scenarios of extreme events caused by climate change. These require multivariate, multisite models that mimic the spatial, temporal, and cross correlations of observed data. Existing weather generator models have impressive features, but are limited by dependence on length of historic observations, incapable of preserving all correlations, and inability to produce synthetic climate scenarios that exceed the range of the observations. This study developed a statistical weather generator to assess climate change impacts on water resources systems for cases of limited data. The weather generator is straightforward to implement and can employ any distribution function for variables such as precipitation or temperature. It is based on (1) a First-order, Two-state Markov Chain to simulate precipitation occurrences; (2) use of Wilks' technique to produce correlated weather variables at multiple sites with conservation of spatial, temporal, and cross correlations; and (3) the capability to vary the statistical parameters of the weather variables. The model was applied to studies of the Diyala River Basin in Iraq, which is a case with limited observed records. Results show that it exhibits high values of the Kling–Gupta efficiency, preserves the statistical properties of the observed

[2] Under Review in Climate Dynamics Journal, Saddam Q. Waheed, Neil S. Grigg, Jorge A. Ramirez

variables, and conserves the spatial, temporal, and cross correlations among the weather variables at all sites with good agreement with observations.

3.1. Introduction

Climate change impacts are of increasing concern to hydrologists who assess risks in the management of water resources systems. Their models of climate scenarios for extreme events can be derived from Global Climate Models (GCMs); statistical weather generators (SWGs); or a combination. GCM scenarios are inadequate and limit decision-making options because they represent only specific scenarios for climatic variability and have large uncertainties [Wilby and Dessai, 2010; Hallegatte et al., 2012; Brown and Wilby, 2012; Stephenson et al., 2012; Steinschneider and Brown, 2013; Whateley et al., 2014; Culley et al., 2016]. To address this limitation, SWGs can be used to produce a wide range of scenarios to study system responses and provide more insights about the system performance under climate change [Weaver et al., 2013; Turner et al., 2014; Steinschneider et al., 2015a; Zhang et al., 2018]. Moody and Brown (2013) and Steinschneider et al. (2015b) linked SWG and GCM scenarios to assign a probability of each SWG scenario by fitting a normal distribution to the GCM outcomes. SWG can then be used to generate probabilistic synthetic scenarios that are statistically similar to observed data and used to investigate which climate states cause system failure [Wilks, 1998, 2009; 2011; Furrer and Katz, 2008; Khalili et al., 2011; Steinschneider and Brown, 2013; Chen et al., 2014; Chen and Brissette, 2014a; Chen and Brissette, 2014b; Breinl et al., 2015; Acharya et al., 2017; Mukundan et al., 2019; Verdin et al., 2019]. Where historic records are limited, synthetic weather sequences based on SWGs are especially suitable [Mehrotra et al., 2012]. The main objective of this paper is to develop a SWG that can be used to generate synthetic scenarios in order to evaluate impacts

of long-term climate change on system performance and suggest robust adaptations to cope with anticipated negative impacts. Emphasis is placed on areas with low data availability, and the model is demonstrated for Diyala River Basin in Iraq for the four historic weather variables [e.g., precipitation, maximum and minimum temperature, and wind speed magnitude] with daily time step from 1948 to 2006.

3.2. Literature Review

Generally, SWG can be grouped into parametric, non-parametric, and semi-parametric methods. In the parametric method, the weather variables are assumed to fit one continuous probability distribution or two combined distributions. The parameters are usually estimated from historic observations [e.g., Richardson, 1981; Nicks and Gander, 1994; Wilks 1998; Qian et al., 2002; Fowler et al., 2005; Brissette et al., 2007; Burton et al., 2008; Ailliot et al., 2009; Khalili et al., 2009; Serinaldi, 2009; Pegram, 2009; Bardossy and Pegram, 2009; Baigorria and Jones, 2010]. In the non-parametric method, the weather variables are resampled from historic observations, using techniques such as are empirical distributions, neural networks, and maximum entropy bootstrap [e.g., Rajagopalan and Lall, 1999; Beersma and Buishand 2003; Wilby et al., 2003; Burton et al., 2008; Leander and Buishand 2009; King et al., 2014; King et al., 2015; Srivastav and Simonovic, 2015]. Whereas the semi-parametric method is a mixture between the parametric and non-parametric methods [e.g. Fowler et al., 2005; Apipattanavis et al., 2007; Cannon, 2008; Breinl et al., 2013; Steinschneider and Brown, 2013; Mehrotra et al., 2015; Marcon et al., 2017].

The parametric method is more suitable because the parameters can be altered to simulate different weather scenarios and facilitate climate change studies [Wilks, 2009]. Khalili

et al., (2011); Buishand and Brandsma, (2001); Furrer and Katz, (2008); and Verdin et al., (2019) noted that the non-parametric method has limitations in generating extreme events because values can only be in the range of the observations. Besides violating the climate change impact in altering intensities of the variables, using only the observation sequences, where the extreme events do not change over the time, is insufficient in assessing the future response of water resources system since it leads to single result corresponding only for those observed sequences. [e.g., Richardson ,1981; Mehrotra et al., 2015; Acharya et al., 2017; Seneviratne et al., 2017; Li and Babovic, 2018; Wang et al., 2018; Mukundan et al., 2019].

Most existing SWGs are for single sites and cannot capture the spatial and cross correlations between the variables, which are essential for generating realistic climate change scenarios. Schaake et al., (2010) stated that "relationships between physically dependent variables like precipitation and temperature should be respected". Single site SWGs can miss-capture the extreme events of the generated runoff, which are essential to develop realistic adaptation strategies to cope with flood and drought events, where high runoff in one sub-basin can be offset by low runoff in adjacent sub-basins [e.g., Qian et al., 2002; Li, 2014; Mehrotra et al., 2015].

Moreover, misrepresentation of spatial and cross correlations (e.g., correlations between the precipitation and temperature) leads to biased generated streamflow as this correlation determines the water availability for evapotranspiration and snowmelt [e.g., Li et al., 2014a; Srivastav and Simonovic, 2015; Chen et al., 2018]. Therefore, SWG should capture the characteristics of each site and the spatial dependence among them.

Recently, multi-site and multi-variable SWGs have been developed using different approaches. Steinschneider and Brown, (2013) developed a semi-parametric model using a k-nearest-neighbor resampling scheme to simulate multiple spatially distributed variables using wavelet decomposition and autoregressive model to account for low-frequency oscillations. They used a Markov chain of first order with three states to identify the precipitation states [e.g., dry, wet, and extremely wet]. This model had difficulty in preserving the weather statistics besides the cross correlation. Also, it is not clear how to diagnose the differences between the precipitation states [e.g., wet and extremely wet].

Srivastav and Simonovic, (2015) developed a non-parametric model using the maximum entropy bootstrap technique to capture the time-dependent structure and the statistical characteristics. They used an orthogonal transformation to capture the spatial correlations. Even though the model preserves the historical characteristics very well, Davidson and Monticini, (2014) and Verdin et al., (2019) showed that the maximum entropy bootstrap technique is limited to the historical data range leading to inadequacy in climate change studies. It is difficult to employ this model to create different climate scenarios through direct parameter changing.

Li and Babovic, (2018) proposed a two-stage parametric model using an empirical copula to generate spatial distribution templates. Then, they developed a rank ordering technique that depended on historic data ranks with empirical copula technique to preserve the correlations between the variables. The model preserves correlations between the variables and sites but is limited to the historic record length. For example, the model cannot generate more than 30 years of simulation if the historic observations are 30 years. Therefore, the model is not useful in areas

with limited data length as insufficient projection length may lead to wrong conclusions in risk assessment studies [e.g., Dresen, 2011; Haugen et al., 2018].

Verdin et al., (2019) presented a model using Bayesian hierarchical technique. The precipitation amounts are modeled using gamma distributions and maximum and minimum temperatures are modeled using a normal distribution. The statistical coefficients within them are modeled as spatial Gaussian processes to account for the correlations. Besides the complexity of model structure, the model has difficulty in preserving the statistical properties of the variables (especially the standard deviation of minimum temperature is extremely underestimated by the model). Also, the model underestimates the spatial correlation between the variables. Furthermore, their results do not demonstrate the model ability to preserve the cross correlation between the variables as well as the temporal correlation.

In this study, our objective is to develop a Parametric Regional Weather Generator (PR-WG) that preserves the statistical parameters (e.g., mean, standard deviation, … etc.) of the weather variables as well as spatial, temporal, and cross correlations among them. It should be easy to implement and adapt by altering the statistical parameters to generate synthetic future climate scenarios. The generated scenario must exceed the historic record length and observation range.

3.3. Model Description

The novel contribution here is to use the parametric approach to create a flexible model that can adapt to any continuous probability distribution. This will enable use of the most accurate distribution for each weather variable, and the user can employ other distributions according to data availability and scope of the study.

3.3.1. Precipitation States

The first step in developing the PR-WG is to establish the precipitation states. They are defined here as: *wet* days if the daily amounts equal or exceed 0.1 mm and *dry* days otherwise. This is similar to the approach by Li and Babovic, (2018); Verdin et al., (2019). The approach is to use the First-order Two-state Markov Chain (FTMC), which is the most popular method to produce dry and wet precipitation occurrences. It works well in different climate types and performs as well as higher Markov chain orders [Chen and Brissette, 2014b; Acharya et al., 2017].

Let $S_{(k,\,t,\,m)}$ denote the precipitation state (S=0 is a dry day and S=1 is a wet day) at spatial location k ∈ ℕ, time index t ∈ ℕ in days, and month index m = {1,2, … 12}. The dry or wet day occurrence is obtained from the following conditional probabilities:

$$Pr\left(S_{(k,t,m}=0\,\middle|S_{k,t-1,m}=0\right)=\ \kappa_0 \quad ; \quad Pr\left(S_{(k,t,m}=1\,\middle|S_{k,t-1,m}=0\right)=1-\ \kappa_0 \tag{3.1}$$

$$Pr\left(S_{(k,t,m}=1\,\middle|S_{k,t-1,m}=1\right)=\ \kappa_1 \quad ; \quad Pr\left(S_{(k,t,m}=0\,\middle|S_{k,t-1,m}=1\right)=\ 1-\ \kappa_1 \tag{3.2}$$

Where, κ_0 is the probability of a dry day following a dry day, and κ_1 is the probability of a wet day following a wet day. These probabilities were estimated from the daily historical precipitation observations for each month.

3.3.2. Precipitation Amount

Precipitation amounts were calculated by using the joint probability distribution between the occurrence and amount. For example, once a wet day is predicted from the FTMC, the precipitation amount is calculated. A skewed normal distribution (SN) was selected because it estimates the daily precipitation amount better than other distributions such as exponential, Gamma, Weibull, mixed-exponential, and generalized Pareto in capturing the mean, standard deviation, and extreme values, and recommended by other researchers [e.g., Li et al., 2014b;

Chen and Brissette, 2014a; Chen and Brissette, 2014b; Mehan et al., 2017; Wang et al., 2018]. Let P denote the precipitation amount in [mm/day] and $\mathbb{I}_{\Psi}$ denote the indicator of precipitation state condition ψ. In which, P returns to a value (obtained implicitly form equation (3.4); Nicks and Gander, 1994) if the condition ψ holds ($\mathbb{I}_{[S=1]}$) and returns to zero otherwise ($\mathbb{I}_{[S=0]}$), as follows:

$$P_{(k,t,m)} = \begin{cases} SN\ (\mu_P, \sigma_P, \gamma_P) & for \quad \mathbb{I}_{[S(k,t,m)=1]} \\ 0 & for \quad \mathbb{I}_{[S(k,t,m)=0]} \end{cases} \tag{3.3}$$

$$\theta_{(k,t,m)} = \frac{6}{\gamma_{p(k,m)}} \left\{ \left[\frac{\gamma_{p(k,m)}}{2} \left(\frac{P_{(k,t,m)} - \mu_{p(k,m)}}{\sigma_{p(k,m)}} \right) + 1 \right]^{\frac{1}{3}} - 1 \right\} + \frac{\gamma_{p(k,m)}}{6} \tag{3.4}$$

Where **θ** is the matrix of the standard normal deviates θ ~ N(0,1) ϵ $\mathbb{R}$; and μ_p, σ_p, and γ_p, are the mean, standard deviation, and skew coefficient of the precipitation for month m. Values of the parameters μ_p, σ_p, and γ_p were estimated from the daily historical observations.

3.3.3. Maximum and Minimum Air Temperature

The maximum and minimum daily air temperature are usually modeled by the normal distribution (N) [e.g., Harmel et al., 2001 and Harmel et al., 2002]. Let T_X and T_N denote the maximum and minimum daily air temperature in [°C], respectively. In which, T_X is (and T_N) is:

$$T_{X(k)} \sim N(\mu_{X(k)}, \sigma_{X(k)}) \tag{3.5}$$

Where μ_X and σ_X are the mean and standard deviation of T_X, respectively. Solving equation (3.5) for each month m according to $\mathbb{I}_{\Psi}$ (to account for precipitation state effects), T_x and T_N can be computed as;

$$T_{X(k,t,m)} = \mu_{x0(k,m)} + \sigma_{X0(k,m)} \times \upsilon_{(k,t,m)} \qquad for \quad \mathbb{I}_{[S(k,t,m)=0]} \tag{3.6}$$

$$T_{X(k,t,m)} = \mu_{\mu x1(k,m)} + \sigma_{X1(k,m)} \times \upsilon_{(k,t,m)} \qquad for \quad \mathbb{I}_{[S(k,t,m)=1]} \tag{3.7}$$

$$T_{N(k,t,m)} = \mu_{\mu N0(k,m)} + \sigma_{N0(k,m)} \times \delta_{(k,t,m)} \quad for \quad \mathbb{I}_{[S(k,t,m)=0]} \tag{3.8}$$

$$T_{N(k,t,m)} = \mu_{\mu N1(k,m)} + \sigma_{N1(k,m)} \times \delta_{(k,t,m)} \quad for \quad \mathbb{I}_{[S(k,t,m)=1]} \tag{3.9}$$

Where, μ_{X0}, μ_{X1}, μ_{N0}, μ_{N1}, σ_{X0}, σ_{X1}, σ_{N0}, and σ_{N1} are the monthly mean and standard deviation for maximum and minimum air temperature [^{o}C/day] for S= 0 and 1, respectively, and **υ** and **δ** are the matrices of standard normal deviates, such that **υ** and **δ** ~ N (0,1) ϵ $\mathbb{R}$. Parameter values of equations (3.6), (3.7), (3.8), and (3.9) were estimated from the historic observations.

3.3.4. Wind Speed Magnitude

Pobocikova et al., (2017) showed that the most accurate function to simulate the daily wind speed magnitude (WS) is Weibull with 3 and 2 parameters, respectively, followed by Gamma. Given the condition that wind speed is affected by precipitation states and amount [Back and Bretherton, 2005], the selected distribution must be decomposed into the same distribution type. As the Weibull distribution cannot be decomposed into two Weibulls (although Gamma can be) [Nadarajah, 2008], wind speed magnitude was modeled by the Gamma distribution (GM) in this study. Let WS denote the daily wind speed magnitude [m/s] for k locations, as follows:

$$WS_{(k)} \sim GM\ (\alpha_{(k)}, \beta_{(k)}) \tag{3.10}$$

Where α and β are the shape and scale parameters, respectively. Similarly for the temperature, WS for each month m and according to $\mathbb{I}_{\Psi}$ was estimated implicitly from the following equations:

$$\lambda_{(k,t,m)} = \frac{\beta_{0(k,m)}^{-\alpha_{0(k,m)}}}{\Gamma\left(\alpha_{0(k,m)}\right)} \int_0^{WS_{(k,t,m)}} h^{\alpha_{0(k,m)}-1}\, e^{-h/\beta_{0(k,m)}}\, dh \quad for \quad \mathbb{I}_{[S(k,t,m)=0]} \tag{3.11}$$

$$\lambda_{(k,t,m)} = \frac{\beta_{1(k,m)}^{-\alpha_{0(k,m)}}}{\Gamma\left(\alpha_{1(k,m)}\right)} \int_0^{WS_{(k,t,m)}} h^{\alpha_{1(k,m)}-1}\, e^{-h/\beta_{1(k,m)}}\, dh \quad for \quad \mathbb{I}_{[S(k,t,m)=1]} \tag{3.12}$$

Where α_0, α_1, β_0, and β_1 are the shape and scale parameters for S=0 and 1, respectively, for each month m, h is an independent parameter, and λ is the cumulative probability, which is distributed uniformly; $\lambda \sim U[0, 1], \epsilon \mathbb{R}$.

3.4. Model Implementation

The parametric SWG should conserve the spatial, temporal, and cross correlations of historic observations of the four weather variables. The concept is to study the behavior of the variates θ, υ, δ, and λ, hereafter referred to as anomalies. The correlations between those anomalies should be identified so the generated weather values are statistically similar to observed values and conserve spatial, temporal, and cross correlations. The implementation of the PR-WG consists of two stages, namely preprocessing and postprocessing.

3.4.1. Preprocessing: Parameter Estimation and Matrix Preparation

In order to specify the wet and dry occurrences, a random uniform variate y ~U[0, 1] must be drawn and compared with transition probabilities obtained from equations (3.1) and (3.2). For multi-site precipitation, their anomalies (referred to as $\mathbf{Y} \epsilon \mathbb{R}$) that identify the states in k locations must be correlated so that the generated states **S** are correlated as the historic observations. Wilks' method was selected to generate correlated anomalies $\mathbf{Y} \sim N(0,1)$ at multiple sites. It is simple and more efficient than hidden Markov and *k*-nearest neighbor methods [Mehrotra et al., 2006], accurate in generating the correlations of monthly interstation [Khalili et al., 2007], and the most cited method comparing with other approaches [Chen et al., 2015].

Assume S (1,m) and S (2,m) are the precipitation states on month m at sites k=1 and k=2. To generate realistic sequences of precipitation states at these two sites, the correlation (ω) between their corresponding anomalies **Y**, $\omega_{(1,2)} = \text{corr}\ (Y_{(1,m)}, Y_{(2,m)})$, must be computed. The

parameter ω was determined by generating different sets of **Ý** at the two sites with different arbitrary correlation values {ώ$_1$, ώ$_2$, …}, ώ$_1$ =corr(Ý$_{(1,m)}$, Ý$_{(2,m)}$, identifying the precipitation states at the two locations Ś$_1$ and Ś$_2$, and calculating the corresponding correlation {έ$_1$, έ$_2$, …}, έ$_{1(1,2)}$ = corr (Ś$_{(1,m)}$, Ś $_{(2,m)}$). Then, a regression line between έ and ώ sets is fitted to identify the relationship between them. Using this regression equation with the observed precipitation state correlation ξ, the parameter ω can then be found. An example is shown in Figure 3.1 a., in which selecting 0.858 correlation between the pair anomalies (ω) will produce 0.785 correlation between the pair states (ξ) at the two locations.

The process should be repeated for each station pair and lead to the number of realizations of k (k-1)/2 and repeated for each month m to create the anomalies matrix $\boldsymbol{\omega_s} \in \mathbb{R}$. The $\boldsymbol{\omega_s}$ matrix is then used to develop **Y** that produces correlated precipitation states in k locations for month m, using the multi-variate normal distribution as follows:

$$Y = f\left(\mu_y,\, \Sigma\right) = \frac{1}{\sqrt{\Sigma\,(2\pi)^d}} exp\left(-\frac{1}{2}\left(y - \mu_y\right)\Sigma^{-1}\left(y - \mu_y\right)\right) \tag{3.13}$$

The variable $\boldsymbol{\mu_y}$ denotes the 1-D mean vector for the anomalies **Y**, **Σ** denotes the covariance matrix, and d is an independent parameter. In this case, $\boldsymbol{\mu} = [0, 0, \dots, 0]_{k\times1}$ and the variance is 1, so the covariance matrix $\boldsymbol{\Sigma_s}$ becomes the correlation matrix $\boldsymbol{\omega_s}$.

The matrix $\boldsymbol{\omega_s}$ must be a positive-definite matrix (e.g., symmetric and all eigenvalues are positive) to be implemented in equation (3.13). Since the elements of $\boldsymbol{\omega_s}$ were calculated empirically, $\boldsymbol{\omega_s}$ is usually a non-positive matrix. Comparing to the work of others, the most precise method to obtain a positive-definite matrix is the Iterative Spectral with Dykstra's Correction (ISDC) [Maree, 2012], as follows:

1- Assume $\omega_i = \omega$, $\Delta\Omega_i = 0$, and $i = 1$, in which ω is a non positive-definite correlation matrix.

2- Let $R_i = \omega_i - \Delta\Omega_i$.

3- Find L_i and Ω_i, such that $R_i = \Omega_i L_i \Omega_i^T$.

4- Replace the negative eigenvalues of L_i by a small positive value to construct L_i^+.

5- Set $\omega_{i+1} = \Omega_i L_i^+ \Omega_i^T$ and $\Delta\Omega_{i+1} = \omega_{i+1} - R_i$. Then, replace all ω_{i+1} diagonal elements by 1.

6- Test whether ω_{i+1} is a positive-defined matrix or not. If not, repeat the steps from 2 to 6 by making $i = i + 1$ and $\omega_i = \omega_{i-1}$.

After generating the matrix **S** at k and m, the next step is to simulate the weather variables (e.g. P, T_X, T_N, and WS). The idea here is to examine the anomalies of those variables and generate the weather variables with same observation properties**.** To account for all spatial and cross-correlation between the variables, their anomalies (**θ**, **υ**, **δ**, and **λ**) must be correlated. The temporal correlation, identified by auto-correlation lag-1 day, for T_X, T_N, and WS must also be considered. Since the precipitation amount is an intermittent variable, the auto-correlation is not considered. The following procedure was suggested to achieve the purpose. First, arrange the weather variable matrix **V** as follows:

$$\begin{bmatrix} V_{1,1}^1 & V_{1,2}^1 & \cdots & V_{1,k}^n \\ V_{2,1}^1 & V_{2,2}^1 & & V_{2,k}^n \\ \vdots & \vdots & \ldots & \vdots \\ V_{t,1}^1 & V_{t,2}^1 & \cdots & V_{t,k}^n \end{bmatrix} \quad (3.14)$$

Where, V represents the observed weather variable value and n denotes the weather variable rank (P, T_X, T_N, and WS), n= {1, 2, 3, 4}. The total number of the rows will be T = month

days × year numbers, the columns will be K × N, and the aisle will be M. This matrix arrangement enables us to consider all spatial and cross correlations between the weather variables. Next, extract the anomalies matrix $\mathbf{Z} \in \mathbb{R}$ from **V** using equations (3.3) and (3.4) for P; (3.6), (3.7), (3.8), and (3.9) for T_x and T_N; and (3.11) and (3.12) for WS after estimating their parameters (e.g., μ_p, σ_p, γ_p for P, μ_{X0}, μ_{X1}, σ_{X0}, σ_{X1} for T_X , μ_{N0}, μ_{N1}, σ_{N0}, σ_{N1} for T_N, and α_0 ,α_1 β_0,, β_1 for WS).

The **Z** matrix represents the anomalies of the weather variables and their elements have spatial, cross, and auto correlation magnitudes. To generate the **Z** matrix with same observation properties, those correlations must be preserved. The first step done here was to estimate autoregressive model of order 1, AR(1), coefficients for the anomalies ($\boldsymbol{\phi_z}$) so that generated variables have the observed AR(1) value ($\boldsymbol{\phi_v}$) applying the Wilks' technique. For example, let assume the μ_{X0}, μ_{X1}, σ_{X0}, σ_{X1} are 11.72, 9.12, 3.71, 2.21 [C^o/day], respectively, and ϕ_v is 0.82 at station k of month m. The adopted procedure for obtaining the ϕ_z, as follows:

1) Generate standard normal random deviate set y; y ~ N (0,1).
2) Use equations (3.1) and (3.2) to identify the dry and wet days.
3) Generate standard normal random deviate set x; x ~ N (0,1).
4) Apply the AR of arbitrary values between -1 and 1 (e.g., ϕ'_z).
5) Obtain the anomalies z by standardizing x of step 4.
6) Apply equations (3.6) and (3.7) to obtain T'_X.
7) Calculate AR (1) of T_X (e.g., ϕ'_v) and plot versus the ϕ'_z, then regress them.
8) Use the regression equation obtained in step 7 with the observed value ϕ_v (e.g., 0.82) to determine ϕ_z. In this case 0.88 (as shown in Figure 3.1 b).

This procedure has to be done for all T_X and T_N of each k and m. For WS, the procedure is same except step 5, converting x into uniform distributed to get WS anomalies. For example, let us assume α_0, α_1, β_0, and β_1 are 4.04, 3.22, 0.62, 0.71 respectively, and the ϕ_v is 0.54. The corresponding ϕ_z will be 0.56, as shown in Figure 3.1 c. This procedure allows us to preserve the auto-correlation of T_x, T_N, and WS.

The final step of the preprocessing stage is to construct the positive-definite correlation matrix of variable anomalies $\boldsymbol{\omega_V}$, as done for precipitation states using ISDC. Building $\boldsymbol{\omega_V}$ allows us to preserve all spatial, temporal, cross correlations between the variables.

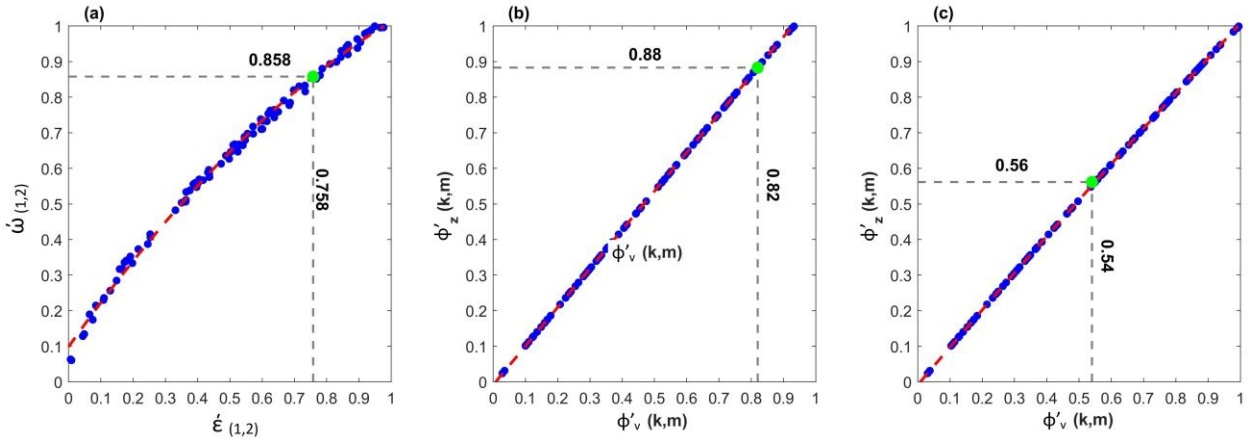

Figure 3.1: (a) An example of Wilks' technique for precipitation states. (b) and (c) examples of Wilks' technique to obtain ϕ_z for T_X and WS, respectively for station k of month m.

3.4.2. Post-processing Stage: Variable Generation

After building all matrices and estimating the parameters in the preprocessing stage, the four weather variables can be generated for any time length of interest, as follows:

1) Use equation (3.13) with $\boldsymbol{\omega_s}$ to generate **Y** anomalies that denote **S**. The length of Y denotes the day's number of the generated time series. In this case, the user can generate any length (independently on the historic observation length).

2) Use equations (3.1) and (3.2) with the estimated FTMC parameters (κ_0 and κ_1) to identify the dry and wet day occurrences.

3) Apply equation (3.13) with $\boldsymbol{\omega_v}$ to generate **Z** anomalies that denote the variable values. Off course, the length of **Z** must be the same of **Y**.

4) Obtain **P** for the wet days using equations (3.3) and (3.4) with the estimated parameters μ_p, σ_p, and γ_p. This will make sure the generated **P** have similar observed statistics.

5) Apply AR (1) with coefficients Φ_z for $\mathbf{T_X}$, $\mathbf{T_N}$, and **WS** anomalies to consider the auto-correlation magnitude for the variables.

6) Re-standardized the anomalies for $\mathbf{T_X}$ and $\mathbf{T_N}$, as follows:

$$Z_{std(k)} = \frac{Z_{(k)} - \mu(Z_{(k)})}{\sigma\,(Z_{(k)})} \tag{3.15}$$

Where, $\mathbf{Z_{std}}$ is the standardized anomalies **Z** of step 5, and μ(Z) and σ(Z) are the mean and standard deviation of **Z**, respectively.

7) Apply $\mathbf{Z_{std}}$ in equations (3.6), (3.7), (3.8), and (3.9) with the estimated parameters (μ_{X0}, μ_{X1}, μ_{N0}, μ_{N1} ,σ_{X0}, σ_{X1}, σ_{N0}, and σ_{N1}) to calculate $\mathbf{T_X}$ and $\mathbf{T_N}$.

8) Convert the anomalies **Z** of **WS** to be uniform distributed between 0 and 1 $\mathbf{Z_U}$, as follows;

$$Z_{U(k)} = 0.5 \times erf\left(\frac{Z_{(k)} - \mu\left(Z_{(k)}\right)}{\sqrt{2}\,\sigma\left(Z_{(k)}\right)}\right) + 0.5 \tag{3.16}$$

9) Apply $\mathbf{Z_U}$ in equations (3.11) and (3.12) with the estimated parameters (α_0, α_1, β_0, and β_1) to calculate **WS**. Steps 3 to 9 enable us to preserve observation statistics of $\mathbf{T_X}$, $\mathbf{T_N}$ and **WS** and the auto, spatial, and cross correlations with consideration of the precipitation states effects through decomposing their distribution functions.

10) Repeat steps 1 to 9 for all months m.

3.5. Case Study and Data

The developed PR-WG was tested in the Diyala River Basin, which is a transboundary basin between Iran and Iraq with total stream length of 217 km and basin area of 16,760 km^2 above Derbendikhan Dam, as shown in Figure 3.2. In previous work, Waheed et al., (2019) implemented the daily weather data [e.g., precipitation, maximum and minimum temperature, and wind speed] in this basin at 0.5^o spatial resolution from 1948 to 2006 and explained the implementation procedure.

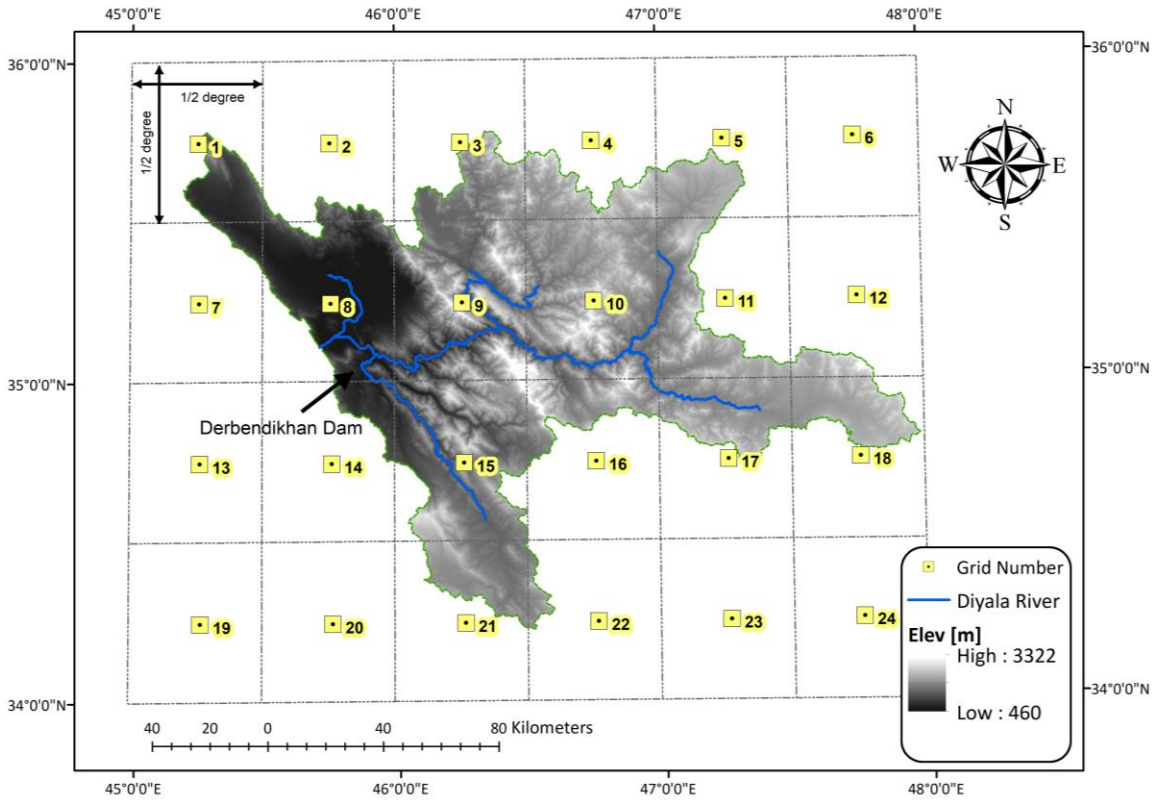

Figure 3.2: Diyala River basin in Iraq with grid numbers.

3.6. Results and Discussion

3.6.1. Model Performance Evaluation

The PR-WG was tested for its daily performance with historic observations for the period between 1948 and 2006 in a grid composed of 24 grid-cells. The Kling–Gupta efficiency [KGE; Gupta et al., 2009], was used to evaluate the PR-WG's ability to produce spatially correlated precipitation states S similar to the observed values. The KGE examines the bias of mean, standard deviation, and correlation [Steinschneider et al., 2015a], as follows:

$$KGE = 1 - \sqrt{\left(\frac{\mu_{sim}}{\mu_{obs}} - 1\right)^2 + \left(\frac{\sigma_{sim}}{\sigma_{obs}} - 1\right)^2 + (\rho - 1)^2} \quad (3.17)$$

Where μ_{obs}, σ_{obs}, μ_{sim}, and σ_{sim} are the mean and standard deviation of the observations and simulations (e.g., the PR-WG outcomes), respectively, and ρ is the correlation coefficient between the observations and simulations.

Figure 3.3 shows the comparison of 10 daily simulations of PR-WG of monthly dry and wet occurrences in gray color dots, and the average of those 10 simulations is plotted in blue dots. It is evident that the model works well to produce the number of dry and wet days, with a KGE of 0.97. This result demonstrates the ability of FTMC to produce the precipitation states well [e.g., Chen and Brissette, 2014b; Acharya et al., 2017]. Figure 3.4 shows a comparison of pairwise correlations of precipitation states for each calendar month with a 1-1 line for reference. It can be seen that the correlations are captured well by the PR-WG. The overall KGE value is 0.98.

Figure 3.5 demonstrates the PR-WG performance to produce the statistical parameters (e.g. mean, standard deviation, and skewness) of the four weather variables. The comparisons were done on monthly basis for the 24 grid-cells with a 1-1 line for reference. A series of 1000 years was generated to reduce the sampling bias and uncertainty in the simulations. However, the monthly means of all variables and the standard deviations for T_X, T_N and WS perfectly

produced by the model (KGE ≈1), while σ_p, and γ_p are reasonably preserved (KGE =0.97 and 0.89).

The slight discrepancies are due to the stochastic nature of the process [Chen et al., 2012].

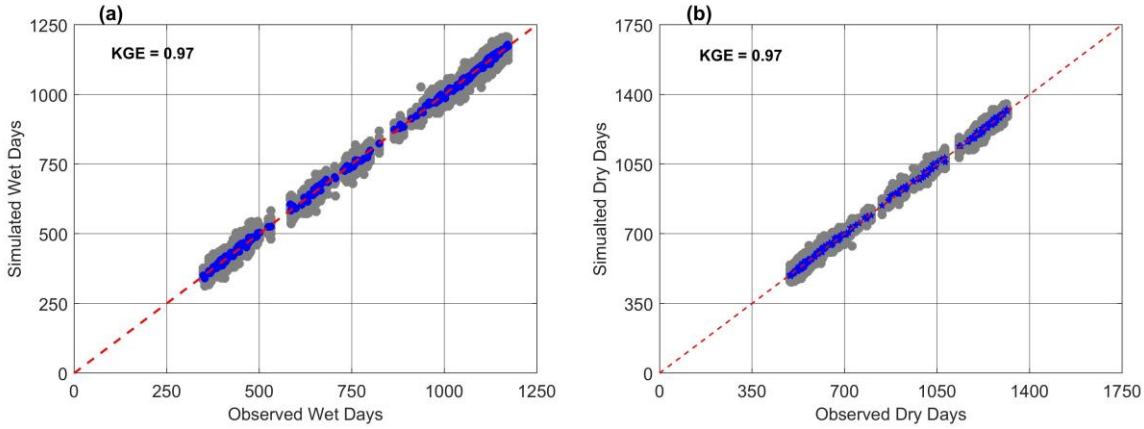

Figure 3.3: Comparison of the precipitation states between the observations and simulations for all months with 1-1 line for reference.

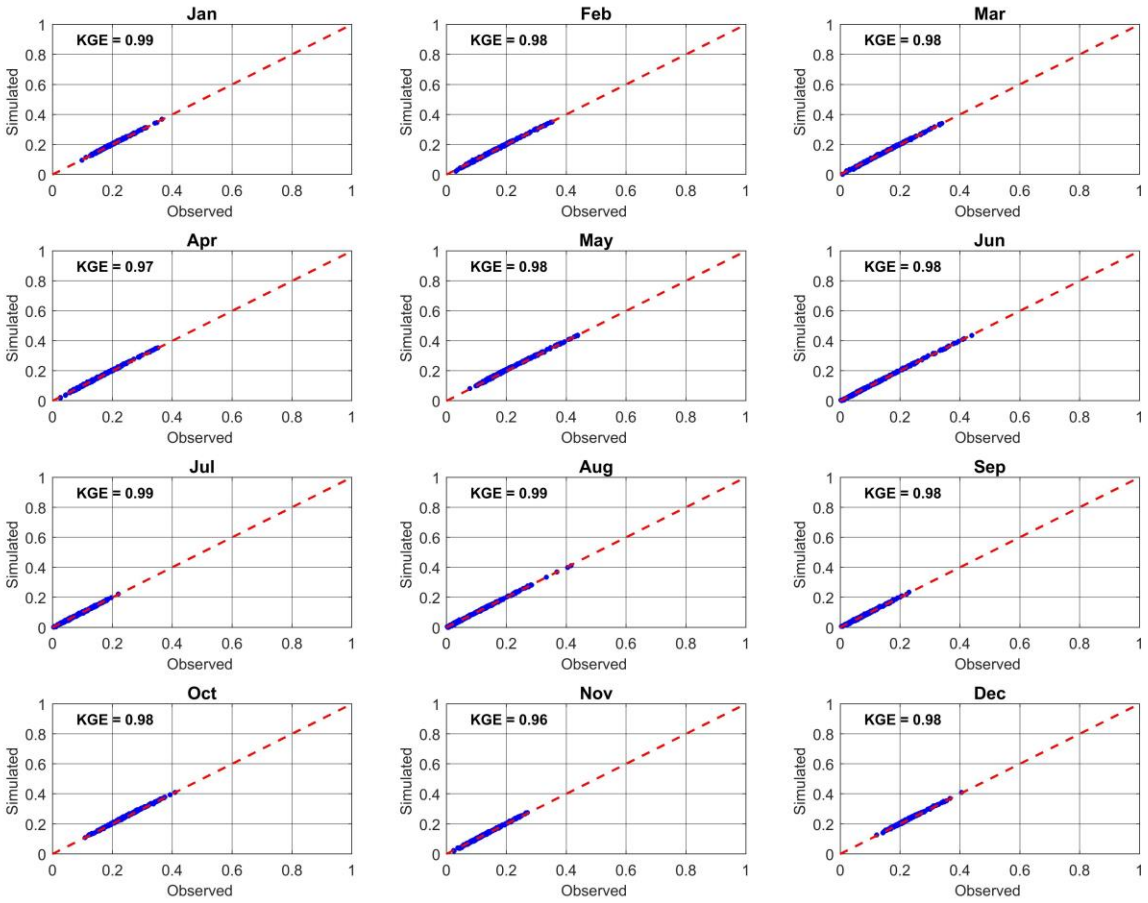

Figure 3.4: Comparison of the precipitation state correlation between the observations and simulations for each month with 1-1 line for reference.

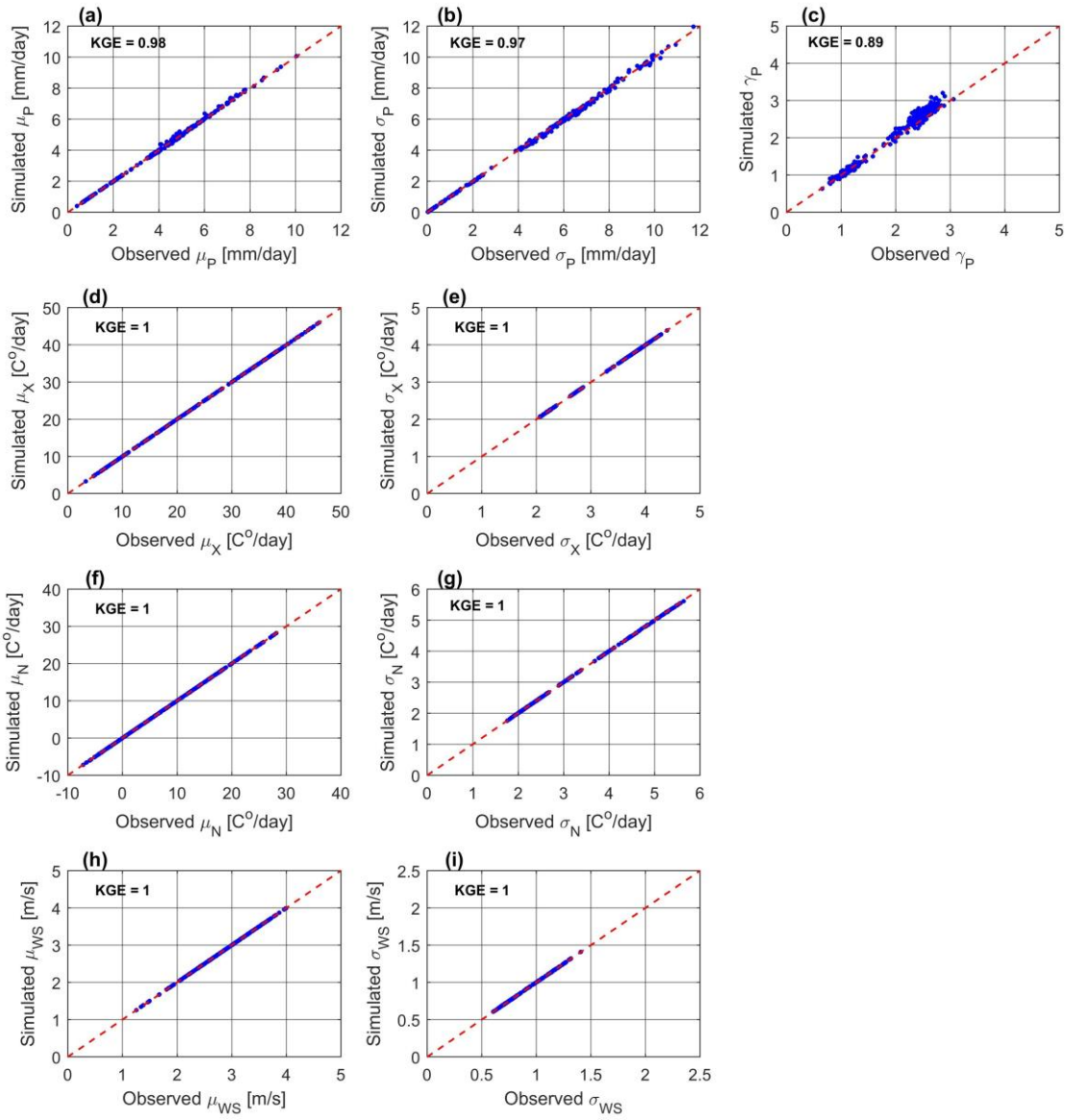

Figure 3.5: Comparisons of the monthly statistic parameters of the observations and simulations with 1-1 line for reference. (a), (b), and (c) mean, standard deviation, and skewness of P. (d), (e) (f), and (g) mean and standard deviation of T_X and T_N. (h) and (i) mean and standard deviation of WS.

Figure 3.6 shows the spatial and cross correlation coefficient matrices of the observations and simulations for one month (e.g., m=1), while Figure 3.7 show the spatial and cross correlation comparison for all variable for each m. The number of columns of **V** matrix [see section 3.4.1.] are 4 × 24 = 96. Therefore, the **V** dimensions are 96 × 96, in which, 1 to 24 for P, 25 to 48 for T_X, 49 to 72 for T_N, and 73 to 96 for WS. It can be observed from Figure 3.6 that the observed

correlation among the variables varies greatly across them. P and WS are slightly less spatially correlated as compared with T_X and T_N. Those facts are in line with Srivastav and Simonovic, (2015) and Verdin et al., (2019). It is also noticeable form Figure 3.6 and Figure 3.7 that the model preserves well the spatial and cross correlation among the variables. The overall KGE value is 0.96.

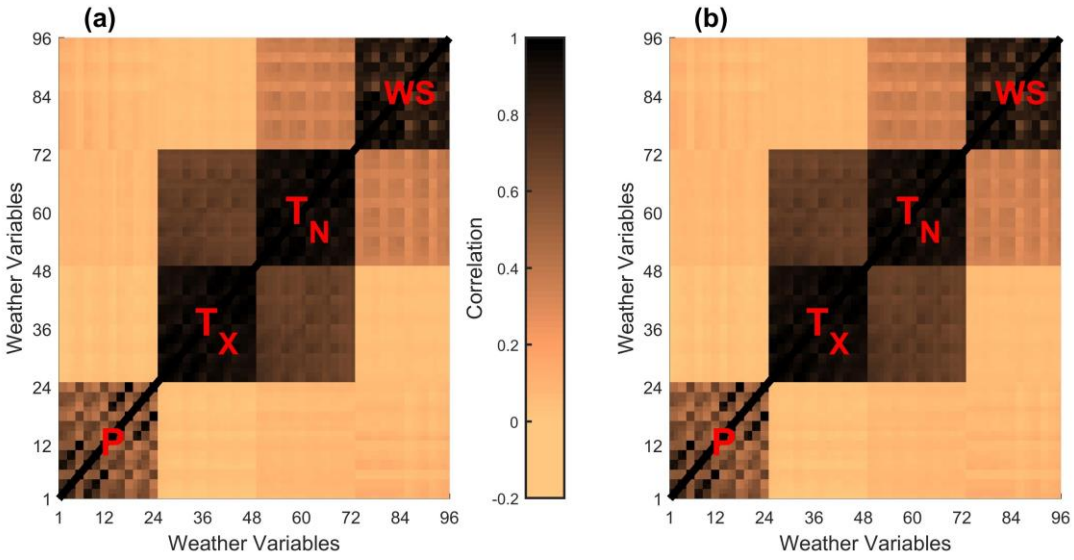

Figure 3.6: Spatial and cross correlation coefficients of observed and simulated variables.

Finally, Figure 3.8 demonstrates the performance of the PR-WG to preserve the lag-1 day auto-correlations of T_X, T_N, and WS. It is noticeable that the values differ from month to month, and less for WS comparing with T_X and T_N. However, the PR-WG captures those monthly variations very well regardless of their magnitudes with overall KGE value of 0.97.

3.6.2. Model Validation

In some cases, the proposed SWG produces negative values for precipitation. Meyer, (2011) indicated that the SN is not suitable when the skewness is greater than 4.5. However, in the study area, values of the skewness have not exceeded 4.5 [see Figure 3.5 c],], therefore SN is applicable. The negatives were checked and found to be less than 3% of the whole 1000-year

time series in the 24 grid-cells. The suggestion of Srivastav and Simonovic (2015) to round the negative values to zero was considered, but it affects the number of wet and dry calculations and the statistical parameters of precipitation. Instead, the negatives were rounded to 0.1 mm/day, which is assumed to be the minimum precipitation amount [see Section 3.3.1.]. This correction approach for negative values illustrates the slight differences in the simulated σ_p, and γ_p [see Figure 3.4 b and c]. The user could apply another distribution function in cases where SN is not applicable such as mixed-exponential [Roldan and Woolhiser, 1982; Wilks, 1999], log-normal, gamma, … etc. The key advantage of PR-WG is its flexibility in adopting any distribution of interest, such as these.

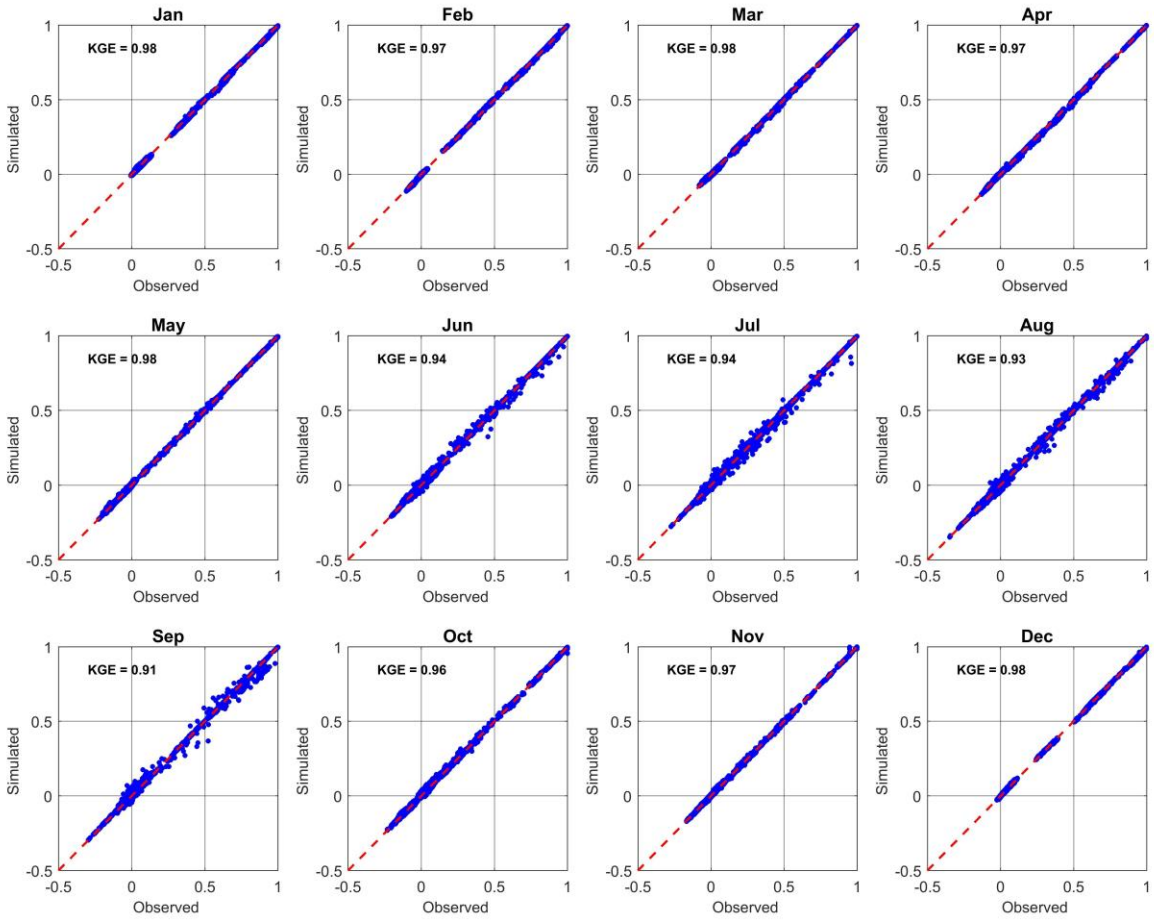

Figure 3.7: Spatial and cross correlation comparison of the weather variables for each month with 1-1 line for reference.

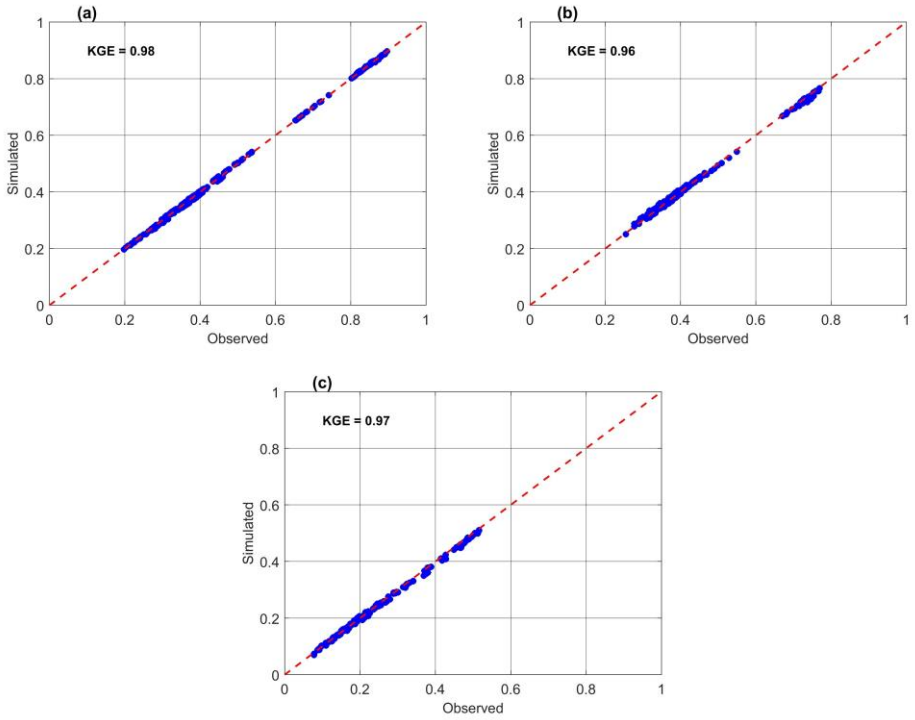

Figure 3.8: Autocorrelation Lag-1 of the weather variables of the weather variables T_x, T_N, and WS, respectively for all months with 1-1 line for reference.

The second validation was done by checking if T_N is greater than T_X and found to be less than 1% of the whole 1000-year time series in the 24 grid-cells. Li and Babovic, (2018) suggested to force T_X to be greater than T_N through setting T_N equal to T_X minus 1. This procedure will affect the auto-correlation of the T_N. Instead, Chen et al., (2012) approach was applied as follows, If T_X <T_N then,

$$T_{X(k,t,m)} = T_{N(k,t,m)} + (\mu_{\mu x(k,m)} - \mu_{\mu N(k,m)}) + \sqrt{\sigma^2_{X(k,m)} - \sigma^2_{N(k,m)}} \times z_{std(k,t,m)} \quad (3.18)$$

$$for \ \mathbb{I}_{[\sigma X_{(k,t,m)} \geq \sigma N_{(k,t,m)}]}$$

$$T_{X(k,t,m)} = T_{N(k,t,m)} + (\mu_{\mu x(k,m)} - \mu_{\mu N(k,m)}) + \sqrt{\sigma^2_{X(k,m)} - \sigma^2_{N(k,m)}} \times z_{std(k,t,m)} \quad (3.19)$$

$$for \quad \mathbb{I}_{[\sigma X_{(k,t,m)} < \sigma N_{(k,t,m)}]}$$

Equations (3.18) and (3.19) are conditioned on the precipitation states. For example, the σ and μ will turn to condition 0 if S=0. In this case, the T_X is guaranteed to be greater than T_N and

the auto, spatial, and cross correlations are preserved since they are multiplied by the anomalies z_{std}.

3.7. Conclusions

It was shown that PR-WG accurately preserves the statistical properties (mean, standard deviation, and skewness coefficient) of the weather variables (overall KGE test value was 0.98). The PR-WG also preserves the spatial, temporal, and cross correlations among the weather variables. While other SWGs may have more features, the one developed in this study enables the risk assessment study to be implemented in areas subjected to limited data availability.

PR-WG effectively estimates the dry and wet day occurrences using FTMC with an overall KGE value of 0.97, a result that is in line with those of Chen and Brissette, (2014b) and Acharya et al., (2017). The results also demonstrate the effectiveness of Wilks' technique to produce spatially correlated precipitation states (KGE of 0.98) and spatially and cross correlated weather variables (KGE of 0.96) beside the temporally correlated (KGE of 0.97).

While the PR-WG was validated in the Diyala River basin, it should be effective and applicable in other places and with other weather variables, such as solar radiation. The advantages of PR-WG are its flexibility to select any distribution function for each weather variable, ability to simulate any number of years within or beyond the historic observation length, capability to generate values outside the observation range, and ability to produce synthetic scenarios through alteration of the weather variable parameters for study of climate change impacts. The PR-WG is easy to construct and understand with little computational intensity to build spatial and cross correlation matrices of the anomalies. Increasing computational power will facilitate the work.

References

Acharya, Nachiketa, Allan Frei, Jie Chen, Leslie DeCristofaro, and Emmet M. Owens. "Evaluating stochastic precipitation generators for climate change impact studies of New York City's primary water supply." Journal of Hydrometeorology18.3 (2017): 879-896.

Ailliot, Pierre, Craig Thompson, and Peter Thomson. "Space–time modelling of precipitation by using a hidden Markov model and censored Gaussian distributions." Journal of the Royal Statistical Society: Series C (Applied Statistics) 58.3 (2009): 405-426.

Apipattanavis, Somkiat, Guillermo Podestá, Balaji Rajagopalan, and Richard W. Katz. "A semiparametric multivariate and multisite weather generator." Water Resources Research43.11 (2007).

Back, Larissa E., and Christopher S. Bretherton. "The relationship between wind speed and precipitation in the Pacific ITCZ." Journal of climate 18.20 (2005): 4317-4328.

Baigorria, Guillermo A., and James W. Jones. "GiST: A stochastic model for generating spatially and temporally correlated daily rainfall data." Journal of Climate 23.22 (2010): 5990-6008.

Bardossy, A., and G. G. S. Pegram. "Copula based multisite model for daily precipitation simulation." Hydrology and Earth System Sciences 13.12 (2009): 2299.

Beersma, Jules J., and T. Adri Buishand. "Multi-site simulation of daily precipitation and temperature conditional on the atmospheric circulation." Climate Research 25.2 (2003): 121-133.

Breinl, Korbinian, Thea Turkington, and Markus Stowasser. "Simulating daily precipitation and temperature: a weather generation framework for assessing hydrometeorological hazards." Meteorological Applications 22.3 (2015): 334-347.

Breinl, Korbinian, Thea Turkington, and Markus Stowasser. "Stochastic generation of multi-site daily precipitation for applications in risk management." Journal of hydrology 498 (2013): 23-35.

Brissette, F. P., M. Khalili, and Robert Leconte. "Efficient stochastic generation of multi-site synthetic precipitation data." Journal of Hydrology 345.3 (2007): 121-133.

Brown, Casey, and Robert L. Wilby. "An alternate approach to assessing climate risks." Eos, Transactions American Geophysical Union 93.41 (2012): 401-402.

Buishand, T. Adri, and Theo Brandsma. "Multisite simulation of daily precipitation and temperature in the Rhine basin by nearest-neighbor resampling." Water Resources Research37.11 (2001): 2761-2776.

Burton, A., Chris G. Kilsby, Hayley J. Fowler, P. S. P. Cowpertwait, and P. E. O'connell. "RainSim: A spatial–temporal stochastic rainfall modelling system." Environmental Modelling & Software 23.12 (2008): 1356-1369.

Cannon, Alex J. "Probabilistic multisite precipitation downscaling by an expanded Bernoulli–Gamma density network." Journal of Hydrometeorology 9.6 (2008): 1284-1300.

Chen, J., Brissette, F. P., Leconte, R., & Caron, A. "A versatile weather generator for daily precipitation and temperature." Transactions of the ASABE 55.3 (2012): 895-906.

Chen, Jie, and François P. Brissette. "Comparison of five stochastic weather generators in simulating daily precipitation and temperature for the Loess Plateau of China." International Journal of Climatology 34.10 (2014b): 3089-3105.

Chen, Jie, and François P. Brissette. "Stochastic generation of daily precipitation amounts: review and evaluation of different models." Climate Research 59.3 (2014a): 189-206.

Chen, Jie, Chao Li, François P. Brissette, Hua Chen, Mingna Wang, and Gilles RC Essou. "Impacts of correcting the inter-variable correlation of climate model outputs on hydrological modeling." Journal of Hydrology 560 (2018): 326-341.

Chen, Jie, François P. Brissette, and Xunchang J. Zhang. "A multi-site stochastic weather generator for daily precipitation and temperature." Transactions of the ASABE 57.5 (2014): 1375-1391.

Chen, Jie, François P. Brissette, and Xunchang J. Zhang. "Hydrological modeling using a multisite stochastic weather generator." Journal of Hydrologic Engineering 21.2 (2015): 04015060.

Culley, Sam, S. Noble, A. Yates, M. Timbs, S. Westra, H. R. Maier, Matteo Giuliani, and Andrea Castelletti. "A bottom-up approach to identifying the maximum operational adaptive capacity of water resource systems to a changing climate." Water Resources Research 52.9 (2016): 6751-6768.

Davidson, Russel, and Andrea Monticini. Heteroskedasticity-and-autocorrelation-consistent bootstrapping. No. 12. Working Paper, 2014.

Dresen, Martin "What kind of data is needed to identify climate impacts? How can data be managed and organized through data catalogues?" A Desk-Study. geoSYS, Nansenstr. 17, 12047 Berlin, Germany (2011).

Fowler, H. J., C. G. Kilsby, P. E. O'connell, and A. Burton. "A weather-type conditioned multi-site stochastic rainfall model for the generation of scenarios of climatic variability and change." Journal of Hydrology 308.1 (2005): 50-66.

Furrer, Eva M., and Richard W. Katz. "Improving the simulation of extreme precipitation events by stochastic weather generators." Water Resources Research 44.12 (2008).

Gupta, Hoshin V., Harald Kling, Koray K. Yilmaz, and Guillermo F. Martinez. "Decomposition of the mean squared error and NSE performance criteria: Implications for improving hydrological modelling." Journal of hydrology 377.1-2 (2009): 80-91.

Hallegatte, Stéphane, Ankur Shah, Robert Lempert, Casey Brown, and Stuart Gill. "Investment decision making under deep uncertainty." Policy research working paper 6193 (2012): 1-41.

Harmel, R. D., C. W. Richardson, C. L. Hanson, and G. L. Johnson. "Evaluating the adequacy of simulating maximum and minimum daily air temperature with the normal distribution." Journal of applied meteorology 41.7 (2002): 744-753.

Harmel, R. D., C. W. Richardson, C. L. Hanson, and G. L. Johnson. "Simulating maximum and minimum daily temperature with the normal distribution." 2001 ASAE Annual Meeting. American Society of Agricultural and Biological Engineers, (2001).

Haugen, Annika, Chiara Bertolin, Gustaf Leijonhufvud, Tone Olstad, and Tor Broström. "A Methodology for Long-Term Monitoring of Climate Change Impacts on Historic Buildings." Geosciences 8.10 (2018): 370.

Khalili, Malika, François Brissette, and Robert Leconte. "Effectiveness of Multi-Site Weather Generator for Hydrological Modeling." JAWRA Journal of the American Water Resources Association 47.2 (2011): 303-314.

Khalili, Malika, François Brissette, and Robert Leconte. "Stochastic multi-site generation of daily weather data." Stochastic environmental research and risk assessment 23.6 (2009): 837-849.

Khalili, Malika, Robert Leconte, and François Brissette. "Stochastic multisite generation of daily precipitation data using spatial autocorrelation." Journal of hydrometeorology8.3 (2007): 396-412.

King, Leanna M., A. Ian McLeod, and Slobodan P. Simonovic. "Improved weather generator algorithm for multisite simulation of precipitation and temperature." JAWRA Journal of the American Water Resources Association 51.5 (2015): 1305-1320.

King, Leanna M., A. Ian McLeod, and Slobodan P. Simonovic. "Simulation of historical temperatures using a multi-site, multivariate block resampling algorithm with perturbation." Hydrological Processes 28.3 (2014): 905-912.

Leander, Robert, and T. Adri Buishand. "A daily weather generator based on a two-stage resampling algorithm." Journal of hydrology 374.3 (2009): 185-195.

Li, Chao, Eva Sinha, Daniel E. Horton, Noah S. Diffenbaugh, and Anna M. Michalak. "Joint bias correction of temperature and precipitation in climate model simulations." Journal of Geophysical Research: Atmospheres 119.23 (2014a): 13-153.

Li, Xin, and Vladan Babovic. "A new scheme for multivariate, multisite weather generator with inter-variable, inter-site dependence and inter-annual variability based on empirical copula approach." Climate Dynamics (2018): 1-21.

Li, Zhi, Francois Brissette, and Jie Chen. "Assessing the applicability of six precipitation probability distribution models on the Loess Plateau of China." International Journal of Climatology 34.2 (2014b): 462-471.

Li, Zhi. "A new framework for multi-site weather generator: a two-stage model combining a parametric method with a distribution-free shuffle procedure." Climate dynamics 43.3-4 (2014): 657-669.

Marcon, Giulia, Philippe Naveau, and Simone Padoan. "A semi-parametric stochastic generator for bivariate extreme events." Stat 6.1 (2017): 184-201.

Maree, Stef. Correcting Non Positive Definite Correlation Matrices. (2012). B.Sc Thesis in Applied Mathematics, TU Delft.

Mehan, Sushant, Tian Guo, Margaret Gitau, and Dennis C. Flanagan. "Comparative study of different stochastic weather generators for long-term climate data simulation." Climate 5.2 (2017): 26.

Mehrotra, R., R. Srikanthan, and Ashish Sharma. "A comparison of three stochastic multi-site precipitation occurrence generators." Journal of Hydrology 331.1 (2006): 280-292.

Mehrotra, Rajeshwar, Jingwan Li, Seth Westra, and Ashish Sharma. "A programming tool to generate multi-site daily rainfall using a two-stage semi parametric model." Environmental Modelling & Software 63 (2015): 230-239.

Mehrotra, Rajeshwar, Seth Westra, Ashish Sharma, and Ratnasingham Srikanthan. "Continuous rainfall simulation: 2. A regionalized daily rainfall generation approach." Water Resources Research 48.1 (2012).

Meyer, C. "General description of the CLIGEN model and its history." USDA-ARS National Soil Erosion Laboratory: West Lafayette, IN (2011).

Moody, Paul, and Casey Brown. "Robustness indicators for evaluation under climate change: Application to the upper Great Lakes." Water Resources Research 49.6 (2013): 3576-3588.

Mukundan, Rajith, Nachiketa Acharya, Rakesh K. Gelda, Allan Frei, and Emmet M. Owens. "Modeling streamflow sensitivity to climate change in New York City water supply streams using a stochastic weather generator." Journal of Hydrology: Regional Studies 21 (2019): 147-158.

Nadarajah, Saralees. "A review of results on sums of random variables." Acta Applicandae Mathematicae 103.2 (2008): 131-140.

Nicks, A. D., and G. A. Gander. "CLIGEN: A weather generator for climate inputs to water resource and other models." Proc. Fifth Int. Conf. on Computers in Agriculture. 1994.

Pegram, Geoffrey GS. "A nested multisite daily rainfall stochastic generation model." Journal of Hydrology 371.1 (2009): 142-153.

Pobocikova, Ivana, Zuzana Sedliackova, and Mária Michalkova. "Application of four probability distributions for wind speed modeling." Procedia engineering 192 (2017): 713-718.

Qian, Budong, Joao Corte-Real, and Hong Xu. "Multisite stochastic weather models for impact studies." International Journal of climatology 22.11 (2002): 1377-1397.

Rajagopalan, Balaji, and Upmanu Lall. "A k-nearest-neighbor simulator for daily precipitation and other weather variables." Water resources research 35.10 (1999): 3089-3101.

Richardson, Clarence W. "Stochastic simulation of daily precipitation, temperature, and solar radiation." Water resources research 17.1 (1981): 182-190.

Roldan, Jose., and David. A.Woolhiser. "Stochastic daily precipitation models: 1. A comparison of occurrence processes." Water resources research 18.5 (1982): 1451-1459.

Schaake, John, Jean Pailleux, Jutta Thielen, Ray Arritt, Tom Hamill, Lifeng Luo, Eric Martin, Doug McCollor, and Florian Pappenberger. "Summary of recommendations of the first workshop on Postprocessing and Downscaling Atmospheric Forecasts for Hydrologic Applications held at Météo-France, Toulouse, France, 15–18 June 2009." Atmospheric Science Letters 11.2 (2010): 59-63.

Seneviratne, Sonia I., Neville Nicholls, David Easterling, Clare M. Goodess, Shinjiro Kanae, James Kossin, Yali Luo et al. "Changes in climate extremes and their impacts on the natural physical environment." (2017).

Serinaldi, Francesco. "A multisite daily rainfall generator driven by bivariate copula-based mixed distributions." Journal of Geophysical Research: Atmospheres 114.D10 (2009).

Srivastav, Roshan K., and Slobodan P. Simonovic. "Multi-site, multivariate weather generator using maximum entropy bootstrap." Climate Dynamics 44.11-12 (2015): 3431-3448.

Steinschneider, Scott, and Casey Brown. "A semiparametric multivariate, multisite weather generator with low-frequency variability for use in climate risk assessments." Water resources research 49.11 (2013): 7205-7220.

Steinschneider, Scott, Rachel McCrary, Sungwook Wi, Kevin Mulligan, Linda O. Mearns, and Casey Brown. "Expanded decision-scaling framework to select robust long-term water-system plans under hydroclimatic uncertainties." Journal of Water Resources Planning and Management 141.11 (2015b): 04015023.

Steinschneider, Scott, Sungwook Wi, and Casey Brown. "The integrated effects of climate and hydrologic uncertainty on future flood risk assessments." Hydrological Processes 29.12 (2015a): 2823-2839.

Stephenson, David B., Matthew Collins, Jonathan C. Rougier, and Richard E. Chandler. "Statistical problems in the probabilistic prediction of climate change." Environmetrics23.5 (2012): 364-372.

Turner, Sean WD, David Marlow, Marie Ekström, Bruce G. Rhodes, Udaya Kularathna, and Paul J. Jeffrey. "Linking climate projections to performance: A yield-based decision scaling assessment of a large urban water resources system." Water Resources Research 50.4 (2014): 3553-3567.

Verdin, Andrew, Balaji Rajagopalan, William Kleiber, Guillermo Podestá, and Federico Bert. "BayGEN: A Bayesian space-time stochastic weather generator." Water Resources Research (2019).

Waheed, Saddam, Neil S. Grigg, and Jorge A. Ramirez. "Variable Infiltration Capacity Model Sensitivity, Parameter Uncertainty, and Data Augmentation for the Diyala River Basin in Iraq. Under reviewing, Journal of American Society of Civil Engineers (2019).

Wang, Wenting, Dennis C. Flanagan, Shuiqing Yin, and Bofu Yu. "Assessment of CLIGEN precipitation and storm pattern generation in China." CATENA 169 (2018): 96-106.

Weaver, Christopher P., Robert J. Lempert, Casey Brown, John A. Hall, David Revell, and Daniel Sarewitz. "Improving the contribution of climate model information to decision making: the value and demands of robust decision frameworks." Wiley Interdisciplinary Reviews: Climate Change 4.1 (2013): 39-60.

Whateley, Sarah, Scott Steinschneider, and Casey Brown. "A climate change range-based method for estimating robustness for water resources supply." Water Resources Research 50.11 (2014): 8944-8961.

Wilby, R. L., O. J. Tomlinson, and C. W. Dawson. "Multi-site simulation of precipitation by conditional resampling." Climate Research 23.3 (2003): 183-194.

Wilby, Robert L., and Suraje Dessai. "Robust adaptation to climate change." Weather 65.7 (2010): 180-185.

Wilks, Daniel. S. "Multisite generalization of a daily stochastic precipitation generation model." Journal of Hydrology 210.1 (1998): 178-191.

Wilks, Daniel. S. "Simultaneous stochastic simulation of daily precipitation, temperature and solar radiation at multiple sites in complex terrain." Agricultural and Forest meteorology 96.1 (1999): 85-101.

Wilks, Daniel. S. "A gridded multisite weather generator and synchronization to observed weather data." Water resources research 45.10 (2009).

Wilks, Daniel S. Statistical methods in the atmospheric sciences. Vol. 100. Academic press, 2011.

Zhang, Enze, Xin'an Yin, Zhihao Xu, and Zhifeng Yang. "Bottom-up quantification of inter-basin water transfer vulnerability to climate change." Ecological Indicators 92 (2018): 195-206.

CHAPTER 4

Nonstationary-Probabilistic Decision Framework to Assess the Long-Term Water Resources System Vulnerability under Climate Change and Quantify the Robust Plan and Timing[3]

Chapter Synopsis

Multi-objective water resources systems require long-term operational plans that consider vulnerability to failure under nonstationary conditions due to climate change. The paper presents a probabilistic decision-making framework under nonstationary assumptions to evaluate the robustness of the pre-selected plans and identify the optimal plan using a genetic algorithm approach. The framework incorporates a new metric for maximum allowable time to apply the adaptations and maintaining operational targets without penalties. The framework has four stages for climate exposure identification, production of water supply scenarios, generation of water demand scenarios, and evaluation of system performance. Hydrologic variables considered include precipitation, temperature, and wind speed. The Diyala River Basin in Iraq was used as a case study to test the effectiveness of the framework. Three synthetic pre-selected plans were developed by reducing the demand ratios of the system. Results indicate that current operational rules are robust for flood protection but vulnerable in drought periods. Precipitation changes were dominant in flood and drought management, and temperature and wind speed change effects were significant during drought. Results demonstrated the framework effectiveness to quantify detrimental climate change effects, provide long-term guides for

[3] Under Review in Hydrologic Processes Journal, Saddam Q. Waheed, Neil S. Grigg, Jorge A. Ramirez (2020)

operational planning, and identify the upper limit application time of the adaptation strategies in the system to avert the climate change impact. Framework application suggests an optimal adaptation strategy, robustness examination of the pre-suggested plans, and identify the maximum allowable time for the robust plans. The study represents the first attempt to consider nonstationary hydroclimatic conditions in simulation of supply, demand, and system loss scenarios.

4.1. Introduction

Climate change affects the availability and quality of water in space and time and the frequency of floods and droughts. It requires risk analysis for reservoir operations because conflicts between water supply and demand are increasing and affecting both performance and equity [Wang et al., 2019; Tian et al., 2019]. The resulting non-stationarity in hydroclimatic statistics may invalidate assumptions upon which systems were planned and new approaches may be stimulated [Solomon et al., 2007; Milly et al., 2008; Stocker et al., 2013; Paton et al., 2013; Villarini et al., 2009; Whateley et al., 2014; Culley et al., 2016; Spence and Brown 2016]. Impetus to improve system performance under climate variations and use existing infrastructure better is driven by the high cost of upgrading systems [e.g., Paton et al., 2014; Beh et al., 2015; Steinschneider et al., 2015a; Giuliani et al., 2016].

To address system vulnerability, adaptation strategies such as changes in demand management can reduce risks and avert undesirable impacts [Turner et al., 2014; Whateley et al., 2014; Culley et al., 2016; Azhoni et al., 2018]. In practice, decision makers aim to achieve multiple objectives by evaluating the robustness of the pre-suggested plans and the decision-making process should provide the best strategy from a set of pre-specified possible options

[Herman, et al., 2015; Golfam et al., 2019]. Optimization methods can indicate non-inferior alternatives to maximize performance [Spence and Brown, 2016; Zhang, et al., 2018; Zhu et al., 2019; Taner et al., 2019].

Efforts to develop approaches for climate change impact assessments and adaptation suggestion are either top-down or bottom-up. In the traditional top-down approach, the performance of the water resources system is examined under discrete climate scenarios, often from the Global Climate Model (GCM) outputs. These scenarios are fed into a hydrologic model to generate future water supply scenarios and the performance of a water resources system is tested over those scenarios. GCM scenarios limit decision-making choices because they represent only specific discrete climate scenarios and lead to uncertain decisions [Wilby and Dessai, 2010; Hallegatte et al., 2012; Brown and Wilby, 2012; Stephenson et al., 2012; Whateley et al., 2014; Culley et al., 2016; Taner et al., 2019]. Moreover, GCMs are spatially coarse and do not capture the high-intensity precipitation that occurs at fine spatial scales [Spence and Brown, 2016].

To overcome this problem, a bottom-up approach uses a statistical weather generator (SWG) to produce a range of scenarios including some beyond the GCM bounds. These scenarios are implemented in hydrologic models to produce supply scenarios, and the system responses are evaluated. This provides insights into expected system performance under climate change, enables better testing and leads to the most robust management alternative [Weaver et al., 2013; Turner et al., 2014; Steinschneider et al., 2015a; Zhang et al., 2018]. SWG scenarios can be linked with GCM scenarios and a probability of each scenario generated by the SWG can be estimated [e.g., Moody and Brown, 2013; Steinschneider et al., 2015b; and Taner et al., 2017].

The current approaches quantify climate change impact magnitudes, but not the timing. No study has been found to estimate the best timing (timeframe) to apply adaptation strategies. Also, wind speed magnitude effects have been considered in wind energy production [Pryor and Barthelmie, 2010; Jiang et al., 2010; Najac et al., 2011; Moemken et al., 2017; 2018], but no study was located in decision-making process. Previous work by the writers included preparation of weather data and development of a SWG (Waheed et al., 2020a; Waheed et al., 2020b). This paper builds on the past work to propose a decision-making framework under nonstationary assumptions to examine the robustness of pre-selected plans. The framework bolstered the previous work by Brown, et al., (2011); Whateley et al., (2014); Steinschneider, et al., (2015b); Culley, et al., (2016); Spence and Brown, (2016); Zhang, et al., (2018); Taner et al., (2019). It represents an advance by introducing new performance indicators to identify the timing and magnitude effects of climate change on water resources systems and consider the nonstationary in simulating the future water scenarios. The study includes new indicators and procedures to analyze of the impact of wind speed changes on evaluation of options. The study represents the first attempt to consider the nonstationary assumption on estimating the future water supply, demand, and system loss scenarios.

The proposed approach is also able to identify the theoretical optimal adaptation strategy and suggest the optimal timeframe for all possible climate scenarios and multiple performance objectives. The framework is capable in defending the applicability timeframe of the robust plans and provide the upper limit time of the adaptation strategies in the system to avert the climate change impact. The aim is to help optimize infrastructure operation as part of efforts to cope with negative climate change influences. The goal is to use a probabilistic approach under non-

stationarity hydroclimatic conditions to select the most efficient and robust alternative from Pareto-optimal sets. The paradigm is demonstrated for a case study of the Diyala River Basin (DRB) above Derbendikhan dam, located in Iraq.

4.2. Study Area and Previous Climate Change Studies in DRB

The Diyala River is the third largest tributary of the Tigris River in Iraq. It is transboundary and starts from the Zagros Mountains in Iran and crosses the Iran-Iraq border until its confluence with the Tigris River south of Baghdad. The total river length is about 445 km with total basin area of 32,600 km^2, of which 43% lies in Iraq. The basin is situated between 33.216° N and 35.833° N, and 44.500° E and 46.833° E. The main tributaries are the Sirwan, Tanjeru and Wand Rivers.

Two large dams are constructed within Iraq namely: Derbendikhan and Hemrin Dam [Hamza, 2012; Al-Faraj and Scholz, 2014; Al-Faraj et al., 2015; Abbas et al., 2016]. Derbendikhan Dam is one of the largest dams in Iraq, constructed between 1956 and 1961, and located about 285 km northeast of Baghdad (Coordinates 35°06'46"N and 45°42'23"E). It is a multi-purpose system for drinking, irrigation, flood control, hydroelectric power production, and recreation; and the total reservoir storage is about 3 billion m^3 [Tofiq and Guven, 2014; Al-Jawad et al., 2019; Al-Khafaji and Al-Chalabi, 2019]. This paper is based on a study of the upper part of DRB to examine the operation of Derbendikhan dam. The total river length until Derbendikhan Dam is about 217 km and its basin area is about 16,760 km^2, as shown in Figure 4.1.

Forcing data for the basin was developed by Waheed et al., (2020a) with a daily time step and spatial resolution of 0.5^o, as shown in Figure 1 Figure 4.1 ©. Information on the dam and demand were obtained from the Iraqi ministry of Water Resources (MoWR) and Al-Jawad et al., (2019).

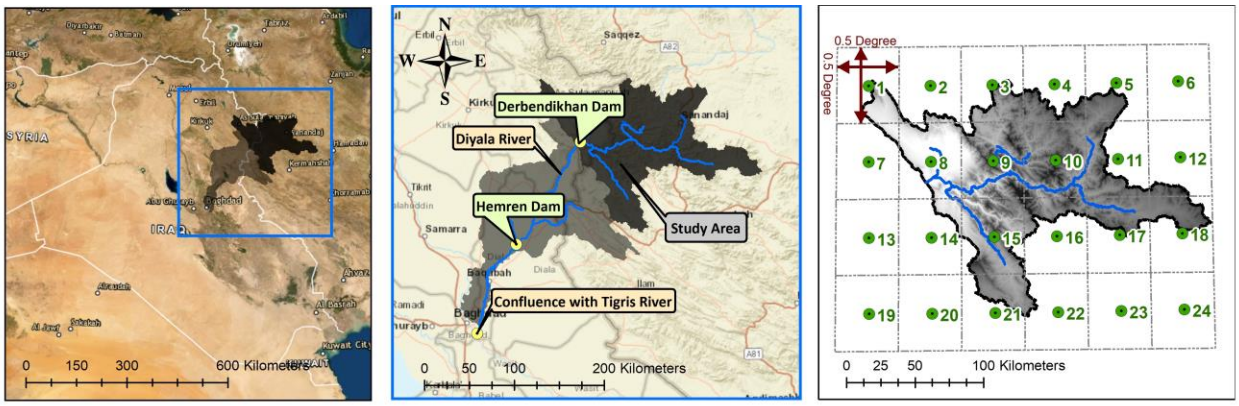

Figure 4.1: DRB location in Iraq with its grid numbers.

Few notable studies were located to investigate climate change impacts on the water availability in DRB. Waheed, (2013) studied the effects of climate change on water availability for the period (1990-2010) using the Hydrologic Engineering Center's Hydrologic Modeling System (USACE-HEC, 1998). The analysis removed the trend in the weather variables, then compared the resultant runoff with the observed. The results showed an increment in the monthly evapotranspiration of 4% to 13%, and a decrement in the surface runoff of 4.7 %. Al-Faraj et al., (2014) examined the sensitivity of the runoff reduction due to climate change. The results showed a change in the median flow between +5.3% to -62.7% for the period (1983–2013), and -28.2% to -77.5% for (1999–2013) and -23.6% to -76.8% for (2004–2013), as a comparison with the period (1955–1982). Abbas et al., (2016) studied the climate impact and the Reconnaissance Drought Index using the Soil and Water Assessment Tool (SWAT) with different six GCM outputs (e.g., top-down approach). With comparison to the period between 1979 and 2004, the results showed a decrease of 56%, 50% and 39% under A2, A1B and B1, respectively; and an increase of 14% under A2 and A1B scenarios. Al-Khafaji and Al-Chalabi, (2019) studied the impact of climate change on the streamflow and sediment yield with aid of SWAT for the period until 2050 of five GCM scenarios. Results showed a decrease in average monthly streamflow up to 49% as

compared with the historic period 1948 to 2013. Neither Abbas et al., (2016) nor Al-Khafaji and Al-Chalabi, (2019) studied or removed the bias in the GCM scenarios, which can explain the huge decrease in the future water availability. Al-Jawad et al., (2019) developed and applied a comprehensive optimal operation technique for a multiple-objective function. The methodology is applied for the historic period from 1981 and 2013 and projected two future scenarios by including the trends in the last seven years and the entire 33 years period. Although their results show improvement in the dam operation using the proposed model to decrease water deficit and recommended guidance to cope with it, they did not provide a framework to compare different plans to overcome the climate change impact. From review of these studies, it is apparent that a more comprehensive study using a bottom-up approach is required to evaluate the climate change impacts as well as to compare adaptation scenarios. In addition, more analysis is needed to examine the future scenario probabilities to help decision makers determine the desirable adaptation strategies.

4.3. Methodology and Proposed Framework

The suggested framework is categorized in four stages: (1) generation of climate exposure (2) calculation of water supply scenarios, (3) calculation of water demand scenarios, and (4) multi-objective assessment of system performance, as shown in Figure 4.2.

4.4.1. Generation of Climate Exposure

The first step is to identify the space of future climate exposure (Θ) in the study area. Climate exposure is defined as the sets of the hydro-climatological scenarios in the study area that will confront the system in the future [Culley et al., 2016]. These exposures were obtained from the GCM outputs in the area. To obtain GCM outputs for the area, the Coupled Model

Intercomparison Project 5 (CMIP5) data were selected for recommended models in the region [e.g., Bucchignani et al., 2016a; 2016b; 2018; Zolghadr-Asli et al., 2018; Ongoma et al., 2019], as shown in Table 4.1.

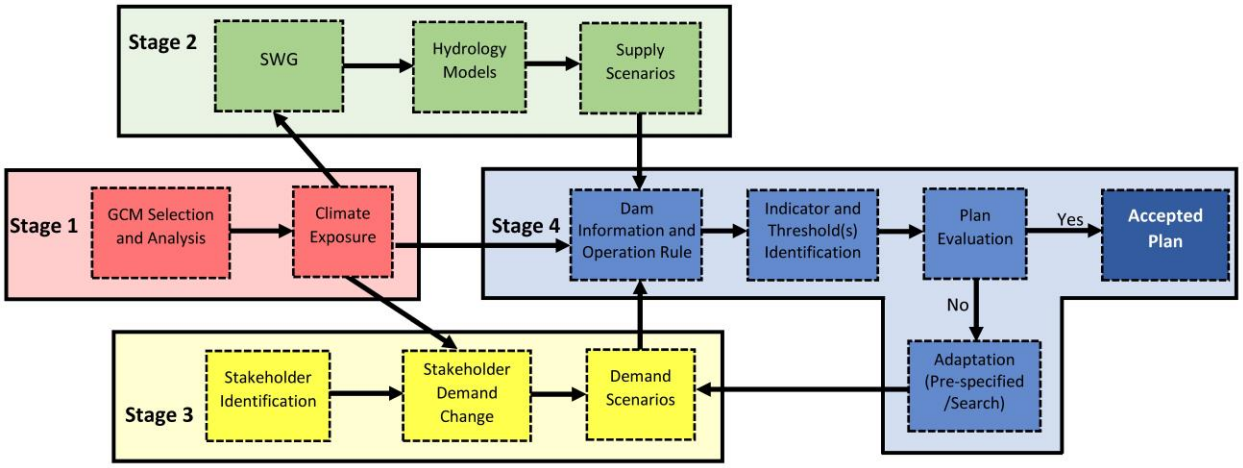

Figure 4.2: Conceptual flow chart of the proposed framework of infrastructure assessment for planning alternatives under climate change and nonstationary assumption.

Table 4.1: The selected CMIP5 assemble of GCMs, institutions, countries, and runs

Model	Institution	Country	Runs
CMCC	Centro Euro-Mediterraneo per I Cambiamenti Climatici	Italy	5
CSIRO-MK3.6.0	CSIRO-QCCCE	Australia	40
CanESM2	Canadian Centre for Climate Modelling and Analysis	Canada	15
		Total runs	60

Bias correction is necessary as the GCMs are afflicted with the systematic errors due to model formulation which precludes their direct application [Ehret et al., 2012; PaiMazumder and Done, 2015]. An empirical distribution correction (EDC) method with 100 integral quantiles was recommended [Lafon et al., 2013; Smitha et al., 2018; Gao et al., 2019]. The main idea of the EDC is to establish the relationship between observed and GCM-simulated daily data at the historical period then apply it to the projected GCM data.

Let gm and ob be the GCM and observed data, respectively with cumulative distribution functions (CDF) F_{GM} and F_{OB}. EDC remaps gm to ob so that their distributions are equivalent $[F_{GM}(gm) = F_{OB}(ob)]$. The corrected gm values are obtained as $\left[gm = F_{GM}^{-1}[F_{OB}(ob)]\right]$ where F^{-1} is the inverse function of CDF, as shown in Figure 4.3.

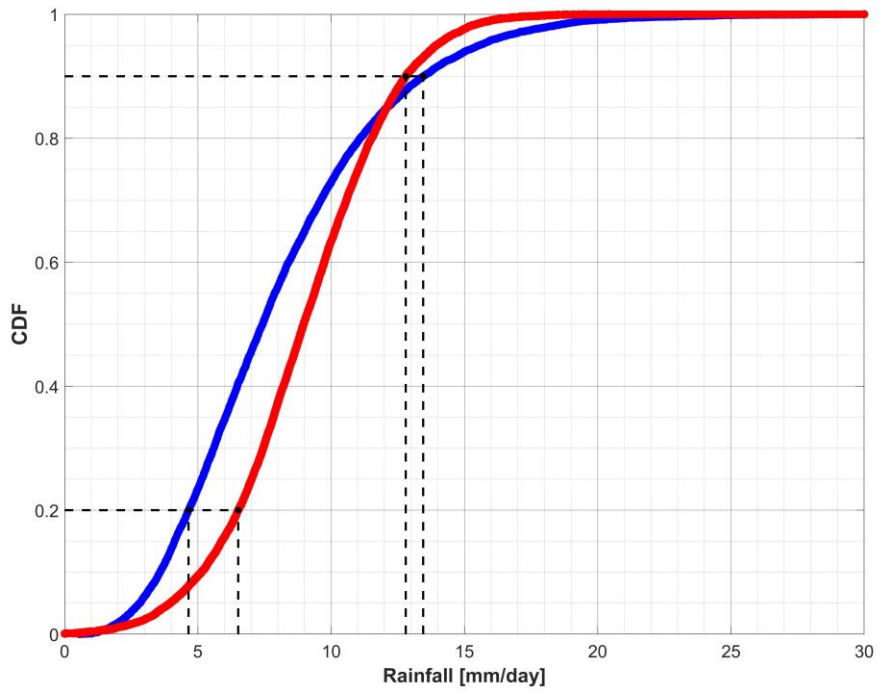

Figure 4.3: Schematic of the EDC with observed (red), simulated-GCM (blue) CDF of daily rainfall and the F^{-1} (black-dashed lines) is used for the correction [adopted from Lafon et al., 2013].

Insights about the total range of change and yearly increment of the weather variables were obtained from the unbiased GCM outputs. In this study, the nonstationary changes in four variables were examined: non-zero daily precipitation mean and its coefficient of variation (CV), temperature mean, and wind speed mean with linear function assumption [Spence and Brown, 2016]. The key innovation was to study the effect of wind speed effect on the decision-making process. Instead of comparing the historic data with the projected data to identify the change in each variable as suggested by other researchers [e.g., Whateley et al., 2014; Steinschneider et

al., 2015a; 2015b; Spence and Brown, 2016; Taner et al., 2017; 2019], a moving average function was applied to remove the noise in the projected data obtained from the EDC. Although the window length of the moving average is an open research question, a 30-year function was applied following the suggestion by Carter et al., (2000) and Ummenhofer and Gerald, (2017). To consider all the future variations, a linear regression line was applied to obtain the yearly increment in the four weather variables. Such that, $\mu\,(t) = \mu_o + \alpha_\mu\, t$ and $\gamma\,(t) = \gamma_o + \alpha_{CV}\, t$ where μ_o and γ_o are the intercepts, and α_μ and α_γ are the slope of the regression line for the mean and CV, respectively which represent their yearly increments. Then, multiplicative factors (for the precipitation mean and CV and wind speed mean) were used starting from 0% change in the historical precipitation and linearly increasing (or decreasing) up to the specified value in the final period (e.g., +30% of the historical value). For temperature changes, additive factors are applied starting from 0 °C and linearly increasing to the specified temperature increase value in the final period (e.g., +6 °C). According to the obtained range of total change in 80 years (α × 80) for each weather variable [see section 4.5.1.], the climate condition scenarios were suggested. In addition, 10 simulations (I) of each climate condition j were generated to examine the effects of internal climate variability [e.g., Whateley et al., 2014; Steinschneider et al., 2015a; 2015b]. The total number of climate exposures is K = J × I; $\Theta = \{\theta_1, \theta_2, \ldots. \Theta_k\}$; $\Theta \in \Omega$.

4.4.2. Calculation of Water Supply Scenarios

study utilized a SWG developed by Waheed et al., (2020b) to produce the future climate scenarios using the climate exposure Θ. The key benefit of the SWG is its ability to change the parameter according to the climate exposure Θ over the study area with linearly increment, as defined before in section 4.4.1. following the nonstationary assumption. These climate scenarios

were then implemented in Variable Infiltration Capacity (VIC) and routing (RVIC) models built and calibrated by Waheed et al., (2020a) to generate time series of streamflow at the basin outlet. These streamflows represent the water supply scenarios (S; ∀s ={s_1,s_2 … s_k}) for Derbendikhan reservoir simulation. Relative weights (W) were assigned to each of the climate exposure J using a fat-tailed Cauchy distribution, which is superior to the widely used multi-variate normal distribution [Taner et al., 2017; Taner et al., 2019]. With uniform distribution assigned for the internal climate iteration I [Steinschneider et al., 2015b], W was obtained as follows:

$$W_{(j,i)} = \frac{\phi_c\left[{\Phi_c}^{-1}\left(\theta_j\right)\right]}{\int_1^J \phi_c\left[{\Phi_c}^{-1}\left(\theta_j\right)\right]} \times \frac{1}{I} \tag{4.1}$$

Where $\phi_c(.)$ and ${\Phi_c}^{-1}(.)$ are the density and distribution function of the fat-tailed Cauchy distribution.

4.4.3. Calculation of Water Demand Scenarios

The first step in this stage is to identify the demand stakeholder categories, which are: municipality demand per capita, irrigation, industry, and the environmental requirement (using Tennant 1975 method) for the next downstream dam in the basin (e.g., Hemrin dam). Then, the future developments were examined for each sector and their corresponding demands were calculated. The key innovation here is to combine the water supply condition exposure with the demand exposure. This enables the analyst to consider the nonstationary assumption in the demand simulation to capture nonlinear relationship and monotonic interactions between them. The impact of climate change for each sector was also considered by changing the water need. For the population demand, Opalinski, (2018) showed that 1 C^o increase in temperature causes 3.2 and 3.9% demand increases in winter and summer months, respectively in dry regions. This

increment ratio was assigned for all climate exposure Θ with linearly increment. Similarly, the water demand was calculated for the irrigation projects using Penman-Monteith equation for each crop. Then, the future demand scenarios for all climate exposure Θ were obtained by applying the linearly increment in each variable using Penman-Monteith equation for each crop.

4.4.4. Assessment of System Performance

The first step for this stage is to identify the dam reservoir capacity and its operational rule (rule curve) obtained from MoWR. The water balance of the reservoir was modeled as:

$$ST_{t+1} = (ST_t + S_t) - (RE_t + R_t + E_t + SL_t) \quad , \quad \forall t = 1,2,\ldots.T;\ t \in \mathbb{N} \tag{4.2}$$

Where ST is the reservoir water storage, RE is the water release, R is the direct rainfall on the reservoir, E is the evaporation of the reservoir, and SL is the seepage loss. E was modeled using the Penman equation. E and R were calculated simultaneously according to the climate exposure linearly increment under the nonstationary assumption, similarly to the crop demand for the irrigation projects. This enables the analyst to consider the nonlinear relationship and monotonic increment (or decrement) in future scenarios estimating K of supply, demand and system losses.

Then the system performance was evaluated to provide an understanding of how specific climate conditions from the exposure lead to vulnerable outcomes according to multiple system performance. This involved an assessment of the dam's ability to regulate the available water and release enough to meet all stakeholder demands (D) at each month t during the system design life (SDL). The definition of Whateley et al., (2014); Steinschneider et al., (2015b); Taner et al., (2019) of reliability, a ratio of number of months that the reservoir meets the specified demand threshold (ψ) divided to the total simulated number of months (T), was extended. A new

term was introduced called First Deficit Occurrence (FDO), defined as the first time [in months] in T when the water release cannot meet ψ of the demand, as follows:

$$FDO(i,j) = min_t\big(\psi\, D(i,j,t) \;>\; RE(i,j,t)\big) \tag{4.3}$$

The assumed value of ψ is 1. The key innovation here is to consider the system design life (SDL) in the calculation, as follows:

$$FDI(i,j) = \begin{cases} 1, & if\ FDO\ (i,j) \geq SDL \\ \dfrac{FDO\ (i,j)}{SDL}, & if\ FDO\ (i,j) < SDL \end{cases} \tag{4.4}$$

Where FDI is an indicator of FDO in years; FDI Є [0,1]. Then, the Demand Meeting Efficiency (DME); DME Є [0,1], is calculated as:

$$DME = \int_{i=1}^{I} \int_{j=1}^{J} W(i,j) \times FDI(i,j)\, dj\, di \tag{4.5}$$

This assumes that if a deficit occurs at time t there will be higher probability of deficit in the following period due to the monotonic increment and the non-linear relationship between the supply, demand, and system losses. The idea of this indicator is to avoid encountering a failure during SDL. Similarly, the second indicator for Flood Protection Efficiency (FPE) in years, is developed using the following system:

$$FLO(k) = min_t(SE_{t+1} \;>\; SE_{max} \mid RE_t = \; RE_{max}\,) \tag{4.6}$$

$$FLI(i,j) = \begin{cases} 1, & if\ FLO\ (i,j) \geq SDL \\ \dfrac{FLO\ (i,j)}{SDL}, & if\ FLO\ (i,j) < SDL \end{cases} \tag{4.7}$$

$$FPE = \int_{i=1}^{I} \int_{j=1}^{J} W(i,j) \times FLI(i,j)\, dj\, di \tag{4.8}$$

Here, FLO is the First Flood Occurrence [month], ST_{max} and RE_{max} are the maximum storage (or the conservation level) and release of the reservoir respectively, and FLI is the FLO indicator, with FLI and FPE Є [0,1]. The two objective functions (DME and FPE) can be used to evaluate the status quo performance and compare different pre-specified adaptation strategies. The plan is considered robust if $DME \geq Th_D$ and $FPE \geq Th_F$, and vulnerable otherwise. Th_D and Th_F are the minimum threshold values of DME and FPE respectively and assumed 0.5. However, with the procedure applied to calculate the supply and demand monotonically and probabilistically, the time-probability of the system to encounter a failure in DME and FPE can also be evaluated, as shown later in the results section.

Once the pre-specified plans are examined, the maximum allowable time (MAT) to start applying the plan(s), conjugated on maintain $DME \geq Th_D$ and $FPE \geq Th_F$, can be identified. i.e, MAT is defined as the maximum operational time to switch from the status quo rules into the selected adaptation strategy rules ($Ru_o \rightarrow Ru_z$) and the expected DME and FPE exceed their minimum thresholds during SDL, as follows (an illustration example is shown in Figure 4.4):

$$MAT = max_t \left(Ru_o \rightarrow Ru_z \mid DME \geq Th_D \,\&\, FPE \geq Th_F\right) \tag{4.9}$$

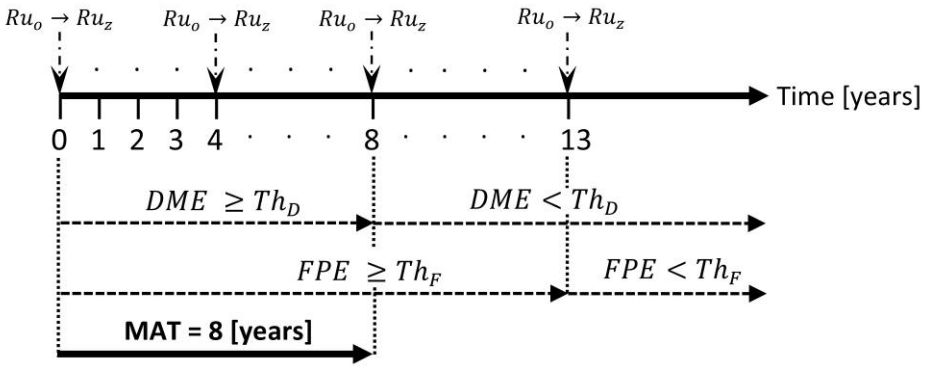

Figure 4.4: Schematic of the MAT definition. The symbol $Ru_o \rightarrow Ru_z$ represents the time to switch from the status quo rules to the alternative rules.

In this study, the demand reductions for each sector were considered as alternative plans [e.g., Pareto sets]. Consequently, a third objective function to rank the solution economically was used. As the water is priceless in some sectors in Iraq, the default economic indicators are not applicable. To overcome, the Net Economic Return term (NER) of Tian et al., (2019) was modified by assigning a power to rank the importance of each demand sector, as follows:

$$NER(z) = \sum_{m=1}^{M} MR(m,z)^{1+m/M} \times A_m \quad (4.10)$$

Where MR is the Meeting Ratio, m is the index of the water sector (higher number represents the higher priority), z is the index of adaptation plan; ∀z= 0,1,2 … Z; 0 represents the system status quo, and A is the net water allocation portion for m^{th} sector (after subtracting the conveyance loss); $\sum_M A_m = 1$. MR was calculated by dividing the meeting ratio after the adaptation is applied by the status quo. For example, if the z plan is to reduce the irrigation sector water allocation by 10%, MR is (10-100)/100= 0.90. Furthermore, A was calculated according to the exposure condition effect on each sector. For example, increment in temperature mean causes increment in the water allocations for municipality and irrigation comparing to the industry and environmental requirements. However, applying an adaptation strategy may affect the corresponding generation of hydropower. Therefore, the hydropower generation efficiency (HPE) was calculated by dividing the average of hydropower (HP) produced after applying the adaptation (HP_z) by the HP of the status quo (HP_o), as follows:

$$HPE(z) = \int_{i=1}^{I} \int_{j=1}^{J} \frac{HP_z(i,j)}{HP_o(i,j)} \times W(i,j)\, dj\, di \quad (4.11)$$

$$HP_z(i,j) = \frac{1}{min[FDO_z(i,j), FLO(i,j)]} \int_{1}^{min[FDO_z(i,j),FLO(i,j)]} \beta\ \rho\ H_{z(i,j,t)}\ RE_{z(i,j,t)}\ dt \qquad (4.12)$$

Where β is the hydropower efficiency, H is the net water head [m], and ρ is the water density.

The fast Non-dominated Sorting Genetic Algorithm (NSGA-II) developed by Deb and Pratap (2002) was employed to identify the optimal adaptation strategy. NSGA-II is highly capable in performing complex multi-objective water resources optimization problems and recognized as one of the most efficient and adequate multi-objective evolutionary algorithms [e.g., Yusoff et al., 2011; Yu et al., 2015; Delgarm et al., 2016; Zheng et al., 2016; Roach et al., 2018; Tian et al., 2019]. NSGA-II is a heuristic search technique for solving mono-criterion optimization problems based on the biological evolution (inheritance, crossover, and mutation operators) with non-dominated and a crowding distance sorting procedure. First, NSGA-II generates initial population (size Z) based on each sector range (e.g., 0.7 ≤ MR ≤1); and sorts them based on non-domination criteria (e.g., DME, FPE, NER, HPE, and MAT). Then, the crowding distance, measure of how close each individual is to the neighbors, is calculated. The high values called parents (size Z/2) are selected, which represent high diversity degree. Then, the crossover and mutation processes are applied to the parents to generate their children (size Z/2). The parents and children are combined to form the next generation set (size Z). The process is repeated G iterations (number of generations) and the final set is obtained which represents the optimal solution. Further explanation of the NSGA-II can be found in Deb and Pratap (2002). The general flowchart of the suggested top-down methodology (demand, supply, and dam losses model + reservoir simulation

model) with NSAG-II is shown in Figure 4.5. In this study, G is assumed 40, Z is 100. However, mutation and crossover probabilities are assumed 0.2 and 0.7, respectively [Roach et al., 2018].

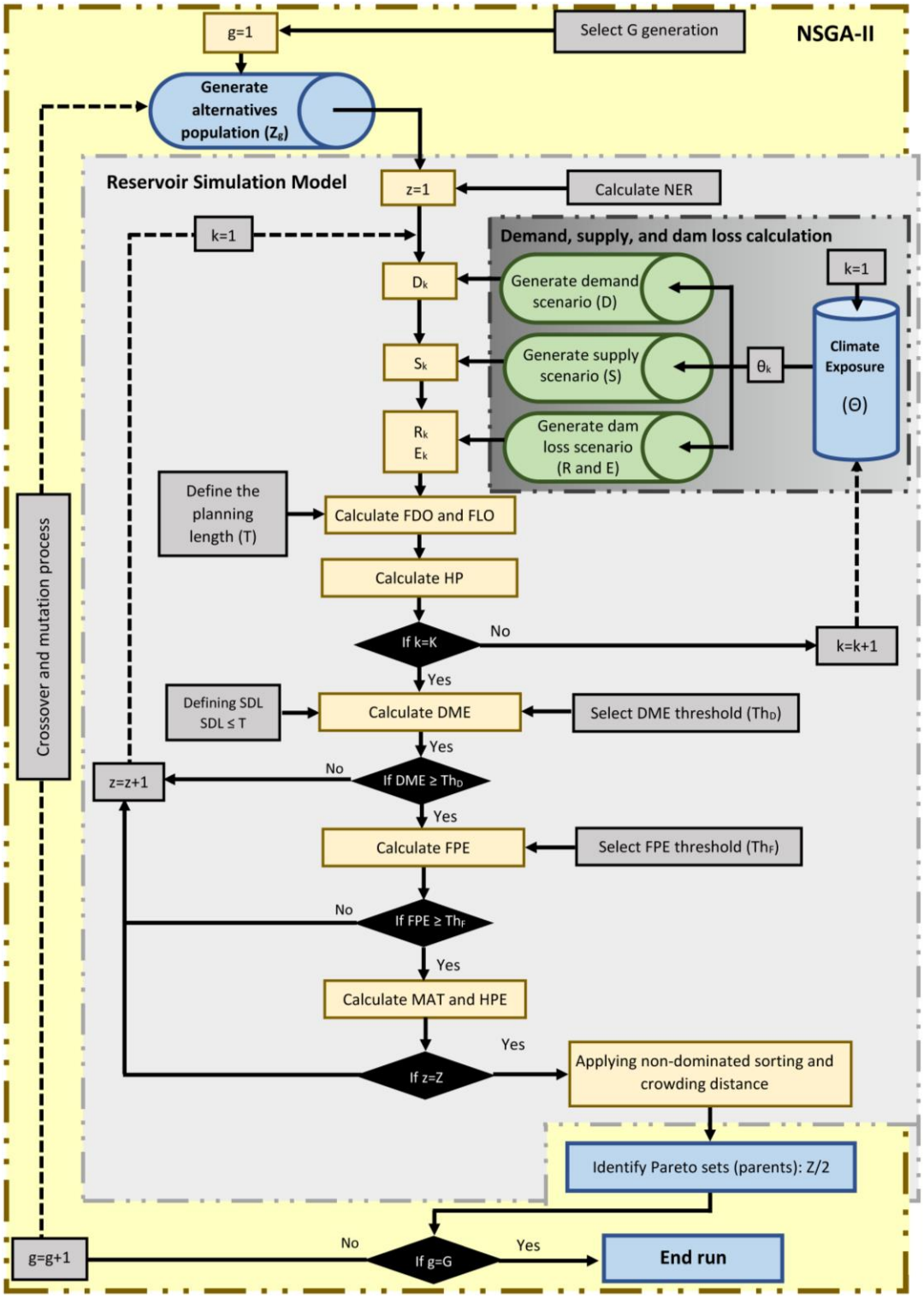

Figure 4.5: The general flowchart of the study to identify the best (optimal) adaptation strategy.

In summary, the objective functions are to maximize the vector of 5 indicators:

$$F(\boldsymbol{z}) = max\,\{DME(z), FPE(z), HPE(z)\ NER(z), MAT(z)\} \quad (4.13)$$

Subject to,

$$1 \geq MR(m) \geq 0.7\ ;\ \forall m = 1,2,3,4 \quad (4.14)$$

$$DME \geq Th_D \quad (4.15)$$

$$FPE \geq Th_F \quad (4.16)$$

However, in order to achieve a single optimum solution form NSGA-II after implementing G iteration, the following equation is used [Delgarm et al., 2016]:

$$Z_{opt} = max(\frac{1}{\Lambda}\sum_{1}^{\Lambda}\frac{f_\lambda(z) - f_\lambda(z)^{min}}{f_\lambda(z)^{max} - f_\lambda(z)^{min}}) \quad (4.17)$$

Where Z_{opt} is the optimal solution (Z), Λ is the number of objective functions given in equation (4.14) which is 5, $f_\lambda(z)^{max}$ and $f_\lambda(z)^{min}$ are maximum and minimum values of each objective function λ. However, for consistency purposes as all objectives are unitless, MAT is normalized by dividing by the upper limit value of MAT (e.g., MAT_{max}), $f_{MAT}(z) = MAT_z/MAT_{max}$.

4.4. Results and Discussion

The analysis leads to results about the GCM outputs, climate change risk assessment under the status quo rules, and the multi-objective robustness evaluation of the pre-suggested alternatives and the optimization process, as follows.

4.5.1. GCM outputs

Figure 4.6, Figure 4.7, and Figure 4.8 show the analyzed CMIP5 ensemble of GCM outputs of the 3 selected models (60 outputs) after applying EDC then a moving average of 30 years. It is seen that the precipitation mean change ranged from -37.4% to +31.3% (average of -4.8%) and precipitation CV change ranged from -38.2% to 34.0% (average of +2.5%), temperature mean change ranged from +0.4 ^{o}C to +5.1 ^{o}C (average of +2.3 ^{o}C), temperature CV change ranged from -45.8% to +30.8% (average of -8.2%), wind speed magnitude mean change ranged from -22.3% to 11.7% (average of -4.9%), and wind speed magnitude CV change ranged from -29.1% to 32.2% (average of -0.1%). However, these results are in line with other studies of analysis the future change in different locations around the world, as summarized in Table 4.2.

Table 4.2: Summary of some literatures of analyzing GCMs in different locations.

Author	Location	Model Phase	Comparison Periods (Projected/Historic)	Precipitation Mean [%]	Temperature Mean [^{o}C]
Turner et al., (2014b)	Thomson & Yarra River Basins, Australia	CMIP3	(2040 - 2070)/ (1974 - 2004)	-25 to +5	+0.5 to +2.5
Whateley et al., (2014)	Connecticut River Basin, US	CMIP3 & CMIP5	(2025 - 2075)/ (1950 - 1999)	-5 to +10	+1.5 to +3.5
Steinschneider et al., (2015a)	Coralville Basin, US	CMIP3 & CMIP5	(2041 - 2070)/ (1970 - 2000)	-15 to +20	+0.5 to +4
Steinschneider et al., (2015b)	Belton Lake, US	CMIP3	(2041 - 2070)/ (1971 - 2000)	-10 to +13.7	+1.6 to +3.3
Abbas et al., (2016)	DRB, Iraq	CMIP3	(2046 - 2064)/ (1980 - 2010)	-26 to +40	+1 to +2.7
			(2080 - 2100)	-80 to +25	+1.2 to +5.7
Taner et al., (2017)		CMIP5	(2016to 2050)/ (1974 to 2008)	-0.2 to +2.5	-30 to +18
				Precipitation CV [%]	
Steinschneider et al., (2015b)	Belton Lake, US	CMIP3	(2041 - 2070)/ (1971 - 2000)	-24 to +91	
				Wind Speed [%]	
Pryor et al., (2006)	Europe	CMIP3	(1960 -1989)/ (2065 - 2094)	-5 to +12	
Moemken et al., (2018)	Europe	CMIP5	(2071-2100)/ (1970 – 2000)	-10 to +15	

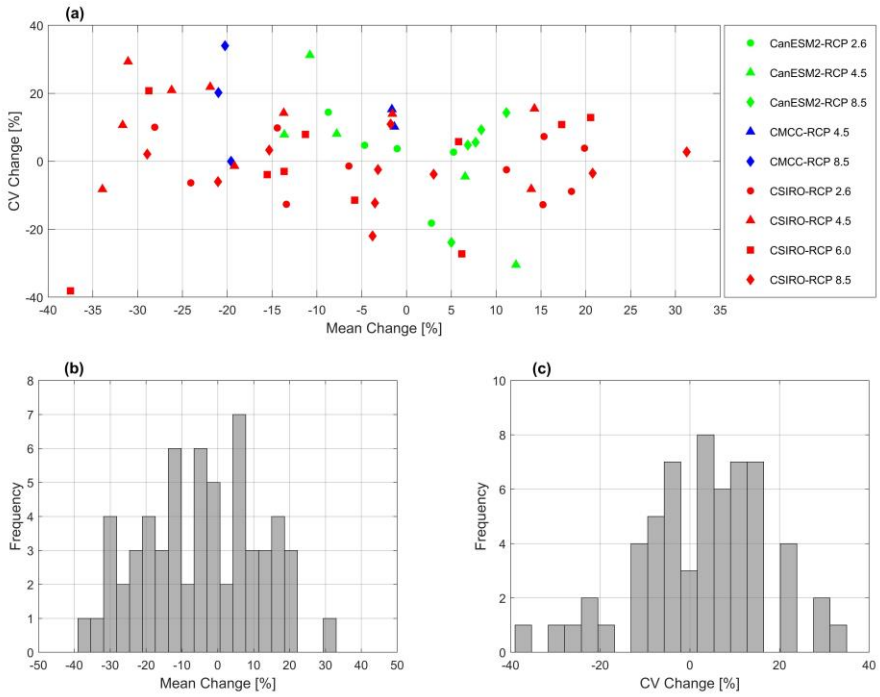

Figure 4.6: The analyzed 60 outputs of the three selected GCMs for the precipitation corresponding to their Representative Concentration Pathway (RCP) values. (a) the plot of the mean versus the CV change; (b) and (c) the histogram of the mean change and C.V change.

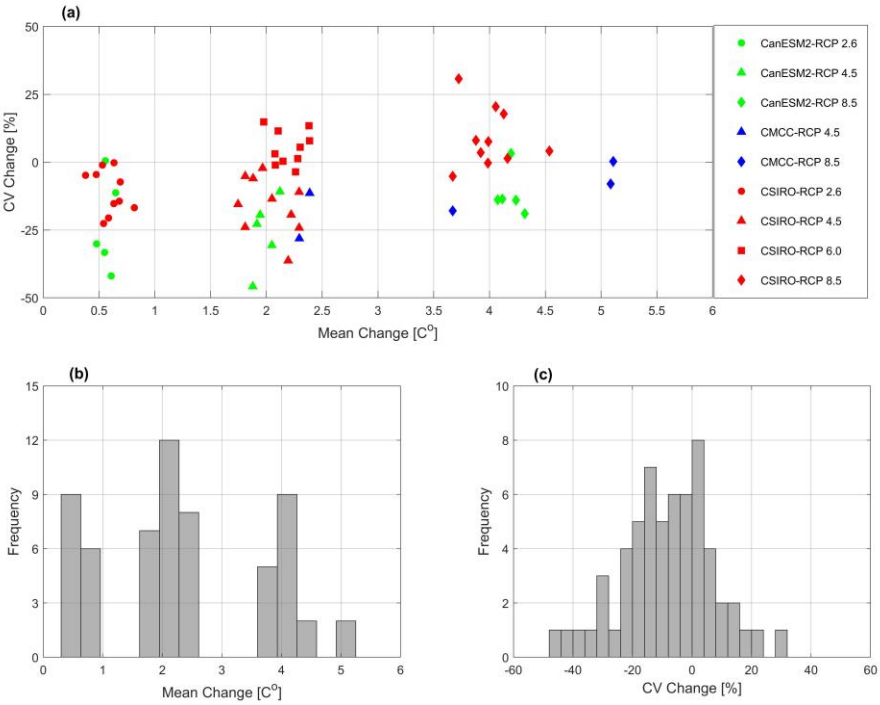

Figure 4.7: The analyzed 60 outputs of the three selected GCMs for the temperature corresponding to their RCP values. (a) the plot of the mean versus the CV change; (b) and (c) the histogram of the mean change and C.V change.

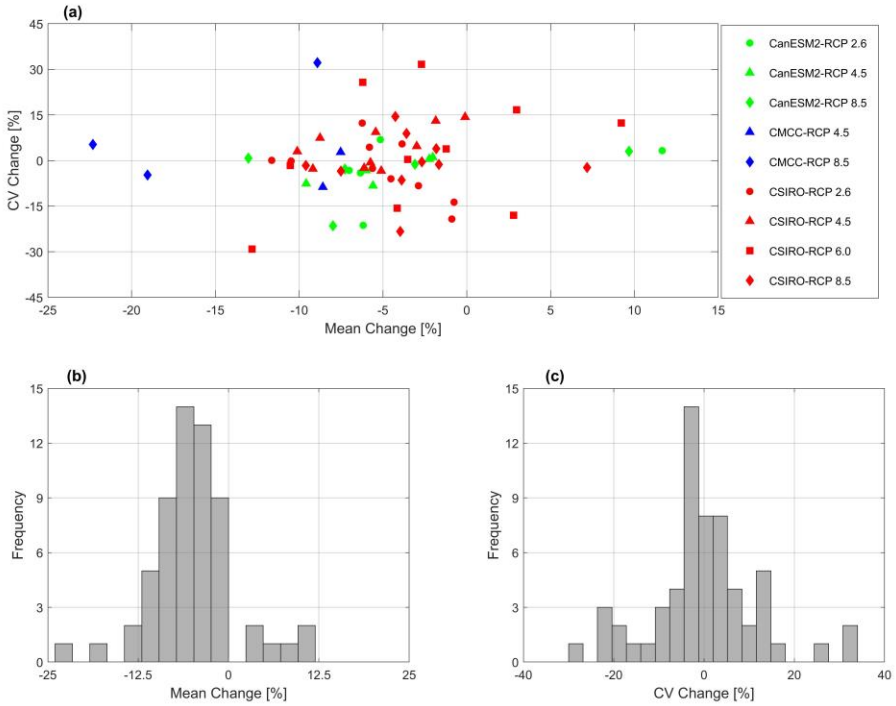

Figure 4.8: The analyzed 60 outputs of the three selected GCMs for the wind speed magnitude corresponding to their RCP values. (a) the plot of the mean versus the CV change; (b) and (c) the histogram of the mean change and C.V change.

However, based on those ranges, the climate exposure Θ was identified as follows. (1) precipitation mean alteration ranged from -40% to +30% with 10% increment (8 alterations); (2) precipitation CV alteration ranged from -40% to +40% with 20% increment (5 alterations); (3) temperature mean alteration ranged from 0 to 6 C^o with 2 C^o increment (4 alterations); (4) wind speed mean alteration ranged from -50% to 25% with 25% increment (4 alterations). The total number of alterations (J) is 8 × 5 × 4 × 4 = 640, and the total number of climate exposures is K = J × I = 640 × 10 = 6400. However, a test was done for the temperature and wind speed CV and results indicated their insignificant effect. Therefore, they were not included.

4.5.2. Climate Change Risk Assessment

The suggested bottom-up methodology was used to parse the capability of system status quo to manage the flood and drought occurrence against the climate exposure. Figure 4.9 shows

the cumulative probability of the system status quo with respect to FLO, equation (4.6), and FDO, equation (4.3), as the time propagates, and different findings emerge from this figure. First, it is apparent that the system status quo rules to manage the flood risks promote robustness. They can foresee across wide swath of climate trajectories to hedge against flood risk. The FLO is anticipated to occur after 18 years with probability of 3.7%. The inherent FPE is 0.605, which is deemed to be acceptable as it is above the threshold value. Thus, for long-term the operation dam is well managed to maintain adequate performance against the flood occurrence and able to handle a wide range of climate scenarios during the SDL. In contrast, the system status quo is vulnerable with respect to drought management. The FDO is anticipated to occur after 3 years with probability of 1.7%. The probability rises very sharply and reaches 31.2% after 10 years. Also, after 23 years the probability reaches 90.2%. Thus, there is a significant deficit chance that system performance will encounter under the status quo plan. Moreover, the system is no longer viable after 48 years. The inherent DME is 0.178, which signaling a risk as it is much below the minimum acceptable threshold value. This implies that it is utmost urgency for the decision-makers to pay special attention to drought and water scarcity for sustainable water management.

Figure 4.10 shows the results of FDO and FLO response surfaces of the status quo under the range of climate exposure. The change in precipitation mean and CV are represented in the x-axis and y-axis, respectively in a and c. The temperature mean change and wind speed mean are represented in the x-axis and y-axis, respectively in b and d. The obtained values of FDO and FLO due to internal climate variability (I) were averaged out and represented in the z-axis. Also, the analyzed GCM outputs are shown in white dots. Many interesting insights can be learned from this figure. First, the system is most sensitive to changes in mean precipitation for drought

and flood occurrences, it has relatively sharp changes over all other variables. This suggests that the precipitation mean change dominates the system response to both flood and drought risks. With no change in other variables, the range of FDO and FLO are 8 to 33 and 80 to 20 years, respectively for the rate change of -40 to +30%. In other words, 10% reduction in precipitation mean can degrade the system performance to meet the demand by 3.5 years (on average). Similarly, 10% reduction can improve the flood protection by 8.5 years (on average). As the precipitation amount falls, higher demands would be expected for the irrigation sector, in conjunction with supply reduction, leading for faster demand deficit. This is because the demand requirements were generated dependently with the supply. In contrast, flood mostly occurs with increase in precipitation volume due to the augmented rainfall from the large rainfall events.

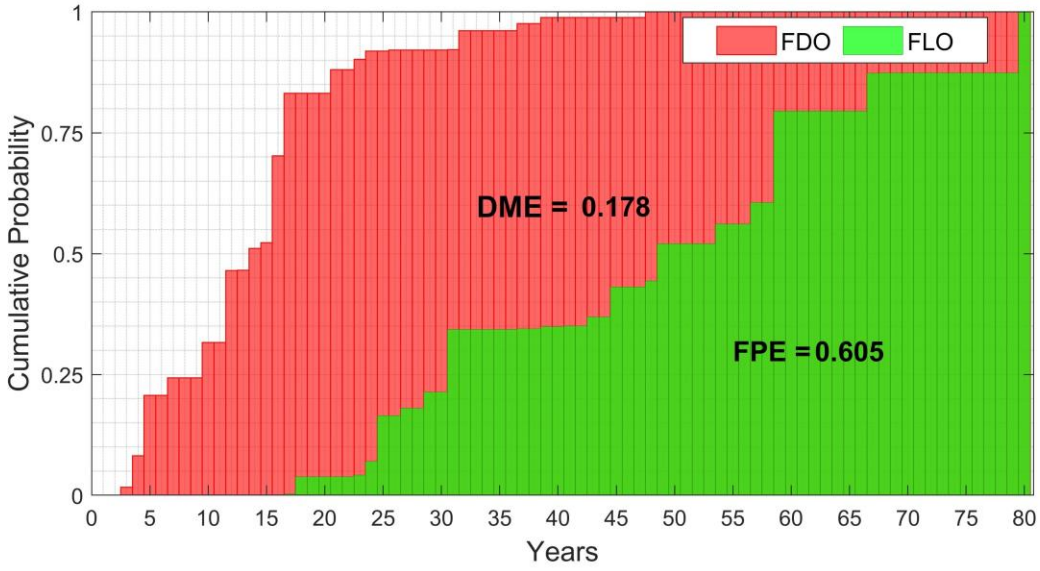

Figure 4.9: Cumulative probability of FLO and FDO of the system under status quo rules during the SDL.

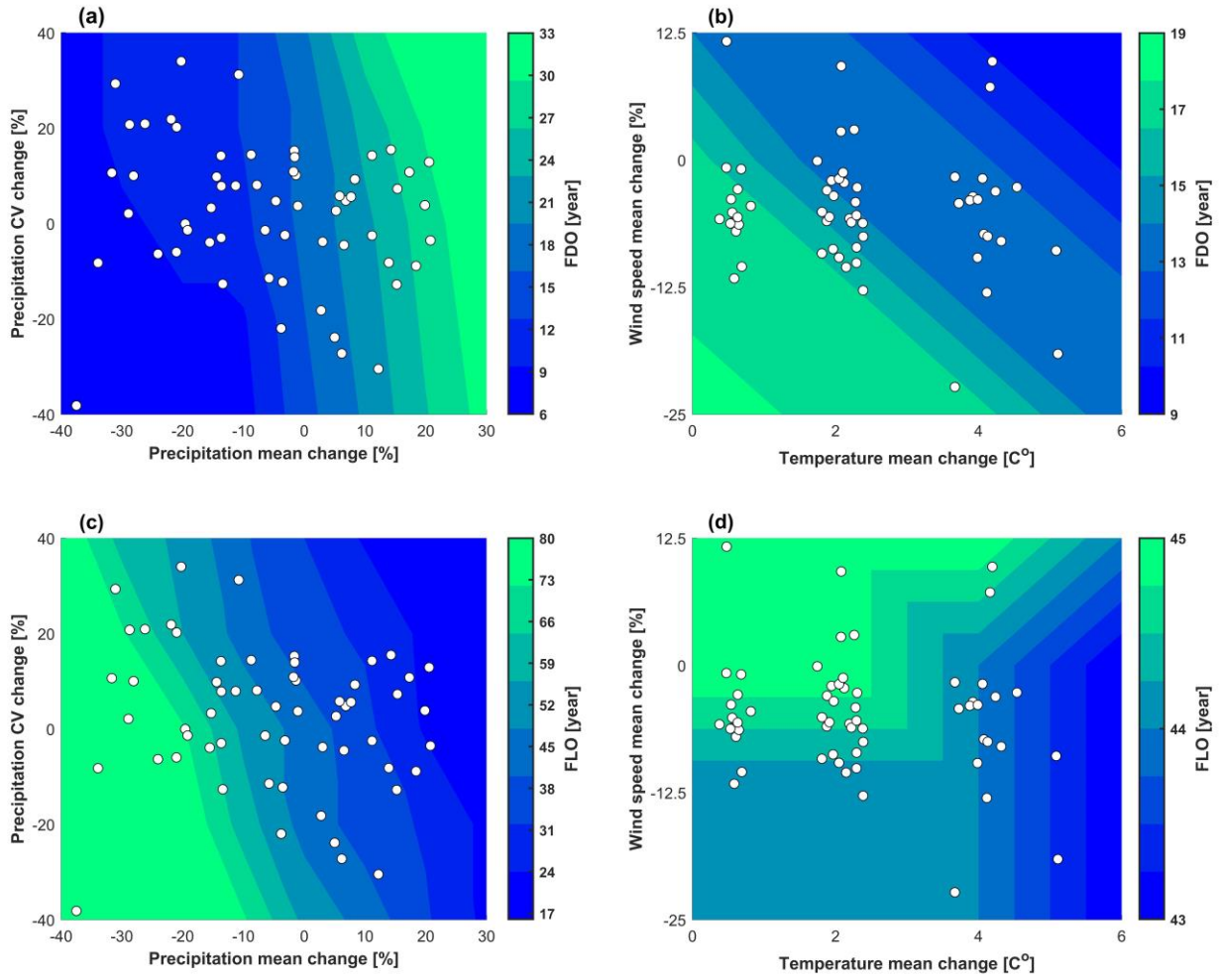

Figure 4.10: FDO and FLO response surfaces over climate exposure for precipitation mean, CV, temperature mean, and wind speed mean alterations.

Interestingly, the system is more sensitive for the precipitation CV changes for floods compared with the droughts. With no change in other variables, the range of FDO and FLO is 15 to 19 and 54 to 32 years, respectively for the rate change of -40 to +40%. On average, 10% reduction in precipitation CV can degrade the system performance to meet the demand by 0.5 years. Likewise, 10% reduction can improve the flood protection by 2.7 years. With higher daily precipitation variability, caused by CV increment, more runoff would be generated in the upstream basin, leading to increases in flood occurrence and deficit; although to a lesser degree.

This means that the system is more capable to buffer out the precipitation variability effects to allocate the demand requirement than the flood protection. This might be because the precipitation variability has more influence on the supply compared to the demand, since the reservoir operation [see equation (4.2)] and demand calculations were done on a monthly basis while the runoff generation by VIC and RVIC [Waheed et al., 2020a] was performed on daily basis. Therefore, CV is less sensitive for drought management comparing with flood risk.

Contrastingly to the precipitation CV, the system is more sensitive for the temperature mean increment for droughts compared to the floods. With no change in other variables, the range of FDO and FLO are 17 to 10 and 54 to 43 years, respectively for the change of 0 to +6 C^o. On average, 1 C^o increment can degrade the demand meet ability 1.7 years and can help the flood protection by 0.3 years. Likewise, the system is more sensitive for the wind speed mean change for the droughts compared to the floods. With no change in other variables, the ranges of FDO and FLO are 19 to 14 and 44 to 45 years, respectively for the rate change of -25 to +12.5%. On average, 10% increment can degrade the system performance to meet the demand by 1.3 years and improve the flood protection by 0.3 years. When the temperature and wind speed increase, the corresponding evapotranspiration magnitude increases. Also, the temperature increment leads to less precipitation held as snow. Then, the generated runoff would experience less availability from snowmelt. Therefore, with the warm and windy condition, the water demands would increase substantially, in conjunction with supply reduction, leading to faster deficit occurrence especially in the system with big majority for irrigation projects.

It is inferred from above that the precipitation amount change is dominant for flood and drought occurrences, followed by precipitation CV, then temperature change and wind speed.

Also, it would be more important to include the temperature and wind speed mean effects in drought management purposes. The results of precipitation and temperature effects obtained are consistent with other studied [e.g., Whateley et al., 2014; Steinschneider et al., 2015a; 2015b; Culley et al., 2016; Spence and Brown., 2016; Taner et al., 2017; 2019; Zhang et al., 2018; Van Tra et al., 2018], while wind speed influence is considered an innovative analysis in this study.

4.5.3. Multi-objective Robustness Evaluation of the Alternatives

Figure 4.11 (a) illustrates the system performance measures under the status quo rules for the four objectives: DME, FPE, HPE, and NER. The MR for the four sectors is 1, since no reduction for any sector was applied yet. Therefore, NER is 1. It is seen that the status quo operation rules provide adequate performance for FPE across a wide range of future changes but the DME is below the threshold target. Therefore, an alternative plan is needed to cope with drought effects. The case study focused on three synthetic pre-specified plans of reducing the MR of the demand sectors to demonstrate the framework ability to evaluate their robustness. Plan 1 is to reduce the water requirement for municipality and industry by 30% (MR_{Mun} = MR_{Ind} = 0.7). Plan 2 is to reduce the irrigation water requirement by 20% (MR_{Irr} is 0.8). Plan 3 is to reduce the environmental water requirement by 20% (MR_{Env} is 0.8), as shown in Figure 4.11 (b). However, the MAT of each robust plan was divided by 14 to convert into a dimensionless ratio ranging from 0 to 1 and to be consistence with the other performances [e.g., DME, FPE, and NER]. It is noticed that the Plan 1 is insufficient to improve the system DME to maintain the minimum threshold value. Its corresponding DME is found of 0.461. This is due to the small water allocation portion for the municipality and industry. However, Plan 2 and Plan 3 are considered acceptable plans to provide adequate performances. The MAT for Plan 2 and Plan 3 are 6 and 8 years,

respectively. Interestingly, the HPE is improved when an adaptation plan is applied. The HPE for Plan 1, 2 and 3 are 1.127, 1.161, and 1.210 respectively. This because the DME value is increased after applying the reduction ratio, the system will have more flexibility to generate HP and for longer time before encountering a failure of FDO or FLO [see equation (4.12)]. Importantly, the Plan 3 is superior to 2 in most performances and has more time window (e.g., MAT) to apply it, but the its NER is less [0.879 and 0.901, for Plan 3 and Plan2, respectively]. Therefore, care must be taken before selecting the best adaptation plan. Interestingly, the upper limit of MAT for system is found to be 14 years where all MR is 0.7. This indicates that an adaptation strategy has to be applied within 14 years to cope with the negative climate change impact.

Figure 4.11 (c) shows the optimal Pareto set obtained from NSGA-II and applying equation (4.17). The optimal MR for municipality, irrigation, industry, and environmental requirement are 0.985, 0.900, 0.915, and 0.925 respectively. The MAT for the optimal set is 9 years. Ultimately, the optimal set is superior to all pre-specified plans. In any cases, the suggested framework of this study is able to suggest the best alternative plan in case the re-specified plans are absent, or to compare with it in selecting the preferred future plan.

Finally, the study focuses on reducing the water requirements of each sector, as one can also study the effect of changing the rule curve as alternative plans to react the negative impact of the climate change. The results of this study are not meant to reduce the productivity of each sector, but to spur new technologies with using less water such as improving the water conveyance efficiency from the dam to each sector, using mechanized irrigation systems … etc.

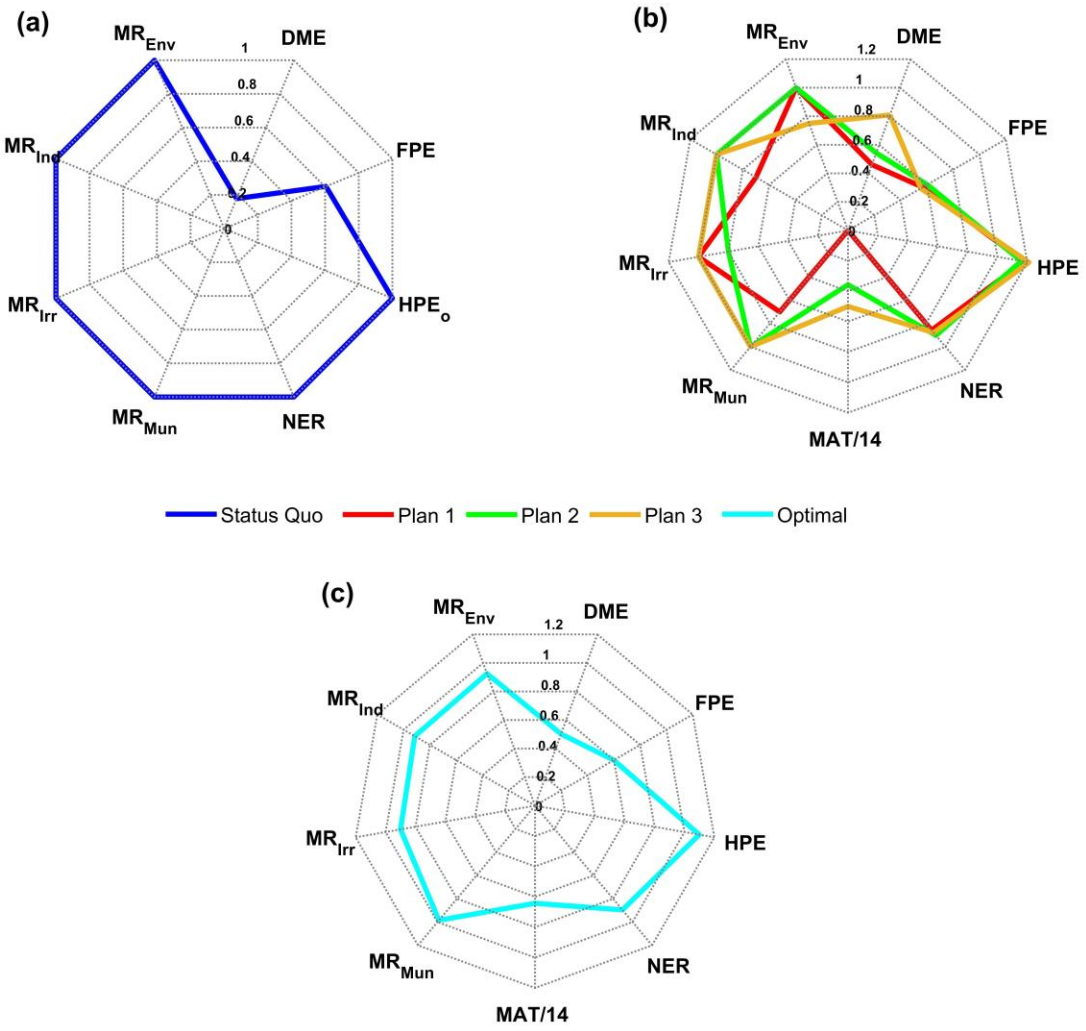

Figure 4.11: Multi-objective robustness assessment of the system. (a) evaluation of the status quo rules. (b) evaluation of the three pre-specified plans. (c) Optimal plan obtained from NSGA [see Figure 4.5].

4.5. Conclusions

This study presented a decision-making framework to evaluate the status quo of the system to long-term climate change influence and gain insight about the risk characteristics. The framework is designed to facilitate identifying the optimal-robust (or the best among pre-suggested plans) to alleviate the anticipated future vulnerability. New approaches were used to analyze the future change and project the number of future realizations of climate change conditions. Also, new robustness metrics (FPE, DME, HPE, NER) were presented to examine long-

term planning alternatives that are robust under difference climate changes with a nonstationary assumption. The case study focused on demand ratio reduction as an adaptation to long-term climate examination to urge water resources managers to focus on sustainable water management, such as increasing water use efficiency to ensure higher reliability and lower vulnerability among different sectors. Moreover, the study presented a novel term MAT to identify the theoretical time window of the plan to maintain the threshold target value of each objective. However, the study represents the first attempt to evaluate the wind speed magnitude effect in decision-making processes, and first bottom-up case study inside Iraq.

Results obtained of analyzing the GCM outputs show that the precipitation mean are subject to vary from -37.4% to +31.3% (average of -4.8%); precipitation CV change will vary from -38.2% to 34.0% (average of +2.5%), temperature mean change will increase from +0.4 C^o to 5.1 C^o (average of +2.3 C^o), temperature CV change will vary from -45.8% to 30.8% (average of -8.2%), wind speed magnitude mean will vary from -22.3% to 11.7% (average of -4.9%), and wind speed magnitude CV will vary from -29.1% to 32.2% (average of -0.1%).

However, parsing the system status quo capability to manage flood and drought occurrence against the climate exposure showed that the system is vulnerable in drought management and robust for flood protection for long-term future climate exposure. The overall DME and FPE are 0.178 and 0.605, respectively. This implies that the project managers should comprehensively pay attention to the drought and water scarcity management.

The analysis of system to the weather variable changes show that the precipitation mean is most sensitive parameter followed by precipitation CV, then temperature change and wind speed. The results also show that including wind speed is important in the decision-making

process especially in drought management. However, the analysis also indicated insignificance of the temperature and wind speed CV change in DRB. Further investigation is recommended to investigate their effects on other basins. One suggestion is to reduce the operation time step from monthly to bi-weekly or weekly.

Three synthetic plans were evaluated to improve the system performance in meeting the demand ratio and maintain an acceptable performance for the other objectives (e.g., FPE, DME, HPE, and NER). The study considered the reduction of demand sectors as alternative plans. Results reveal that reducing the MR for municipality and industry by 30% is not sufficient to improve the DME above the threshold value of 0.5, while the other two plans of reducing MR for irrigation or environment requirement by 20% can maintain the minimum threshold value for DME and FPE. Of interest of this study, the suggested framework is able to identify the maximum time (MAT) to apply each plan and still achieve the target values of all objectives. The optimal pareto set using NSGA-II was obtained by reducing the MR for municipality, irrigation, industry, and environmental 0.985, 0.900, 0.915, and 0.925 respectively. The DME, FPE, HPE, NER, and MAT were 0.502, 0.599, 1.099, 0.896, and 9 [years] respectively. The analysis glimpsed that the MAT upper limit is 14 years which indicates that an adaptation strategy must be applied within 14 years to avoid with the undesirable climate change influence.

This paper presented a novel approach that bridges the nonstationary assumption of the climate exposure with the supply, demand, and system losses for the multi-objective function to assess the water resources system vulnerability across wide trajectories to investigate the long-time-robust plans. It represents the first attempt to consider the full nonstationary hydroclimatic representation for all supply, demand, and system loses in simulation their suture scenarios. The

future work of this study is to consider nonstationary in the hydrology model parameter changes and consider full uncertainty of the model parameters and forcing data.

References

Abbas, Nahla, Saleh A. Wasimi, and Nadhir Al-Ansari. "Impacts of Climate Change on Water Resources in Diyala River Basin, Iraq." Journal of Civil Engineering and Architecture 10.9 (2016): 1059-1074.

Adams, Richard M., and Dannele E. Peck. "Effects of climate change on water resources." Choices 23.1 (2008): 12-14.

Al-Faraj, Furat AM, and Miklas Scholz. "Assessment of temporal hydrologic anomalies coupled with drought impact for a transboundary river flow regime: the Diyala watershed case study." Journal of hydrology 517 (2014): 64-73.

Al-Faraj, Furat AM, Miklas Scholz, and Dimitris Tigkas. "Sensitivity of surface runoff to drought and climate change: Application for shared river basins." Water 6.10 (2014): 3033-3048.

Al-Jawad, Jafar Y., Hassan M. Alsaffar, Douglas Bertram, and Robert M. Kalin. "A comprehensive optimum integrated water resources management approach for multidisciplinary water resources management problems." Journal of environmental management 239 (2019a): 211-224.

Al-Khafaji, Mahmoud S., and Rana D. Al-Chalabi. "Assessment and Mitigation of Streamflow and Sediment Yield under Climate Change Conditions in Diyala River Basin, Iraq." Hydrology 6.3 (2019): 63.

Azhoni, Adani, Simon Jude, and Ian Holman. "Adapting to climate change by water management organisations: Enablers and barriers." Journal of Hydrology (2018).

Beh, Eva HY, Holger R. Maier, and Graeme C. Dandy. "Scenario driven optimal sequencing under deep uncertainty." Environmental Modelling & Software 68 (2015): 181-195.

Brown, Casey, and Robert L. Wilby. "An alternate approach to assessing climate risks." Eos, Transactions American Geophysical Union 93.41 (2012): 401-402.

Bucchignani, E., P. Mercogliano, G. Rianna, and H-J. Panitz. "Analysis of ERA-Interim-driven COSMO-CLM simulations over Middle East–North Africa domain at different spatial resolutions." International Journal of Climatology 36.9 (2016b): 3346-3369.

Bucchignani, E., L. Cattaneo, H-J. Panitz, and P. Mercogliano. "Sensitivity analysis with the regional climate model COSMO-CLM over the CORDEX-MENA domain." Meteorology and Atmospheric Physics 128.1 (2016a): 73-95.

Bucchignani, Edoardo, Paola Mercogliano, Hans-Jürgen Panitz, and Myriam Montesarchio. "Climate change projections for the Middle East–North Africa domain with COSMO-CLM at different spatial resolutions." Advances in Climate Change Research 9.1 (2018): 66-80.

Carter, T. R., M. Hulme, and M. Lal. "Guidelines on the use of scenario data for climate impact and adaptation assessment v1." (1999).

Culley, Sam, S. Noble, A. Yates, M. Timbs, S. Westra, H. R. Maier, Matteo Giuliani, and Andrea Castelletti. "A bottom-up approach to identifying the maximum operational adaptive capacity of water resource systems to a changing climate." Water Resources Research 52.9 (2016): 6751-6768.

Deb, Kalyanmoy, Amrit Pratap, Sameer Agarwal, and T. A. M. T. Meyarivan. "A fast and elitist multiobjective genetic algorithm: NSGA-II." IEEE transactions on evolutionary computation 6.2 (2002): 182-197.

Delgarm, Navid, Behrang Sajadi, Saeed Delgarm, and Farshad Kowsary. "A novel approach for the simulation-based optimization of the buildings energy consumption using NSGA-II: Case study in Iran." Energy and Buildings 127 (2016): 552-560.

Ehret, Uwe, Erwin Zehe, V. Wulfmeyer, K. Warrach-Sagi, and J. Liebert. "HESS Opinions" Should we apply bias correction to global and regional climate model data?"." Hydrology and Earth System Sciences 16.9 (2012): 3391-3404.

Gao, Jungang, Aleksey Y. Sheshukov, Haw Yen, Kyle R. Douglas-Mankin, Michael J. White, and Jeffrey G. Arnold. "Uncertainty of hydrologic processes caused by bias-corrected CMIP5 climate change projections with alternative historical data sources." Journal of hydrology 568 (2019): 551-561.

Giuliani, Matteo, Daniela Anghileri, Andrea Castelletti, Phuong Nam Vu, and Rodolfo Soncini-Sessa. "Large storage operations under climate change: expanding uncertainties and evolving tradeoffs." Environmental Research Letters 11.3 (2016): 035009.

Golfam, Parvin, Parisa-Sadat Ashofteh, Taher Rajaee, and Xuefeng Chu. "Prioritization of Water Allocation for Adaptation to Climate Change Using Multi-Criteria Decision Making (MCDM)." Water Resources Management 33.10 (2019a): 3401-3416.

Hallegatte, Stéphane, Ankur Shah, Robert Lempert, Casey Brown, and Stuart Gill. "Investment decision making under deep uncertainty." Policy research working paper 6193 (2012): 1-41.

Hamza, Nahida H. "Evaluation of water quality of Diyala River for irrigation purposes." Diyala Journal of Engineering Sciences 5.2 (2012): 82-98.

Herman, Jonathan D., Patrick M. Reed, Harrison B. Zeff, and Gregory W. Characklis. "How should robustness be defined for water systems planning under change?." Journal of Water Resources Planning and Management 141.10 (2015): 04015012.

Jiang, Ying, Yong Luo, Zongci Zhao, Ying Shi, Yinlong Xu, and Jinhong Zhu. "Projections of wind changes for 21st century in China by three regional climate models." Chinese Geographical Science 20.3 (2010): 226-235.

Lafon, Thomas, Simon Dadson, Gwen Buys, and Christel Prudhomme. "Bias correction of daily precipitation simulated by a regional climate model: a comparison of methods." International Journal of Climatology 33.6 (2013): 1367-1381.

Milly, Paul CD, et al. "Stationarity is dead: Whither water management?." Science 319.5863 (2008): 573-574.

Moemken, Julia, Mark Reyers, Hendrik Feldmann, and Joaquim G. Pinto. "Wind speed and wind energy potentials in EURO-CORDEX ensemble simulations: evaluation, bias-correction and future changes." EGU General Assembly Conference Abstracts. Vol. 19. 2017.

Moemken, Julia, Mark Reyers, Hendrik Feldmann, and Joaquim G. Pinto. "Future changes of wind speed and wind energy potentials in EURO-CORDEX ensemble simulations." Journal of Geophysical Research: Atmospheres (2018).

Moody, Paul, and Casey Brown. "Robustness indicators for evaluation under climate change: Application to the upper Great Lakes." Water Resources Research 49.6 (2013): 3576-3588.

Najac, Julien, Christine Lac, and Laurent Terray. "Impact of climate change on surface winds in France using a statistical-dynamical downscaling method with mesoscale modelling." International Journal of Climatology 31.3 (2011): 415-430.

Ongoma, Victor, Haishan Chen, and Chujie Gao. "Evaluation of CMIP5 twentieth century rainfall simulation over the equatorial East Africa." Theoretical and Applied Climatology 135.3-4 (2019): 893-910.

Opalinski, Nicole. "Response of municipal water use to weather across the contiguous US." PhD diss., Colorado State University. Libraries, 2018..

PaiMazumder, Debasish, and James M. Done. "The roles of bias-correction and resolution in regional climate simulations of summer extremes." Climate dynamics 45.5-6 (2015): 1565-1581.

Paton, F. L., H. R. Maier, and G. C. Dandy. "Including adaptation and mitigation responses to climate change in a multiobjective evolutionary algorithm framework for urban water supply systems incorporating GHG emissions." Water Resources Research 50.8 (2014): 6285-6304.

Paton, F. L., H. R. Maier, and G. C. Dandy. "Relative magnitudes of sources of uncertainty in assessing climate change impacts on water supply security for the southern Adelaide water supply system." Water Resources Research 49.3 (2013): 1643-1667.

Pryor, Sara C., and R. J. Barthelmie. "Climate change impacts on wind energy: A review." Renewable and sustainable energy reviews 14.1 (2010): 430-437.

Roach, Tom, Zoran Kapelan, and Ralph Ledbetter. "A resilience-based methodology for improved water resources adaptation planning under deep uncertainty with real world application." Water resources management 32.6 (2018): 2013-2031.

Smitha, P. S., B. Narasimhan, K. P. Sudheer, and H. Annamalai. "An improved bias correction method of daily rainfall data using a sliding window technique for climate change impact assessment." Journal of Hydrology 556 (2018): 100-118.

Solomon, Susan, Martin Manning, Melinda Marquis, and Dahe Qin. Climate change 2007-the physical science basis: Working group I contribution to the fourth assessment report of the IPCC. Vol. 4. Cambridge university press, 2007.

Spence, Caitlin M., and Casey M. Brown. "Nonstationary decision model for flood risk decision scaling." Water Resources Research 52.11 (2016): 8650-8667.

Steinschneider, Scott, Sungwook Wi, and Casey Brown. "The integrated effects of climate and hydrologic uncertainty on future flood risk assessments." Hydrological Processes 29.12 (2015a): 2823-2839.

Steinschneider, Scott, Rachel McCrary, Sungwook Wi, Kevin Mulligan, Linda O. Mearns, and Casey Brown. "Expanded decision-scaling framework to select robust long-term water-system plans under hydroclimatic uncertainties." Journal of Water Resources Planning and Management 141.11 (2015b): 04015023.

Stephenson, David B., Matthew Collins, Jonathan C. Rougier, and Richard E. Chandler. "Statistical problems in the probabilistic prediction of climate change." Environmetrics23.5 (2012): 364-372.

Stocker, Thomas F., Dahe Qin, Gian-Kasper Plattner, Melinda Tignor, Simon K. Allen, Judith Boschung, Alexander Nauels, Yu Xia, Vincent Bex, and Pauline M. Midgley. "Climate change 2013: The physical science basis." (2013).

Taner, Mehmet Ümit, Patrick Ray, and Casey Brown. "Robustness-based evaluation of hydropower infrastructure design under climate change." Climate Risk Management 18 (2017): 34-50.

Taner, Mehmet Ümit, Patrick Ray, and Casey Brown. "Incorporating Multidimensional Probabilistic Information Into Robustness-Based Water Systems Planning." Water Resources Research (2019).

Tennant, Donald Leroy. "Instream flow regimens for fish, wildlife, recreation and related environmental resources." Fisheries 1.4 (1976): 6-10.

Tian, Jing, Shenglian Guo, Dedi Liu, Zhengke Pan, and Xingjun Hong. "A Fair Approach for Multi-Objective Water Resources Allocation." Water Resources Management 33.10 (2019): 3633-3653.

Tofiq, F. A., and A. Guven. "Prediction of design flood discharge by statistical downscaling and General Circulation Models." Journal of hydrology 517 (2014): 1145-1153.

Turner, Sean WD, David Marlow, Marie Ekström, Bruce G. Rhodes, Udaya Kularathna, and Paul J. Jeffrey. "Linking climate projections to performance: A yield-based decision scaling assessment of a large urban water resources system." Water Resources Research 50.4 (2014b): 3553-3567.

Ummenhofer, Caroline C., and Gerald A. Meehl. "Extreme weather and climate events with ecological relevance: a review." Philosophical Transactions of the Royal Society B: Biological Sciences 372.1723 (2017): 20160135.

Van Tra, Tran, Nguyen Xuan Thinh, and Stefan Greiving. "Combined top-down and bottom-up climate change impact assessment for the hydrological system in the Vu Gia-Thu Bon River Basin." Science of The Total Environment 630 (2018): 718-727.

Villarini, Gabriele, Francesco Serinaldi, James A. Smith, and Witold F. Krajewski. "On the stationarity of annual flood peaks in the continental United States during the 20th century." Water Resources Research 45.8 (2009).

Waheed, Saddam Q. 2013. ”Effects of climate change on water availability in Diyala basin in Iraq”, 2nd International Conference on Hydrology & Groundwater Expo. NC, USA.

Waheed, Saddam Q., Neil S. Grigg, and Jorge A. Ramirez. " Variable Infiltration Capacity Model Sensitivity, Parameter Uncertainty, and Data Augmentation for the Diyala River Basin in Iraq". Journal of American Society of Civil Engineers (2020a), Under Review.

Waheed, Saddam Q., Neil S. Grigg, and Jorge A. Ramirez. "Development of a Parametric Regional Multivariate Statistical Weather Generator for Risk Assessment Studies in Areas with Limited Data Availability". Journal of Climate Dynamics (2020b), Under Review.

Wang, Keyi, Haiyun Shi, Ji Chen, and Tiejian Li. "An improved operation-based reservoir scheme integrated with Variable Infiltration Capacity model for multiyear and multipurpose reservoirs." Journal of hydrology 571 (2019): 365-375.

Weaver, Christopher P., Robert J. Lempert, Casey Brown, John A. Hall, David Revell, and Daniel Sarewitz. "Improving the contribution of climate model information to decision making: the value and demands of robust decision frameworks." Wiley Interdisciplinary Reviews: Climate Change 4.1 (2013): 39-60.

Whateley, Sarah, Scott Steinschneider, and Casey Brown. "A climate change range-based method for estimating robustness for water resources supply." Water Resources Research 50.11 (2014): 8944-8961.

Wilby, Robert L., and Suraje Dessai. "Robust adaptation to climate change." Weather 65.7 (2010): 180-185.

Yu, Wei, Baizhan Li, Hongyuan Jia, Ming Zhang, and Di Wang. "Application of multi-objective genetic algorithm to optimize energy efficiency and thermal comfort in building design." Energy and Buildings 88 (2015): 135-143.

Yusoff, Yusliza, Mohd Salihin Ngadiman, and Azlan Mohd Zain. "Overview of NSGA-II for optimizing machining process parameters." Procedia Engineering 15 (2011): 3978-3983.

Zhang, Enze, Zhihao Xu, and Zhifeng Yang. "Bottom-up quantification of inter-basin water transfer vulnerability to climate change." Ecological Indicators 92 (2018): 195-206.

Zheng, Feifei, Aaron C. Zecchin, Holger R. Maier, and Angus R. Simpson. "Comparison of the searching behavior of NSGA-II, SAMODE, and Borg MOEAs applied to water distribution system design problems." Journal of Water Resources Planning and Management 142.7 (2016): 04016017.

Zolghadr-Asli, Babak, Omid Bozorg-Haddad, Parisa Sarzaeim, and Xuefeng Chu. "Investigating the variability of GCMs' simulations using time series analysis." Journal of Water and Climate Change 10.3 (2019): 449-463.

Zhu, Feilin, Ping-an Zhong, and Yimeng Sun. "Multi-criteria group decision making under uncertainty: Application in reservoir flood control operation." Environmental modelling & software 100 (2018): 236-251.

CHAPTER 5

CONCLUSIONS AND FUTURE WORK

The results of the study comprise a framework to help the government optimize the operation of existing water resources infrastructure as part of an ongoing effort to cope with negative influences of climate change. Developing this framework was established as the main goal of the dissertation, to develop and test a probabilistic decision-making model under non-stationary hydroclimatic conditions to assess the magnitude and timing of climate change effects for management of water resources systems.

The research included data augmentation to overcome data scarcity issues in the test region and to build valid hydrologic models. It led to a new statistical weather generator to apply in areas subject to data limitation. The study explored selection of the most robust alternative over a set of pre-specified plans using the probabilistic framework and the non-stationarity conditions anticipated in the future. The approach was demonstrated in part of the Diyala River Basin, and while analysis of additional basin areas will be more computationally-intensive, we hope to expand the scope of this framework to all of the basin and other river basins in Iraq in the future.

The main work was reported in Chapters 2, 3 and 4, which will be summarized next. Then, the full implications of the study and future work will be explained.

5.1. Conclusions about Variable Infiltration Capacity Model Sensitivity, Parameter Uncertainty, and Data Augmentation for the Diyala River Basin in Iraq

In Chapter 2, the main objectives were to augment the in situ forcing data and quantify sensitivity of the Variable Infiltration Capacity (VIC) platform to forcing data and parameter uncertainty. These enabled us to implement a valid hydrologic model for management purposes. Accurate forcing data for the basin were developed with the aid of TRMM data and GIDAL data (Adam and Lettenmaier, 2003 and Adam et al., 2006). Analysis of the coefficient of determination R^2 and Kling-Gupta Efficiency (KGE) were performed to evaluate TRMM and GIDAL performances. The GLUE and DREAM techniques methods were used for sensitivity and uncertainty analysis, which is the first attempt to implement them in Iraq.

Results of TRMM data performance exhibited smaller means and standard deviations than the ground observed data while GIDAL showed higher values. R^2 and KGE for GIDAL and TRMM were 0.618, 0.219, 0.264 and -0.227, respectively, indicating their inaccuracy without adjustment. To overcome this issue, the daily gridded precipitation data were implemented for D_{MWR} using multiplicative random cascade downscaling and Schaake Shuffle techniques. Evaluation of the MRC technique for the Derbendikhan station showed R^2 at 0.936, a higher value than the 0.705 result from Al-Khafaji and Al-Chalabi, (2019). However, a set of adjustment equations was proposed for the temperature and wind speed of GIDAL to be statistically indistinguishable from the ground observed data. The KGE values were 0.73, -0.11, 0.97, and 0.48 for temperature and wind speed before and after adjustment, respectively. These can demonstrate the validity of the proposed procedure and enable comprise a framework to implement daily gridded forcing data in the DRB.

Among the seven candidate VIC model parameters, the second soil layer depth is the most sensitive according to GLUE and DREAM techniques. On the other hand, the uncertainty analysis results glimpsed the validity of the VIC model to generate reasonable forecasts.

The VIC model outputs were calibrated on a daily time scale with KGE values of 0.743 with residuals free from non-normality, heteroscedasticity, and auto-correlation. The calibrated model performance was superior to the Al-Khafaji and Al-Chalabi, (2019) model and was examined on longer period using a more comprehensive test.

5.2. Conclusions about Development of a Parametric Regional Multivariate Statistical Weather Generator for Risk Assessment Studies in Areas with Limited Data Availability

In Chapter 3, a Parametric Regional Weather Generator (PR-WG) was developed to assess climate change impacts on water resources systems for cases of limited data with the ability to mimic the statistical characteristics of observed data.

The PR-WG features are its flexibility to select any distribution function for each weather variable, ability to produce scenarios within or beyond the historic observation length with wider range, and ability to produce synthetic scenarios through direct parameter alteration.

Results showed that PR-WG accurately preserves the statistical properties (mean, standard deviation, and skewness coefficient) of the weather variables, and the overall KGE test value was 0.98. PR-WG effectively estimates the dry and wet day occurrences using a First-order, Two-state Markov Chain (FTMC) with an overall KGE value of 0.97. The results also confirmed the effectiveness of Wilks' technique to produce spatially correlated precipitation states (KGE of

0.98) and spatially and cross-correlated weather variables (KGE of 0.96) besides the temporal correlation (KGE of 0.97).

Although the PR-WG was tested and validated in the DRB, it is applicable in other places and can be easily extended for other climate variables. The PR-WG is unsophisticated and can effectively facilitate the implementation of risk assessment study in areas with limited data availability.

5.3. Conclusions about Nonstationary-Probabilistic Decision Framework to Assess the Long-Term Water Resources System Vulnerability under Climate Change and Quantify the Robust Plan and Timing

In Chapter 4, a decision-making framework was developed to evaluate the assess responsiveness of the system to long-term climate change and to gain insight about risk characteristics. The framework bridged the nonstationary assumption of the climate exposure with the supply, demand, and system losses for the multi-objective function across wide climate trajectories. The framework is designed to identify the optimal-robust (or the best among pre-suggested plans) to alleviate the anticipated future vulnerability.

New approaches were proposed to analyze the future climate trajectories. Also, new robustness metrics (FPE, DME, HPE, NER) were derived for the long-term robustness examination under wide range of climate changes. Moreover, a novel term MAT was presented to distinguish the theoretical time window of the robust plan(s) under multiple objectives. The reduction of demand ratio (MR) was modeled as an adaptation so as to urge water resources managers to focus on sustainable water management. The study represents the first attempt to evaluate wind

speed magnitude effects in decision-making process. It is also the first bottom-up case study inside Iraq.

Analyzing the GCM outputs showed that the precipitation mean are subject to vary from -37.4% to +31.3% (average of -4.8%); precipitation CV change will vary from -38.2% to 34.0% (average of +2.5%), temperature mean change will increase from +0.4 C^o to 5.1 C^o (average of +2.3 C^o), temperature CV change will vary from -45.8% to 30.8% (average of -8.2%), wind speed magnitude mean will vary from -22.3% to 11.7% (average of -4.9%), and wind speed magnitude CV will vary from -29.1% to 32.2% (average of -0.1%).

Analysis of the status quo system capability glimpsed that the system is vulnerable in drought management and robust for the flood protection. The computed DME and FPE are 0.178 and 0.605, respectively, which implies that project managers should pay attention to drought and water scarcity management comprehensively.

The analysis of weather variable effectiveness indicated that the precipitation mean alteration is the dominant parameter, followed by precipitation CV and then by temperature change and wind speed. The results also show that considering wind speed change is essential in drought management.

Three synthetic adaptations were suggested to improve the system performance in meeting the demand ratio and maintain an acceptable performance for the other objectives (e.g., FPE, DME, HPE, and NER). Results revealed that reducing the MR for municipality and industry by 30% is vulnerable, while the other two plans of reducing MR for irrigation or environment by 20% are robust. Of interest of this study, the upper limit time to apply a robust adaptation is 14 to avoid with the undesirable climate change influence. The optimal pareto set using NSGA-II is

obtained by reducing the MR for municipality, irrigation, industry, and environmental 0.985, 0.900, 0.915, and 0.925 respectively. The DME, FPE, HPE, NER, and MAT were 0.502, 0.599, 1.099, 0.896, and 9 [years] respectively.

5.4. Future work

Many applications were left for future work since running of the models is very time consuming, requiring even months to get the results. The future possible work can be summarized as follows:

1) Examining the applicability of the proposed forcing data framework in other basins in Iraq. Also, examination the applicability of other data sources of finer special resolution than 0.5 degree is of interest, such as Climate Forecast System Reanalysis (CFSR) dataset for spatial resolution of 1/3 degree.
2) The coefficient of variation for temperature and wind speed were not significant in the DRB. Their significance could be examined using a smaller time step for the dam operation plan such as weekly, or bi-weekly.
3) Extend the suggested decision-making framework for all DRB by including the operation rules of Hemrin dam. Also, other indicators can be added to the framework, such as water quality, water pollutant restrictions, sediment transport, and ecosystem requirements, among others. Further assumptions and simplifications are required to facilitate the work in order to reduce the running time of the models. Furthermore, more information and assumptions about the upstream project development are needed to obtain realistic results to plan for the future adaptation strategies for sustainable water uses in Iraq.

4) Examine the effect of the spatial and cross correlations on the suggested decision-making framework. One possible solution to simplify the suggested framework to include only the significant correlations in the weather generator preprocessing stage.
5) Consider the nonstationary in the hydrological model parameters and include the uncertainty of the model parameters and forcing data.

APPENDIX A

Description of Variable Infiltration Capacity (VIC) Macroscale Hydrologic Model

This section describes the VIC model processes and the mathematical formulations. The overall VIC model framework is shown in Figure A.1. First, VIC can be run in two approaches: Water Balance and full water-energy balance. In water balance approach, it assumes that the soil surface temperature is equal to the air temperature for the current time step. This will eliminate the solution of ground heat flux and the iterative processes required to close the surface energy balance, therefore it requires less computational time. This simplification is suitable on daily time step that is the typical of water balance mode simulations, yields a substantial savings in computational time. The full water-energy balance mode solves the complete water balance as well as also minimizing the surface energy balance error through iterative processes to find the surface temperature that yields surface energy fluxes (sensible heat, ground heat, ground heat storage, outgoing longwave and indirectly latent heat) so that balance the incoming solar and longwave radiation fluxes. This mode requires more computational time than the water balance mode as well as requiring a sub-daily simulation time step. Given the condition that we have daily time step time series and we use VIC for thousands or run, we use the water balance approach in our study, and we describe only it here.

A.1. Water Balance Component

The water balance that is used in the VIC model follows the continuous equation for each time-step:

$$\frac{\partial S}{\partial t} = P - E - R \tag{A.1}$$

where *dS/dt, P, E, and R are* the change of water storage, precipitation, evapotranspiration, and runoff, respectively and all in mm. Over vegetated areas, the water balance equation in the canopy layer (interception) is:

$$\frac{\partial W_i}{\partial t} = P - E_c - P_t \tag{A.2}$$

where W_i is canopy intercepted water (mm), E_c is evaporation from canopy layer (mm), and P_t is througfall (mm).

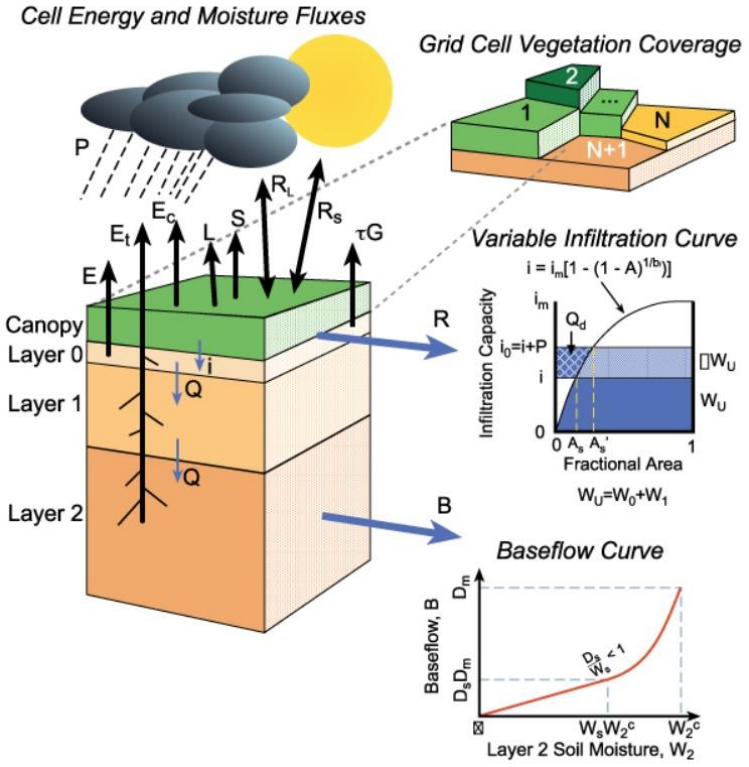

Figure A.1: The general schematic framework of the VIC model (Adapted from Gao et al., 2010).

A.2. Evapotranspiration Component

VIC model computes three different types of evaporation: 1) evaporation from the canopy layer corresponding to each vegetation type, 2) transpiration, E_t, from each of the vegetation

type, and 3) evaporation from the bare soil ,E_1. The Total evapotranspiration over a grid cell is calculated as the sum of the three components multiplied by the weights of the area fractions, as follows:

$$E = \sum_{n=1}^{N} C_n \times \left(E_{c,n} + E_{t,n}\right) + C_{N+1} \times E_l \quad \text{(A.3)}$$

Where C_n is the vegetation fractional area for the n^{th} vegetation type and C_{N+1} is the bare soil fraction in which $\Sigma C_n = 1$.

The canopy evaporation reaches the maximum value, E^*_t, when the intercepted water is present on the canopy and as follows:

$$E_t^* = \left(\frac{W_i}{W_{im}}\right)^{2/3} E_P \frac{r_w}{r_w + r_o} \quad \text{(A.4)}$$

Where W_{im} is the maximum amount of water the canopy can intercept, r_o and r_w are architectural and aerodynamic resistance respectively, and *Ep* is the potential evapotranspiration rate using Penman-Monteith equation. Dickinson, (1984) estimated W_{im} to be the leaf area index, LAI, by 0.2. Deardorff, (1978) described the power of the equation (2/3).

If the intercepted water is not enough to meet the demand within one-time step, the canopy evaporation, E_c, will be:

$$E_c = f \times E_c^* \quad \text{(A.5)}$$

where f is the fraction of the time step for canopy evaporation to evaporate the intercepted water and calculate by:

$$f = min\left(1, \frac{W_i + P + \Delta t}{E_c^* . \Delta t}\right) \quad \text{(A.6)}$$

However, VIC uses the equation developed by Blondin, (1991) and Ducoudre et al., (1993) to compute the transpiration, as follows:

$$E_t = (1 - (\frac{W_i}{W_{im}})^{2/3})\ E_P\ \frac{r_w}{r_w + r_o + r_c} \quad \text{(A.7)}$$

Where r_c is the canopy resistance and calculate as:

$$r_c = \frac{r_{oc}\ g_T\ g_{vpd}\ g_{PAR}\ g_{sm}}{LAI} \quad \text{(A.8)}$$

where r_{0c} is the minimum canopy resistance in s m^{-1}, and g_T, g_{vpd}, g_{PAR}, and g_{sm} are the temperature factor, vapor pressure deficit factor, photo-synthetically active radiation flux (PAR) factor, and soil moisture factor, respectively.

Finally, the bare soil evaporation is calculated according to Franchini and Pacciani, (1991) equation and takes place only form the top soil layer.

$$E_1 = E_p(\int_0^{A_S} dA + \int_{A_S}^{1} \frac{i_o}{i_m \left(1 - (1 - A)^{\frac{1}{b_i}}\right)}\ dA \quad \text{(A.9)}$$

where A_s is the fraction of the bare soil that is saturated, i_0 is the point infiltration capacity, i_m is the maximum infiltration capacity, A is the fraction of the area for which the infiltration capacity is less than i, and b_i is the infiltration shape parameter. i and i_m are expressed as [Zhao et al., 1980]:

$$i = i_m \left(1 - (1 - A)^{\frac{1}{b_i}}\right) \quad \text{(A.10)}$$

$$i_m = (1 + b_i)\ \theta_s\ |z| \quad \text{(A.11)}$$

where ϑ_s is the soil porosity, and z is the soil depth (m).

A.3. Runoff Component

The surface runoff can occur from the upper two soil layers when the precipitation plus the soil moisture storage at the end of the previous time step are more the soil storage capacity.in which, the surface runoff, Q_d, is generated f using the variable infiltration curve [see equation (A.7)] with accounting for the spatial heterogeneity of runoff generation. The subsurface runoff, Q_b, is calculated using Arno model developed by Franchini and Pacciani, (1991) and Todini, (1996), as follows;

$$Q_d = P - z_2(\theta_s - \theta_2) + z_2\,\theta_s\left(1 - \frac{i_o + P}{i_m}\right)^{1+b_1} \qquad if\ P + i_o \le i_m \tag{A.12}$$

$$Q_d = P - z_2(\theta_s - \theta_2) \qquad if\ P + i_o \ge i_m \tag{A.13}$$

$$Q_b = \frac{D_S D_M}{W_S \theta_S}\ \theta_3 \qquad if\ \ 0 \le \theta_3 \le W_s\theta_s \tag{A.14}$$

$$Q_b = \frac{D_S D_M}{W_S \theta_S}\ \theta_3 + \left(D_m - \frac{D_S D_M}{W_S}\right)\left(\frac{\theta_3 - D_S D_M}{\theta_s - W_S\theta_S}\right)^2 \qquad if\ \ 0 \le \theta_3 \le W_s\theta_s \tag{A.15}$$

where D_m is the maximum subsurface flow (mm d^{-1}), D_S is a fraction of D_m,, and W_S is the fraction of maximum soil moisture (soil porosity) ϑ_s. The base flow recession curve is linear below a threshold ($W_S\,\vartheta_s$) and nonlinear above the threshold. Therefore, the total runoff, *Q,* is computed for each n^{th} land cover tile as:

$$Q = \sum_{n=1}^{N+1} C_n\left(Q_{d,n} + Q_{b,n}\right) \tag{A.16}$$

VIC model assumes that there is no lateral flow in the top two soil layers and uses one-dimensional (vertical) Richard's equation to characterize the soil moisture movement. Then Mahrt and Pan, (1984) included the atmospheric forcings into Richard's equation to get an integrated equation of soil moisture for top two soil layers:

$$\frac{\partial \theta_i}{\partial t} Z_i = I - E - K(\theta)|_{-Z_i} + D(\theta)\frac{\partial \theta}{\partial Z}|_{-Z_i} \quad for\ i = 1\ or\ 2 \tag{A.17}$$

where θ is volumetric soil moisture content, z is the soil layer depth, I is the infiltration rate and computed as the difference between the precipitation and surface runoff, (θ) is the hydraulic conductivity, and D(θ) is the soil water diffusivity. However, the soil moisture of the lower soil layer (third) is modeled using water balance with the diffusion between the soil layers:

$$\frac{\partial \theta_3}{\partial t} (Z_3 - Z_2) = K(\theta)|_{-Z_2} + D(\theta)\frac{\partial \theta}{\partial Z}|_{-Z_2} - E - Q_b \tag{A.18}$$

In case it is bare soil, the evapotranspiration term turns to is zero since no evaporation from the lower soil layer. Otherwise, if the vegetation roots reach the lower (third) soil layer, the evapotranspiration is considered.

A.4. Snow Component

Although we only perform VIC on water balance approach, snow model still solves an energy balance between the snowpack; forest canopy and atmosphere using scheme of Andreadis et al., (2009) and Gao et al., (2010), as shown in Figure (A.1). The spatial resolution of model usually ranges from 10 km and up, therefore the snow processes may not be modeled adequately as the spatial resolution of model is larger than characteristic scales of snow processes. Therefore, the VIC model employs a mosaic type representation of each grid cell to model the subgrid variability of topography, vegetation and precipitation through dividing the grid cell by the number of elevation bands. Herein, each elevation band contains N+1 land cover tiles. Then, the energy and mass balance models the snow processes for each land cover tile within each band. In addition, the fluxes of energy and mass are estimated as area averages of the tiles.

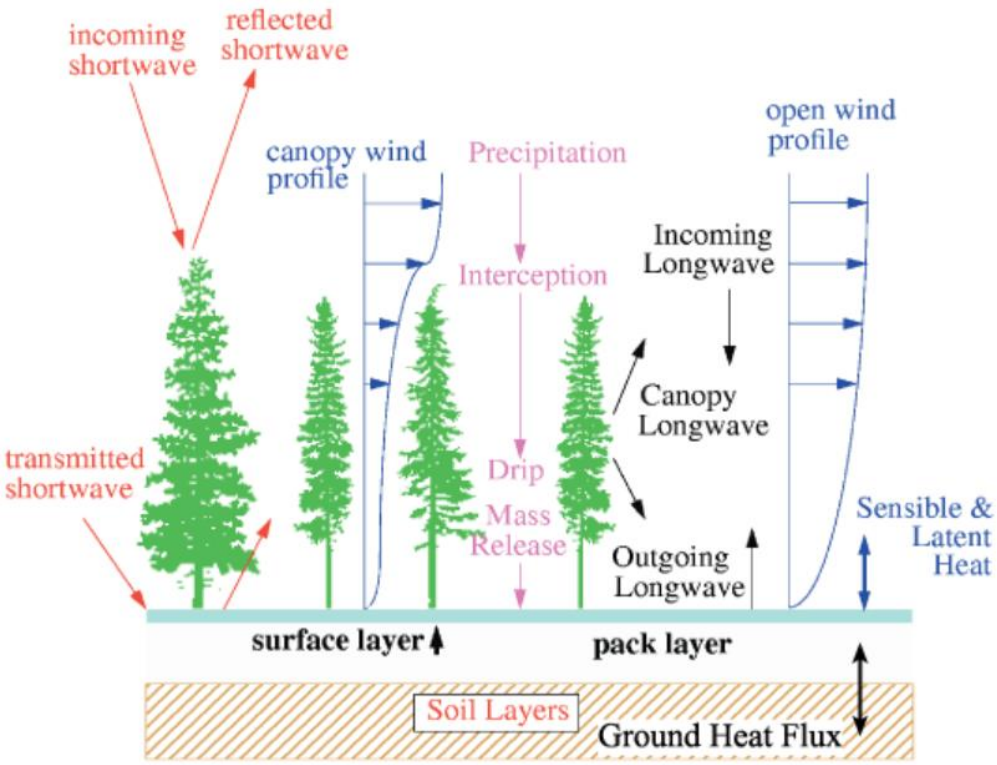

Figure A.2: Schematic framework of snow process of VIC model (Adapted from *Gao et al.,* 2010).

However, the snowpack is processed as a two-layer medium: the surface layer and pack layer. Energy and mass balance is performed for both layers. But, the energy exchange between the atmosphere, forest canopy, and snowpack takes place within the surface layer only. The energy balance of the surface layer is modeled as:

$$p_w \, c_s \, \frac{dWT_s}{dt} = Q_r + Q_s + Q_l + Q_p + Q_m \qquad \text{(A.19)}$$

where c_s is the specific heat of ice (J/kg/K), ρ_w is the density of water (kg/m^3), W is the water equivalent (mm), Ts is the temperature of the surface layer (°C), Q_r is the net radiation flux (W m^{-2}), Q_s is the sensible heat flux (W m^{-2}), Q_l is the latent heat flux (W m^{-2}), Q_p is the energy flux advection to the snowpack by rain or snow (W m^{-2}), and Q_m is the energy flux given to the pack due to liquid water refreezing or removed from the pack during melt (W m^{-2}).

When the snow accumulates on the ground, it goes through a metamorphism process and causes compaction and density increment over time. This compaction is computed as the sum of two fractional compaction rates: compaction due to metamorphism and overburden. However, the snow albedo is assumed to decay with time propagation as:

$$a_a = 0.85\ \lambda_a^{t_d{}^{0.58}} \tag{A.20}$$

$$a_m = 0.85\ \lambda_m^{t_d{}^{0.58}} \tag{A.21}$$

where α_a, α_m are the albedo during the accumulation and ablation seasons, t_d is the time since the last snowfall (in days), λ_a = 0.92, and λ_m = 0.70. Accumulation and ablation seasons are assigned according to the absence or presence of liquid water in the snow surface layer.

During snowmelt, the atmosphere above the snow surface will get warmer. When parcels of cooler air near move upward by turbulent eddies, they tend to infiltrate back into the surface where turbulent exchange is occurred. The aerodynamic resistance of the snow cover is typically corrected for atmospheric stability using the bulk Richardson's, a dimensionless ratio of the buoyant and mechanical forces acting on a parcel of air.

The snow interception is the canopy interception, snowmelt, and mass taking place at the spatial scales of distributed hydrology models. Snowfall is intercepted by the overstore and it reaches the maximum storage capacity according to:

$$I = f\ P_s \tag{A.22}$$

where I is the water equivalent of snow intercepted during a time step (mm), P_s is the snowfall over the time step (mm), and f is the efficiency of snow interception. Storck et al., (2002)

suggested the efficiency of snow interception to be 0.6. The maximum interception capacity (mm), *B*, is given by:

$$B = L_r\, m(LAI) \tag{A.23}$$

where LAI is the single-sided leaf area index of the canopy, m can be found from the observations of maximum snow interception capacity (mm), and Lr is the leaf area ratio as a function of temperature.

The snowmelt is calculated directly from a modified energy balance, similar to that applied for the ground snowpack. A new intercepted rainfall is computed according to the water holding capacity of the intercepted snow. The intercepted snowpack may contain both ice and liquid water. Snowmelt that excesses of the liquid water holding causes meltwater drip. Mass release of snow from the canopy takes place when sufficient snow is available. A 0.4 ratio of 0.4 is derived by Storck et al., (2002) using observations of the ratio of mass release to meltwater drip.

Bowling et al., (2004) developed a blowing snow model to evaluate topographically-induced sub-grid with accounting for the magnitude of wind speed, snow transport, and sublimation. It considers the energy advected by rainfall, throughfall, net radiation, ground heat flux, and sensible and latent heat fluxes. In case the canopy is found, the incoming shortwave and longwave radiation as well as the wind speed are attenuated through the canopy. The time rate of snow water change (W_e) for each vegetation fraction inside the grid cell is calculated as:

$$\frac{dW_e}{dt} = P - M - p\, Q_v - Q_e \tag{A.24}$$

where dW_e/dt is the rate of snow water accumulation, M is snowmelt and drainage, Q_v is the sublimation from blowing snow, and Q_e is evaporation and sublimation from the snowpack, for a time increment dt.

References

Gao, Huilin, Qiuhong Tang, Xiaogang Shi, Chunmei Zhu, Ted Bohn, Fengge Su, Ming Pan, Justin Sheffield, Dennis Lettenmaier, and Eric Wood. "Water budget record from Variable Infiltration Capacity (VIC) model." Algorithm Theoretical Basis Document for Terrestrial Water Cycle Data Records (2010).

Dickinson, Robert E. "Modeling evapotranspiration for three-dimensional global climate models." Climate processes and climate sensitivity 29 (1984): 58-72.

Deardorff, James W. "Efficient prediction of ground surface temperature and moisture, with inclusion of a layer of vegetation." Journal of Geophysical Research: Oceans 83.C4 (1978): 1889-1903.

Blondin, Christian. "Parameterization of land-surface processes in numerical weather prediction." Land Surface Evaporation. Springer, New York, NY, 1991. 31-54.

Ducoudre, Nathale I., Katia Laval, and Alain Perrier. "SECHIBA, a new set of parameterizations of the hydrologic exchanges at the land-atmosphere interface within the LMD atmospheric general circulation model." Journal of Climate 6.2 (1993): 248-273.

Franchini, Marco, and Michele Pacciani. "Comparative analysis of several conceptual rainfall-runoff models." Journal of Hydrology 122.1-4 (1991): 161-219.

Zhao, R-J. "The xinanjiang model." Proceedings of the Oxford Symposium. 1980.

Todini, Ezio. "The ARNO rainfall—runoff model." Journal of hydrology 175.1-4 (1996): 339-382.

Mahrt, Lawrence, and H. Pan. "A two-layer model of soil hydrology." Boundary-Layer Meteorology 29.1 (1984): 1-20.

Andreadis, Konstantinos M., Pascal Storck, and Dennis P. Lettenmaier. "Modeling snow accumulation and ablation processes in forested environments." Water Resources Research 45.5 (2009).

Storck, Pascal, Dennis P. Lettenmaier, and Susan M. Bolton. "Measurement of snow interception and canopy effects on snow accumulation and melt in a mountainous maritime climate, Oregon, United States." Water Resources Research 38.11 (2002): 5-1.

Bowling, L. C., J. W. Pomeroy, and D. P. Lettenmaier. "Parameterization of blowing-snow sublimation in a macroscale hydrology model." Journal of Hydrometeorology 5.5 (2004): 745-762.

APPENDIX B

Description of Routing Model (RVIC)

The routing model (RVIC) is developed by Lohmann, et al., (1996) and Lohmann, et al., (1998) as a post-processor with VIC model to route the total generated runoff by VIC in each grid into the basin outlet(s). The general framework of the RVIC model is shown in Figure B.1. The model assumes that the generated runoff moves inside the grid cell into the channel network before it moves out into another grid cell until it reaches the outlet. The Flow directions can exist in eight possible directions form a grid cell into another and weighted by the fraction of the grid cell that is inside the basin border. i.e, the runoff is first transported to the outlet of the cell using a unit hydrograph and then routed to in the river network up to the basin outlet. Therefore, two routing approaches are exist here: cell routing and channel (river) routing and both are assumed as simple linear transfer functions. They use First Differenced Transfer Function-Excess Rainfall and Unit Hydrograph by a Deconvolution Iterative Technique with a time scale separation and a simple linear routing model [Duband et al., 1993]. The runoff is transported is as a linear, causal, stable, and time invariant with a positive impulse response function.

B.1. Cell Grid Routing

The runoff movement is divided into fast and slow components of the measured discharge with the linear model explained by Duband et al., (1993) in order to simulate the dynamics of the horizontal routing process as:

$$\frac{dQ^s(t)}{dt} = -k\,Q^s(t) + b\,Q^F(t) \qquad \text{(B.1)}$$

$$Q(t) = Q^S(t) + Q^F(t) \quad \text{(B.2)}$$

where $Q^S(t)$ is the slow flow component, $Q^F(t)$ is the fast flow component, and Q(t) is the total flow. The parameters b and k are assumed constant for each basin over the period of simulation. The ratio of b over k is the ratio of slow flow water over the fast flow. Both slow and fast flow components are analytically linked by the following expression:

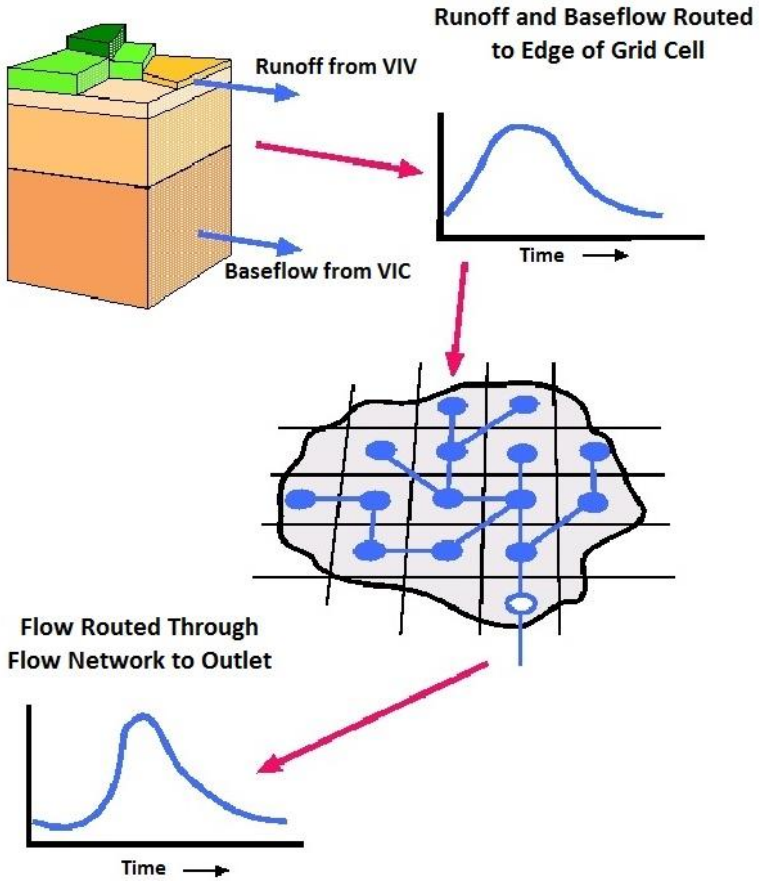

Figure B.1: The overall schematic framework of RVIC model (Adapted from Gao et al., 2010).

$$Q^s(t) = Q^S(0)\, exp(-kt) + b \int_0^t exp\big(-k\,(t-\tau)\big) Q^F(\tau) d\tau \quad \text{(B.3)}$$

The initial condition Q^S (0) is decayed exponentially with the mean residence time of water in the flow (1/k). The half-life decay is then equal to (ln2)/k. the total discharge for the discrete values will then be:

$$Q^s(t) = \frac{exp\ (-k\ \Delta t)}{1 + b\ \Delta t}\ Q^s\ (t - \Delta t) \frac{b\ \Delta t}{1 + b\ \Delta t}\ Q(t) \tag{B.4}$$

The linearity assumption between the streamflow and effective precipitation leads to the impulse response function between the fast flow and effective precipitation based on equation (B.4) and by solving the following equation iteratively:

$$Q^F(t) = \int_0^{t_{max}} UH^F\ (\tau)\ P_{eff}\ (t - \tau) d\tau \tag{B.5}$$

Where UH^F (τ) is the impulse response function, the unit hydrograph, for the fast flow component, t_{max} is the time taken for all fast processes to decay, and P^{eff} is the effective precipitation. The fast flow can then be expressed in discrete format with n data points at the time step of Δt, and t_{max} = (m-1) Δt and solved iteratively for the of UH^F_i as follows:

$$\begin{pmatrix} Q_m^F \\ M \\ Q_n^F \end{pmatrix} = \begin{pmatrix} P_m^{eff} & \Lambda & P_1^{eff} \\ M & O & M \\ P_n^{eff} & \Lambda & P_{n-m+1}^{eff} \end{pmatrix} \begin{pmatrix} UH_0^F \\ M \\ UH_{m-1}^F \end{pmatrix} \tag{B.6}$$

The following constrain is held is each iteration:

$$\sum_{i=0}^{m-1} UH_i^F = \frac{1}{1 + b/k} \quad with \quad UH_i^F \geq \forall_i \tag{B.7}$$

The UH^F is then be solved for the effective precipitation as:

$$\begin{pmatrix} Q_m^F \\ M \\ M \\ Q_n^F \end{pmatrix} = \begin{pmatrix} UH_{m-1}^F & \Lambda & UH_0^F & 0 & \Lambda & 0 \\ 0 & o & o & o & o & M \\ M & o & o & o & o & 0 \\ 0 & \Lambda & 0 & UH_{m-1}^F & \Lambda & UH_0^F \end{pmatrix} \begin{pmatrix} P_1^{eff} \\ M \\ M \\ P_1^{eff} \end{pmatrix} \quad \text{(B.8)}$$

The model keeps holding the constrain ($0 \leq P_i^{eff} \leq P \leq \forall_i$) in each iteration step. Then, the newly computed effective precipitation is inserted back, and the deconvolution procedures are repeated until reaching the convergence. However, the UH of that grid cell is found through the catchment and the river network impulse response function corresponding to the catchment.

B.2. River Routing

A simple linear model based on the linearized Saint-Venant equation is employed to route the computed generated runoff in the basin channel (river) in to the outlet, as follow:

$$\frac{\partial Q}{\partial t} = D\,\frac{\partial^2 Q}{\partial x^2} - C\,\frac{\partial Q}{\partial t} \quad \text{(B.9)}$$

where C is a parameter denoting the wave velocity and D is a parameter denoting the diffusivity. Both C and D characterize the water transport within the cell. They can be found from the measurements or estimated from the bed river data for each gird cell due to their effectiveness and variance in each geographic location. Equation (B.9) is then solved with aid of the convolution integral, as follows:

$$Q(x,t) = \int_0^t U(t-s)\;\, h(x,s)ds \quad \text{(B.10)}$$

And,

$$h(x,t) = \frac{x}{2t\sqrt{\pi\, t\, D}} exp(-\frac{(C\, t - x)^2}{4Dt}) \quad \text{(B.11)}$$

The function h (x,t) represents the impulse response function of the Saint-Venant equation with $h(x,0)=0$ at $x>0$, and $h(0,t) = \delta(t)$ for $t \geq 0$.

References

Lohmann, D., R. Nolte-Holube, and E. Raschke. "A large-scale horizontal routing model to be coupled to land surface parametrization schemes." Tellus A48.5 (1996): 708-721.

Lohmann, D., Raschke, E., Nijssen, B., & Lettenmaier, D. P. "Regional scale hydrology: I. Formulation of the VIC-2L model coupled to a routing model." Hydrological Sciences Journal 43.1 (1998): 131-141.

Gao, Huilin, Qiuhong Tang, Xiaogang Shi, Chunmei Zhu, Ted Bohn, Fengge Su, Ming Pan, Justin Sheffield, Dennis Lettenmaier, and Eric Wood. "Water budget record from Variable Infiltration Capacity (VIC) model." Algorithm Theoretical Basis Document for Terrestrial Water Cycle Data Records (2010).

Duband, D., Ch Obled, and J. Y. Rodriguez. "Unit hydrograph revisited: an alternate iterative approach to UH and effective precipitation identification." Journal of Hydrology 150.1 (1993): 115-149.

APPENDIX C

Ground Observation Gages in the Study Area

Table C.1: The ground gage stations for precipitation in the Diyala River Basin, coverage ranges, and completeness percentages (MoWR, 2011; unpublished data).

No	Station	Longitude	Latitude	Country	Monthly Coverage		Monthly Completeness (%)	Daily Coverage		Daily Completeness (%)
1	Sarpolzohab	45.86	34.45	Iran	Jan/1986	Dec/2005	26.2	Jan/1996	Dec/1999	7.7
2	Sanandaj	47	35.33	Iran	Sep/1959	Dec/2000	40.3	Jan/1971	Dec/1999	28.7
3	Marivan	46.2	35.51	Iran	Jan/1992	Dec/1999	10.6	Dec/1959	Dec/2008	23.4
4	Eslamabadgharb	46.43	34.13	Iran	Jan/1991	Dec/2000	13.2	-	-	0
5	As Sulaymaniya	45.45	35.55	Iraq	Nov/1935	Dec/2011	98.9	Nov/2000	May/2011	17.6
6	Chwarta	45.57	35.71	Iraq	Feb/1942	Sep/1970	26.7	Oct/2001	May/2011	17.1
7	Derbendikhan	45.69	35.11	Iraq	Feb/1957	Sep/1971	70	Dec/1961	Jun/2011	94.2
8	Dokan	44.95	35.92	Iraq	Jan/1959	Sep/2009	67.4	Jan/1959	May/2011	96.6
9	Halabcha	45.98	35.17	Iraq	Jan/1941	Sep/1987	48.3	Oct/2001	May/2011	17.1
10	Kifri	44.96	34.68	Iraq	Feb/1957	May/2011	29.1	-	-	0
11	Penjween	45.94	35.62	Iraq	Oct/1939	Sep/1979	29.5	Jan/2001	May/2011	17.3
12	Qaradagh	45.4	35.3	Iraq	Feb/1958	Sep/1981	8	Oct/2001	May/2011	17.1
13	Hemrin	44.97	34.11	Iraq	May/1936	Sep/2009	24.5	Oct/2003	May/2011	13.9
14	Jalawla	45.15	34.27	Iraq	Nov/1935	Sep/2006	65.8	Oct/2003	May/2011	8.2
15	Khanaqin	45.43	34.3	Iraq	Aug/1937	Dec/2008	91.5	Jan/2001	Dec/2010	20.8
16	Mansuriya El Jabal	45	34.05	Iraq	Jan/1940	Sep/1981	43.5	-	-	0

APPENDIX D

TRMM and GIDAL Performances.

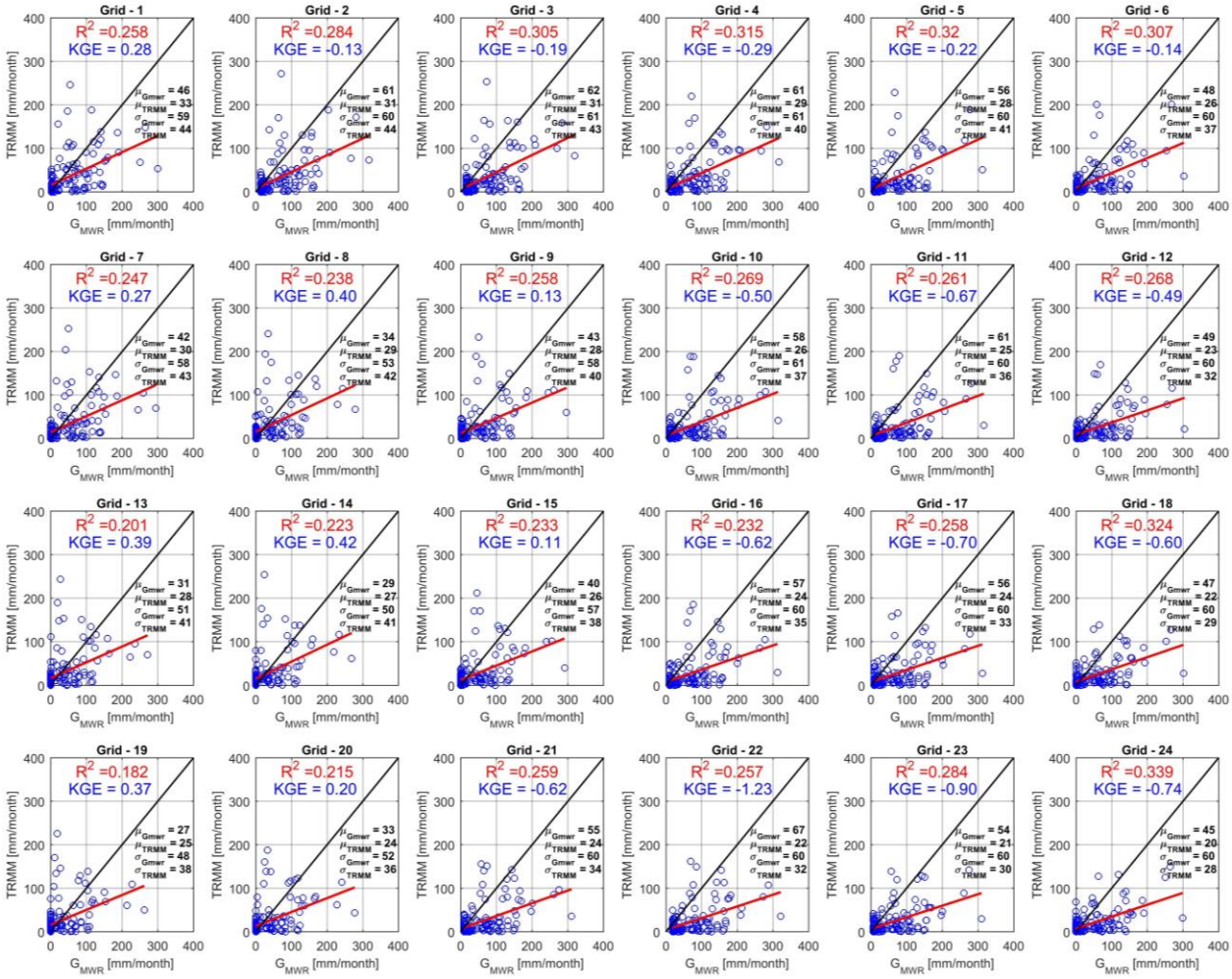

Figure D.1: The monthly precipitation plots observation data (G_{MWR}) data versus TRMM data in the 24 basin grids in blue dots with KGE and R^2 values for the overlap period years (Mar 2000 to Dec 2011). The red line is the regression line between G_{MWR} and TRMM. The black line is a 1:1 line for comparison purpose.

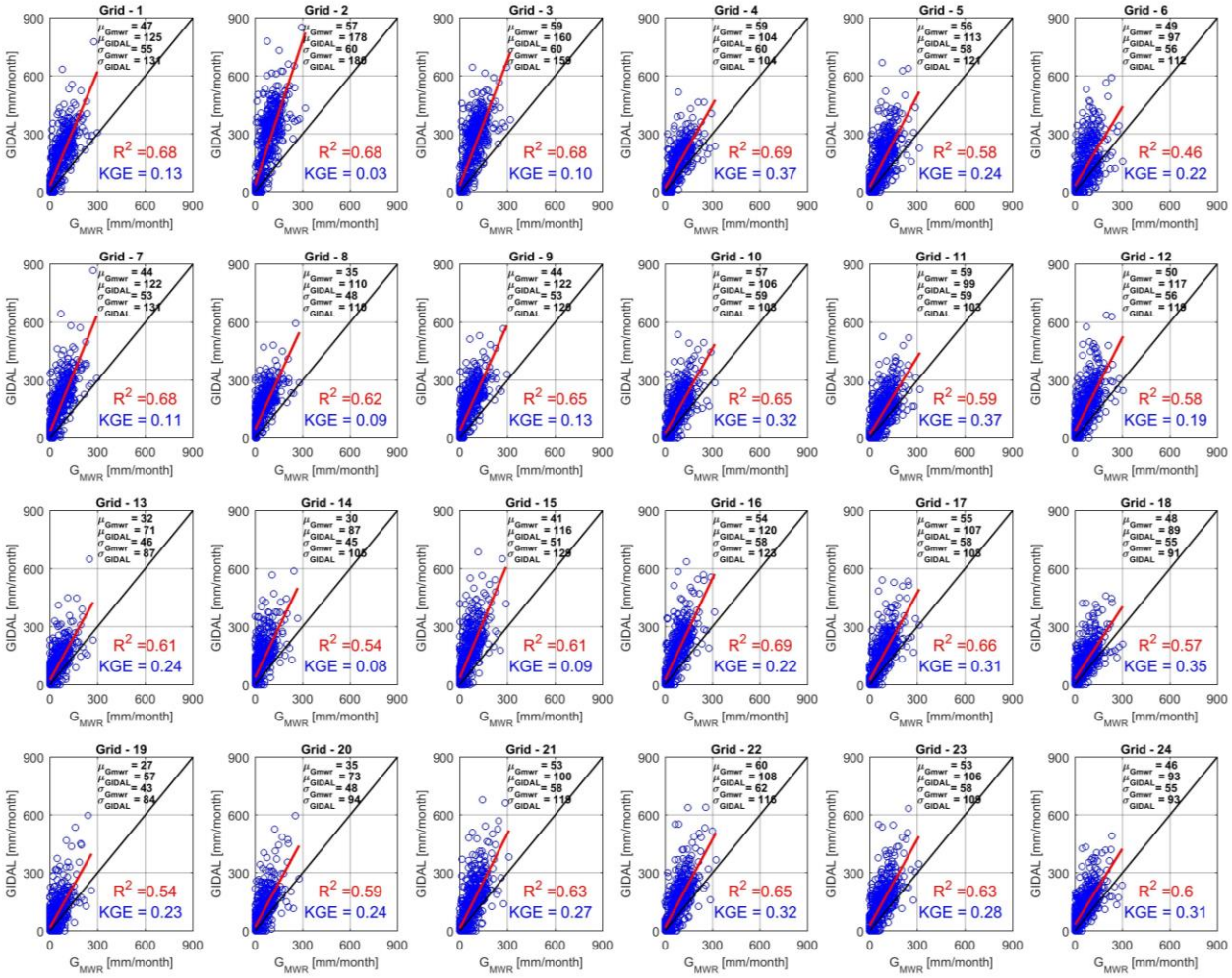

Figure D.2: The monthly precipitation plots of G_{MWR} versus GIDAL in the 24 basin grids in blue dots with KGE and R^2 values for the overlap period years (Jan 1948 to Oct 2007). The red line is the regression line between G_{MWR} data and GIDAL. The black line is a 1:1 line for comparison purpose.

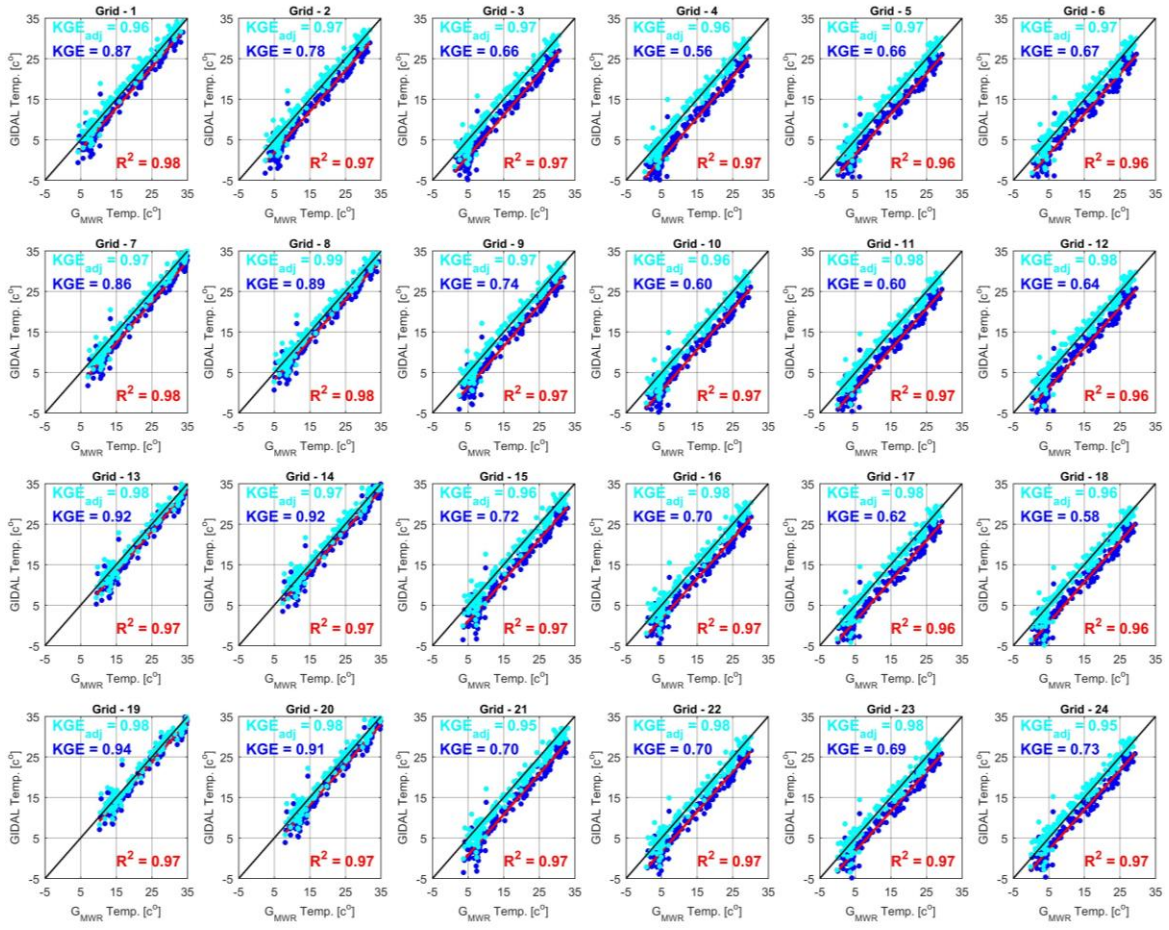

Figure D.3: The monthly temperature plots of G_{MWR} versus the GIDAL (before and after adjustment) in the 24 basin grids, with R^2 and KGE (before and after adjustment) values. The red line is the regression line between G_{MWR} and GIDAL. The black line is a 1:1 line for comparison purpose.

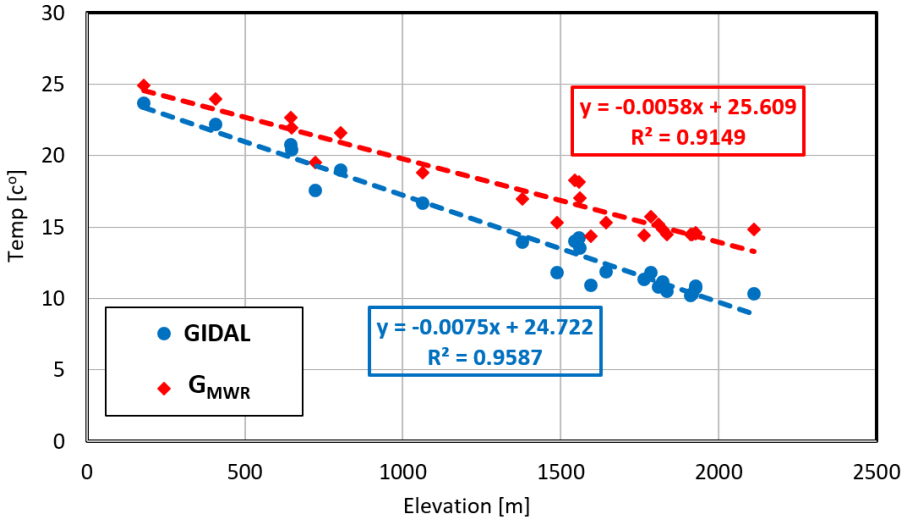

Figure D.4: Relationship of G_{MWR} and GIDAL (temperature) with the average grid elevation DRB.

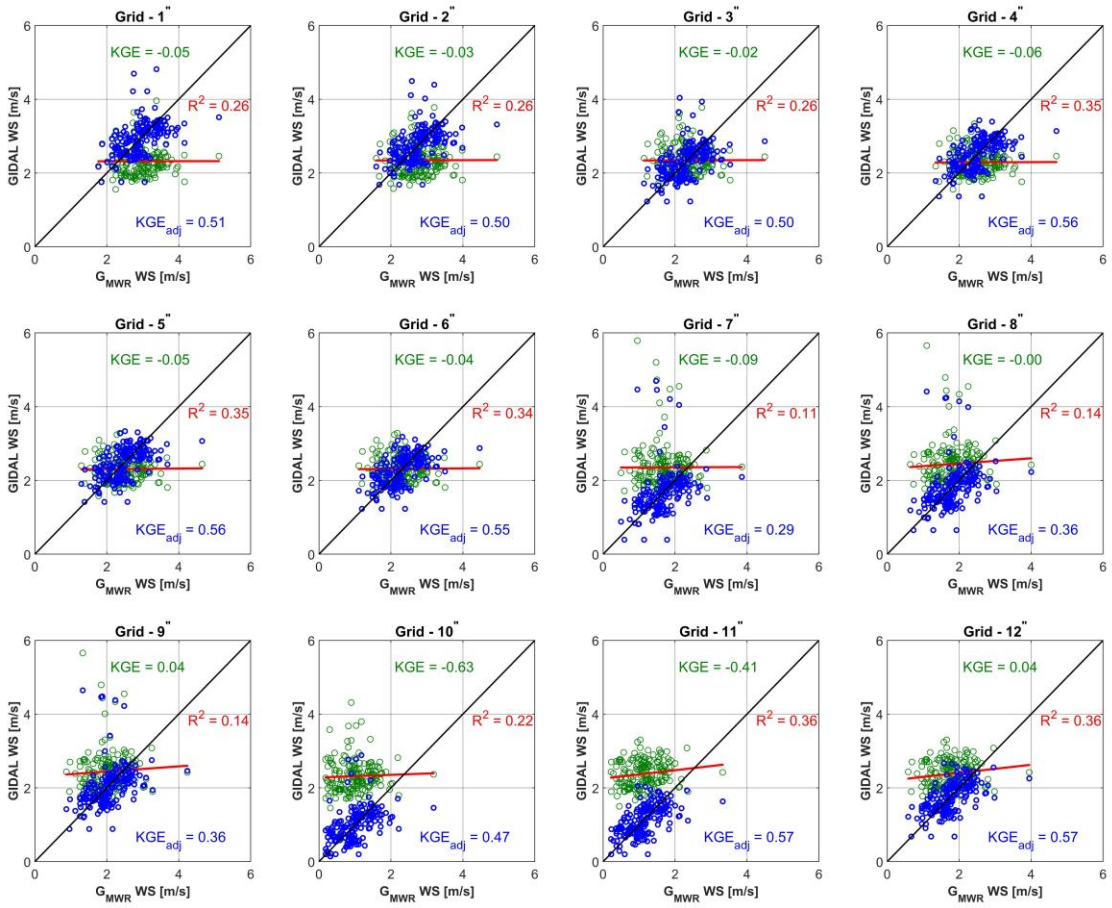

Figure D.5: The monthly wind speed plots of G_{MWR} versus the GIDAL (before and after adjustment) in the 12 basin grids [see Figure 2.4], with R^2 and KGE (before and after adjustment) values. The red line is the regression line between G_{MWR} and GIDAL. The black line is a 1:1 line for comparison purpose.

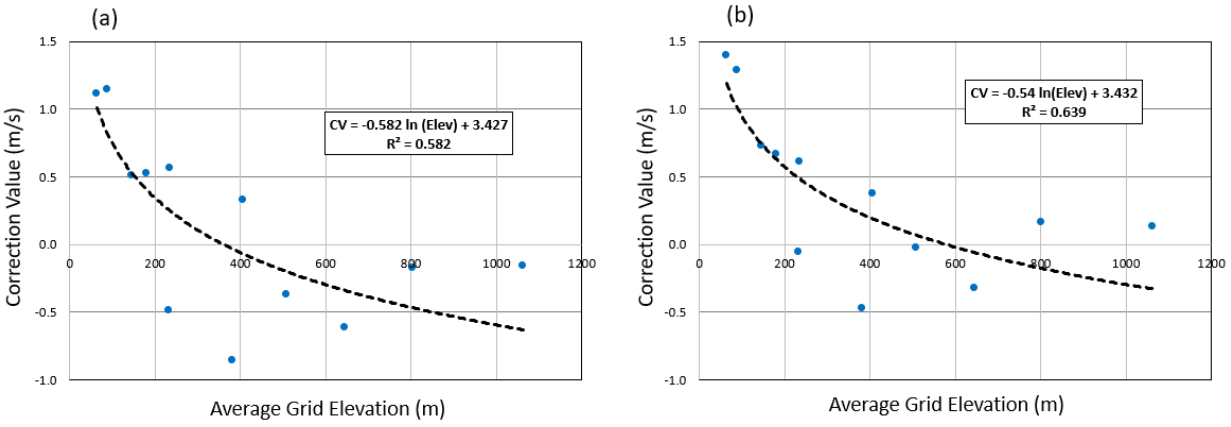

Figure D.6: Correction Value (CV) of GIDAL wind speed, for summer (a) and autumn (b), versus the average grid elevation in DRB.

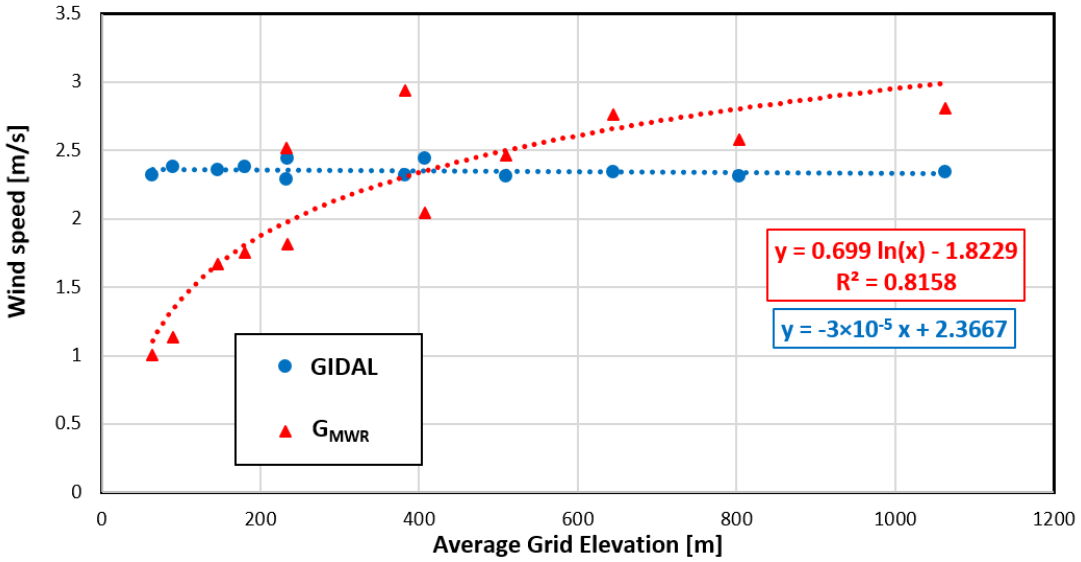

Figure D.7: Relationship of G_{MWR} and GIDAL (wind speed) with the average grid elevation DRB.

APPENDIX E

Statistics of the implemented forcing data of Chapter 2.

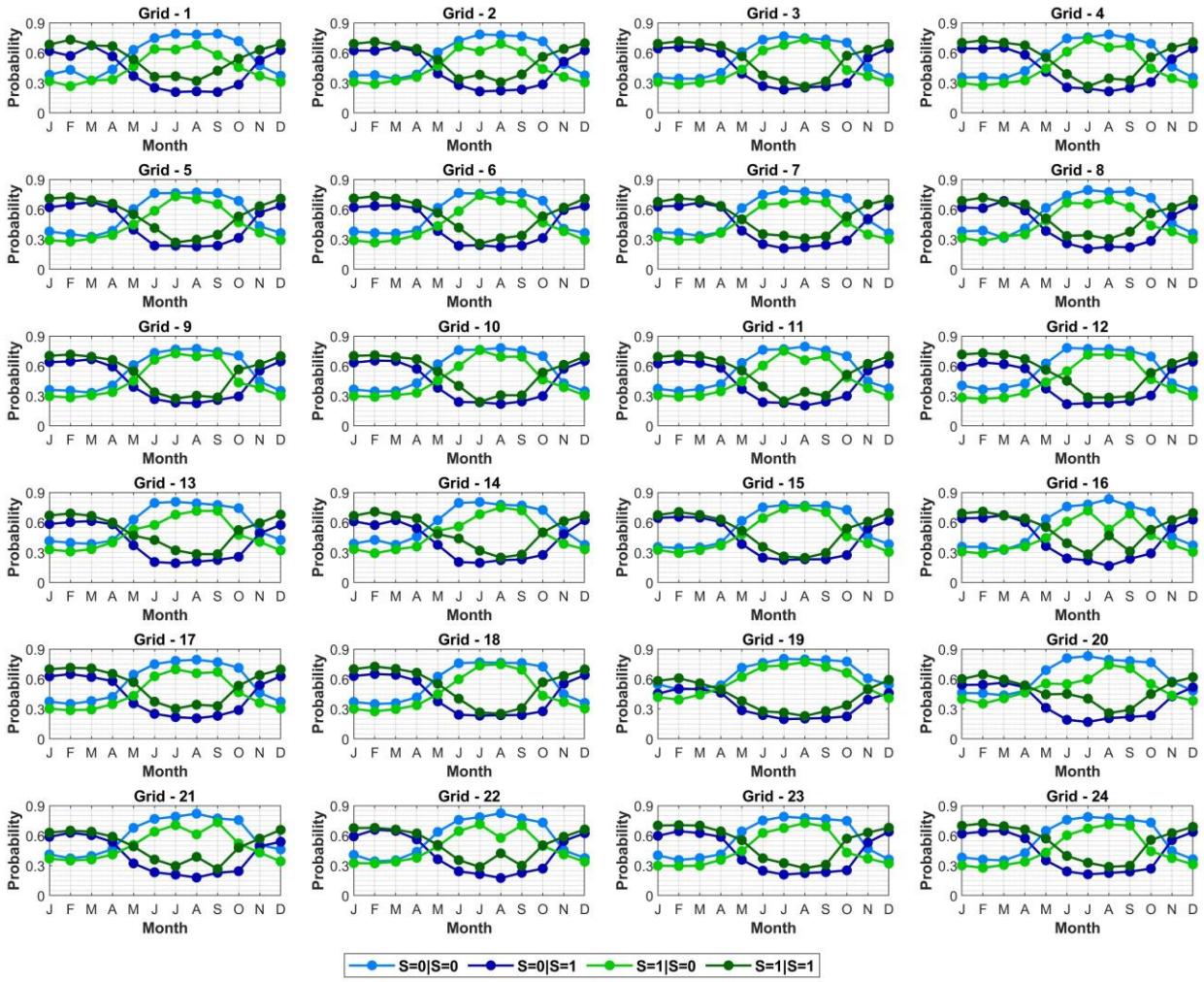

Figure E.1: Conditional probability of precipitation states in the for each grid in DRB.

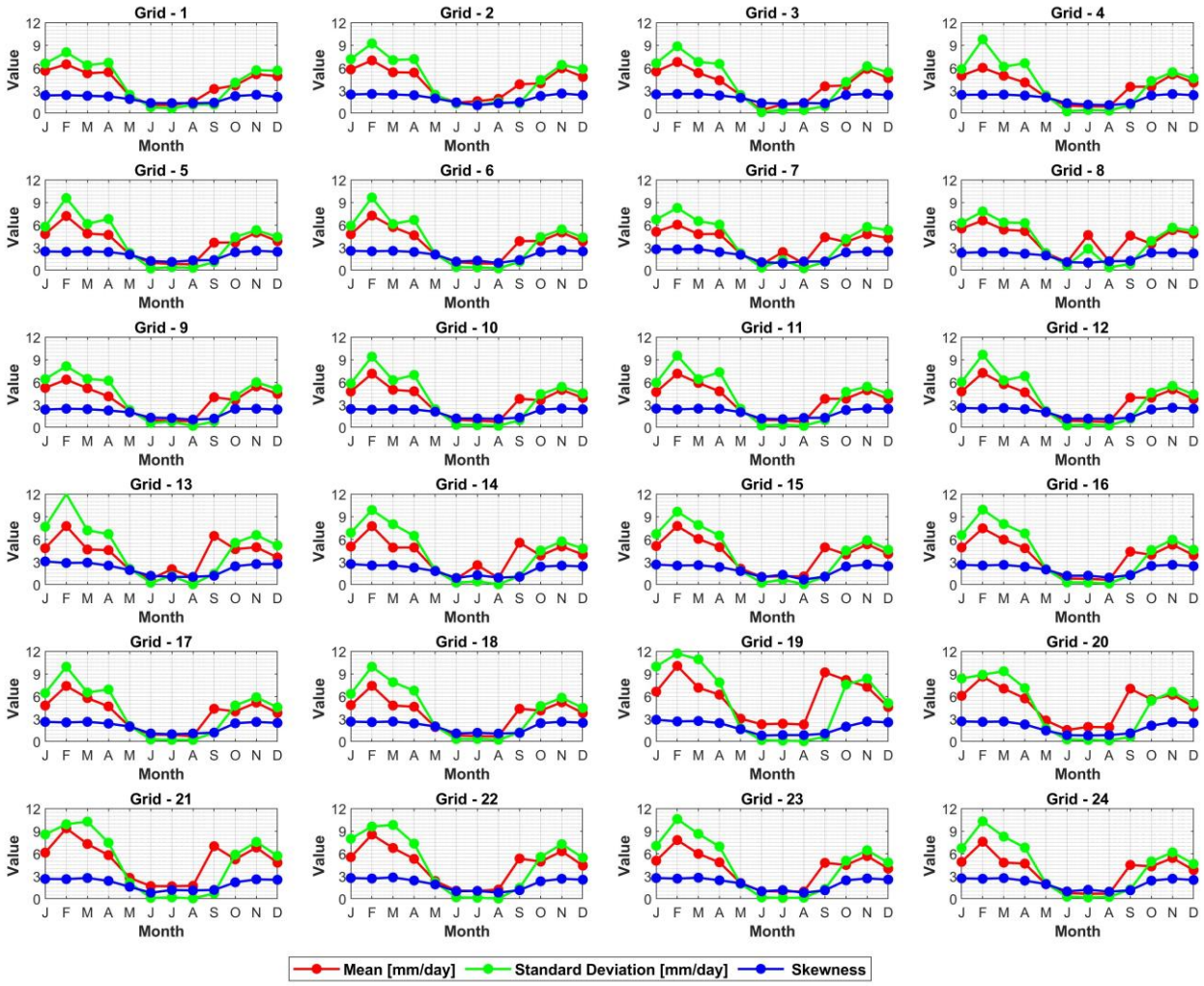

Figure E.2: Monthly precipitation statistics for each grid.

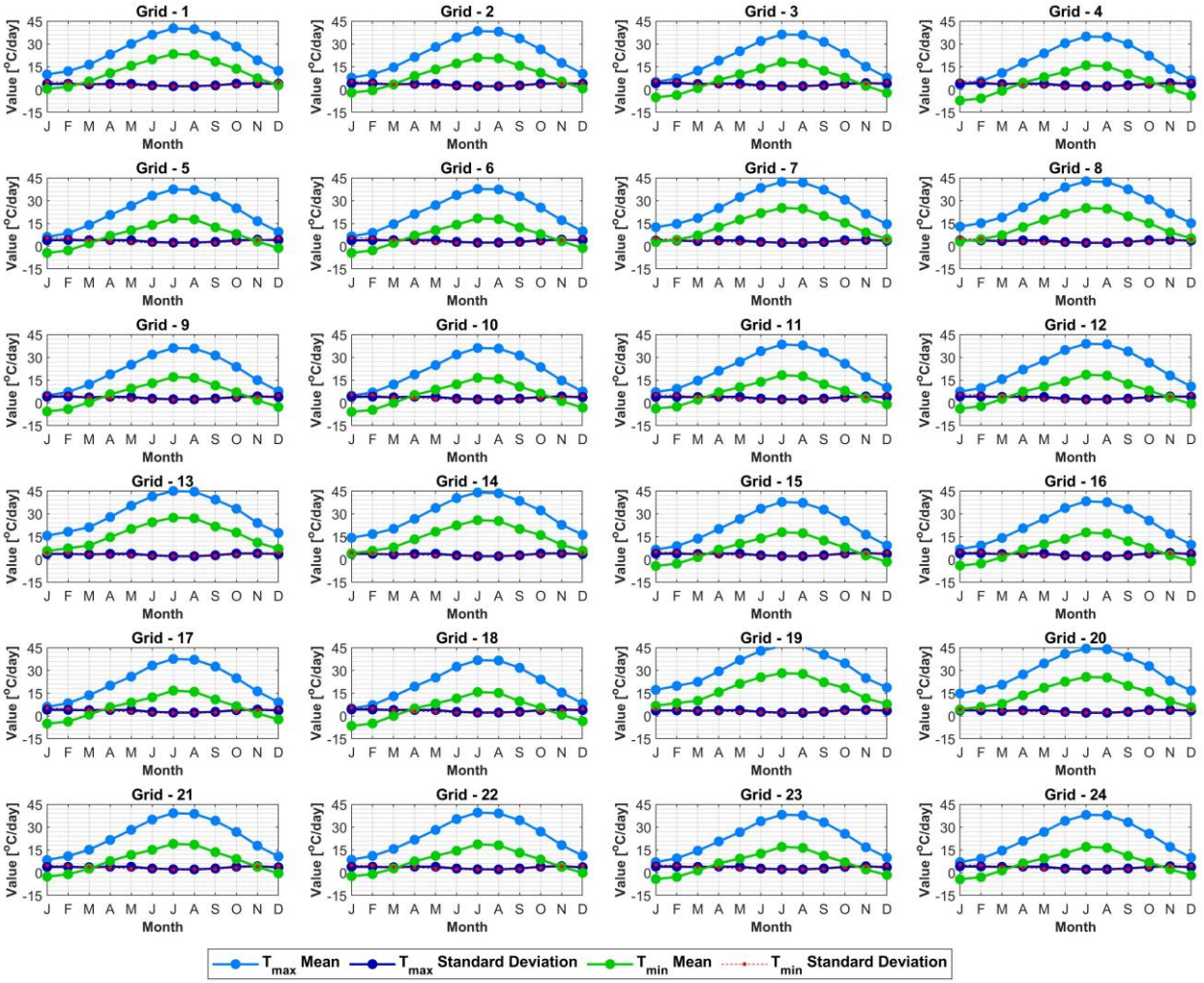

Figure E.3: Monthly temperature statistics for each grid.

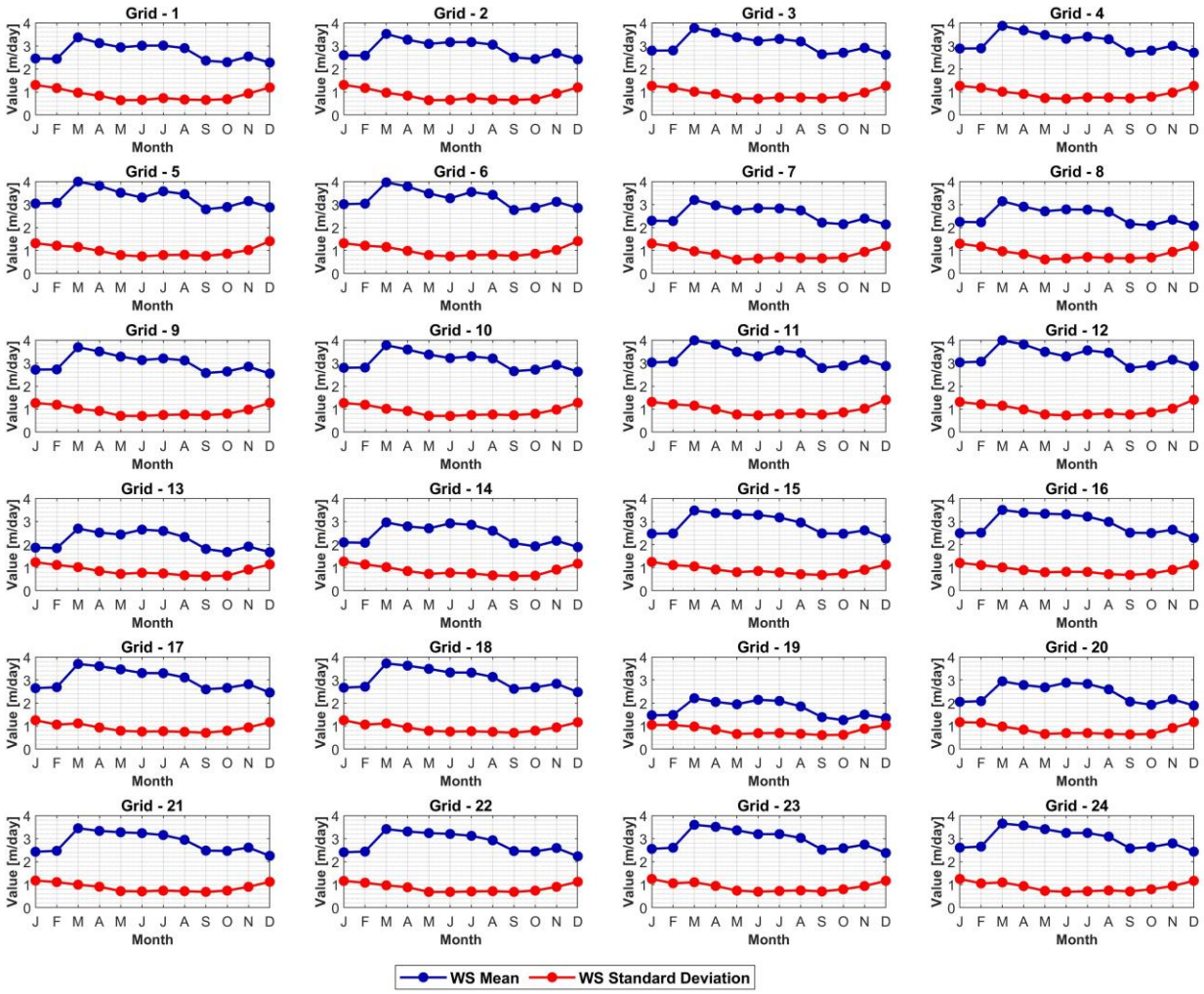

Figure E.4: Monthly wind speed statistics for each grid.